ASTON UNIVERSITY

Disorder Induced Superconductivity in a Quasi One-Dimensional Strongly Correlated System

---

Author:

Adam Lowe

Main Supervisor:

Dr. Igor Yurkevich

Assistant Supervisor:

Prof. David Saad

A thesis submitted in fulfilment of the requirements

for the degree of Doctor of Philosophy

in the

Mathematics Group

School of Engineering and Applied Science

The thesis was submitted on June 6, 2020

Thesis Summary

Aston University

Disorder Induced Superconductivity in a Quasi One-Dimensional Strongly Correlated System

Adam Lowe, Doctor of Philosophy, 2020

This thesis proposes two theoretical models. The first theory that is devised extends a model suggested by Karnaukhov [1] which suggests spontaneously broken time reversal symmetry ($\mathcal{T}$- symmetry) in a superconductor, thus implying a non trivial topology with the system. The first contribution of this thesis provides an analytical derivation for such a system, in contrast to the original paper which relied on numerical techniques. The analytical solutions confirm the results of the original paper. Furthermore, the assumption of the translationally invariant gap field being homogeneous is checked. This yields the result that for zero chemical potential there is a degeneracy of ground states along the diagonals of the Brillouin zone, and thus it can not be claimed that the gap field is homogeneous in all cases [2]. Consequently, it is found that $\mathcal{T}$-symmetry may not be broken in the scenario for a zero chemical potential, but in all other cases it is.

The other theory that is explored within this thesis is a quasi-1D model which is based on Luttinger liquid wires which have superconducting coupling inbetween the wires. From this a disorder term is added, and the relation between disorder and superconductivity is studied. This was inspired by an experiment [3] which claimed that disorder could enhance superconductivity. To solve the model, renormalisation group (RG) theory is applied, and the coupled differential equations were solved. For certain initial conditions, it is found that disorder could enhance superconductivity, which represents a novel piece of research. Moreover, different mechanisms of how this phenomenon occurs are studied, by looking at the competition between charge density wave (CDW), spin density wave (SDW) and the normal state. In an attempt to fully reconcile the experiment with the theory, different properties of the resistivity are studied such that direct comparisons can be made between the predictions of the theory and the experiment itself.

Keywords: Disorder Induced Superconductivity, Topological Superconductors

Acknowledgements

First and foremost I would like to thank my main supervisor Dr. Igor Yurkevich. His guidance and support throughout this project has been nothing short of exceptional. I can only hope to emulate his mathematical precision and insight. I would also like to thank my assistant supervisor Prof. David Saad. He was especially useful when attemping to navigate my way through the administritative world of academia, saving me many hours of time. I also want to thank my collaborators Prof. Miguel Ortuno, and Prof. Victor Kagalovsky. They have both provided useful and stimulating discussions. Victor in particular, has been especially useful for the research conducted within chapter 4 by always provoking new and interesting questions. I would also like to thank the University of Electronic Science and Technology of China in Chengdu, for hosting me for the first month of my PhD. The time I spent there adequately prepared me for the following three years of this PhD.

A special thank you should also be given to everyone within Aston's maths PhD department. The support that I got throughout my time at Aston has all contributed to the completion of this thesis, due to the perfect balance of encouragement, motivation and discussion about football. Additional thanks go to my parents and partner for painstakingly reading my thesis in the past few months. I especially appreciate my partner for putting up with my mood swings and allowing me to pursue my dream.

A final thank you should go to my father for inadvertently igniting my passion for theoretical physics. Little did he know responding to all my questions as a child about how the world works with an answer of "maths and physics" gave me the motivation to continue pursuing until I had all the answers. I now realise I will never have all the answers, and he was simply trying to get me to stop asking annoying questions!

Contents

List of Figures

List of Tables

Chapter 1

Introduction

1.1 Overview of the Thesis

Since superconductivity was discovered [4] at the onset of the 20^{th} century, there has been a focused scientific effort to understand the mechanism underlying superconductivity, in addition to developing the experimental framework. The primary reason for devoting so much research to this problem is inspired by the exciting prospect of room temperature superconductors which would revolutionise our world due to the systems exhibiting vanishing resistivity, thus reducing the world's energy usage. There are also uses for this research in medicine for magnetic resonance imaging (MRI) machines, at CERN for the Large Hadron Collider (LHC) and most recently deploying superconducting qubits in the first testable quantum computer to demonstate quantum advantage [5]. One way to achieve higher temperature superconductors is to use controllable techniques to adjust the physics of the superconductors. A common method for altering the properties of the system is to add disorder. However introducing disorder into a superconducting system was believed to inhibit superconductivity. At least, that was until recently when an experiment [3] showed that increasing disorder in a quasi one-dimensional (1D) system caused the critical temperature of the superconductor to increase. This phenomenon has no accepted scientific theory yet which consistently agrees with experiment. Nonetheless, there is a theory which is widely accepted in 2D which relies on a screened Coulomb interaction [6]. Therefore, the main aim of this thesis is to develop a theory which incorporates the interplay between disorder and superconductivity resulting in an increased critical temperature for the superconductor. A major breakthrough in this field could lead to significant technical and social benefits that would justify the research undertaken in this thesis.

The rest of this chapter describes developments in the field of superconductivity from discovery, up to 1986 where a new type of superconductor was discovered. The pre-1986 superconductivity only focused on what is known as "conventional superconductivity". An experiment at IBM [7] revealed an incomplete understanding of superconductivity, which led to the term "unconventional superconductivity" which shows characteristics not seen in conventional superconductivity. This will be the focus of chaper 2, providing an overview of the theoretical progress and how the theory links to experiment, in what is primarily an experimentally driven field.

The original contributions of this thesis are in chapter 3 [2] and chapter 4. Chapter 3 focuses on how topology is a feature of certain types of superconductors, and how this can be useful. Additionally a new synthetic model is proposed for finding a topological superconductor which has unique properties since it has a continuum of energies at the lowest energy level when the system is at half filling (when the chemical potential is zero).

Chapter 4 is the main focus of the thesis. The Luttinger liquid formalism is introduced since an array of one dimensional chains with weak inter chain coupling is the basis of the model. After this, superconducting coupling and disorder are introduced, and the interplay between disorder and superconductivity is studied. For certain parameters it is seen that disorder can enhance superconductivity which helps explain the key experiment [3] which first observed this unexpected phenomenon and is the inspiration for this theoretical analysis.

Finally conclusions will be drawn and future work proposed with particular focus on finding systems with experimental verification. Additionally, an emphasis will be put on how this new theory can be used and developed for real world applications.

1.2 History of Superconductivity

In 1911, Onnes [4] found that when he cooled liquid helium to approximately 4K, the resistivity vanished. This was the first experimental evidence for superconductivity and was completely unexpected, as it was believed that the resistivity would tend to zero as the temperature tended to zero. There was no theoretical explanation for this, and devising a theory was elusive since the theoretical framework for quantum mechanics had yet to be created.

Early in the 1930s, a further breakthrough occured when Meissner [8] found that when applying a magnetic field to a superconductor, the field is expelled around the superconductor and was duly named the Meissner effect. This allowed theoretical progress since the London brothers [9] subsequently developed a macroscopic explanation of how this Meissner effect occured by way of the London equations which are given by

$$\frac{\partial \mathbf{j}}{\partial t} = \frac{n}{m}\mathbf{E}, \tag{1.1}$$

and

$$\nabla \times \mathbf{j} = -\frac{n}{m}\mathbf{B}, \tag{1.2}$$

where $\mathbf{j} \equiv \mathbf{j}(\mathbf{r}, t)$ is the superconducting current density, $\mathbf{r}$ is the position, t is the time, n is the electron density, m is the electron mass, $\mathbf{E} \equiv \mathbf{E}(\mathbf{r}, t)$ is the electric field, and $\mathbf{B} \equiv \mathbf{B}(\mathbf{r}, t)$ is the magnetic field. These can be succinctly written in the Coulomb gauge as the famous equation

$$\mathbf{j} = -\frac{n}{m}\mathbf{A}, \tag{1.3}$$

where $\mathbf{A}$ is the vector potential. Using these, in combination with Ampere's law

$$\nabla \times \mathbf{B} = \mu_0 \mathbf{j}, \tag{1.4}$$

where μ_0 is the magnetic constant, allows an equation solely in terms of magnetic field to be written as

$$\nabla^2 \mathbf{B} = \frac{1}{\lambda_L^2}\mathbf{B}, \tag{1.5}$$

where $\lambda_L = \sqrt{\frac{m}{\mu_0 n}}$. Equation (1.5) clearly admits exponentially decaying solutions which decays with the penetration length, λ_L and explains why the magnetic field is expelled from a superconductor. Whilst this reveals some interesting physics about a superconductor, it still does not explain the origin or anything about the phase transition. This is addressed in the next section.

1.2.1 Introduction to Phase Transitions and Ginzburg-Landau Theory

Phase Transitions

The theory of phase transitions in the modern era is broadly classified into two categories. The first type of phase transition is a first order phase transition [10]. This type of transition requires latent heat, and a common example is the phase transition from ice to water. This type of transition has been widely understood for many years.

The other type of phase transition is a second order phase transition [11]. This type of transition will be the focus of this thesis. A second order phase transition is continuous, and occurs smoothly with change in temperature. Often, this transition occurs due to some type of symmetry breaking. Subsequently, a superconducting phase transition is described by second order phase transitions. The first phenomenological theory of second order phase transitions was described by Landau, and extended upon to include superconductivity by Ginzburg [12].

Ginzburg-Landau Theory

Ginzburg-Landau theory starts from the postulate that the state, as with all phases, is described by an order parameter Δ which is zero in the normal phase, and becomes non zero in the superconducting phase. In this theory, the free energy F is written in terms of these order parameters, and information can be extracted describing the physics of the phase transition. This order parameter can be heuristically thought of as the superconducting wavefunction, and therefore it must obey

$$n_s(\mathbf{r}) = |\Delta(\mathbf{r})|^2, \tag{1.6}$$

where $n_s(\mathbf{r})$ is the density of the superconducting wavefunction analagous to standard quantum mechanics [13], where $\mathbf{r}$ is the position. To focus on the phase transition, it is logical to think that the order parameter will be small as it will go from a region of being non-zero to zero, and therefore this allows for a small order expansion about the order parameter for the free energy. For a spatially non varying order parameter this yields

$$F = \int d\mathbf{r}\Big(\alpha(\mathbf{r})|\Delta(\mathbf{r})|^2 + \frac{\beta(\mathbf{r})}{2}|\Delta(\mathbf{r})|^4\Big), \tag{1.7}$$

where $\alpha(\mathbf{r})$ and $\beta(\mathbf{r})$ are coupling terms that correspond to the quadratic and quartic terms respectively. These varying parameters determine how the phase transition occurs, and provides insight to the physics of the transition. Generally the superconducting field can vary in space, and therefore this needs to be accounted for. The gradient of the field is incorporated such that

$$F = \int d\mathbf{r}\Big(\alpha(\mathbf{r})|\Delta(\mathbf{r})|^2 + \frac{\beta(\mathbf{r})}{2}|\Delta(\mathbf{r})|^4 + \gamma(\mathbf{r})|\nabla\Delta(\mathbf{r})|^2\Big). \tag{1.8}$$

However, this is still dependent on the choice of the gauge, so to make it gauge invariant, coupling to the vector potential must be added by $\nabla \rightarrow \nabla + 2i\mathbf{A}(\mathbf{r})$. Additionally to add the magnetic field to the free energy, the term $B^2(\mathbf{r})/(8\pi)$ is included. The total equation is then

$$F = \int d\mathbf{r}\Big(\alpha(\mathbf{r})|\Delta(\mathbf{r})|^2 + \frac{\beta(\mathbf{r})}{2}|\Delta(\mathbf{r})|^4 + \gamma(\mathbf{r})|(\nabla + 2i\mathbf{A}(\mathbf{r}))\Delta(\mathbf{r})|^2 + \frac{B^2(\mathbf{r})}{8\pi}\Big). \tag{1.9}$$

From this free energy, the Ginzburg-Landau equations can be found by minimising this free energy with respect to the order parameter and $\mathbf{A}$. After calculations [14] a Ginzburg Landau parameter can be derived and is defined as

$$\kappa = \frac{\lambda_L}{\xi}, \tag{1.10}$$

where ξ is a coherence length. This parameter is interestingly independent of temperature, which is why it is useful experimentally. By using this parameter, certain properties of a superconducting phase transition can be deduced within the Ginzburg-Landau framework.

The interesting physics behind this theory is that it is an entirely macroscopic approach to calculating superconducting behaviour, and phase transitions. This method allows a phenomenological approach when attempting to calculate the type of superconductivity in unconventional superconductivity. This will be shown explicitly in chapter 2. Additionally, the concept of minimising the free energy with respect to the order parameter is a technique that is used in chapter 3.

1.2.2 Bardeen-Cooper-Schreiffer (BCS) Theory of Superconductivity

Whilst Ginzburg-Landau theory is useful and can be used for a wide variety of superconducting systems, both conventional and unconventional, it still does not give a microscopic description, and therefore does not explain any of the underlying mechanisms behind superconductivity. The first microscopic theoretical breakthrough came in the late 1950s by Bardeen, Cooper, and Schreiffer (BCS) [15], which built on the work of Cooper [16], to describe superconductivity due to pairs of electrons which are coupled by phonons to form quasiparticles known as Cooper pairs. When this mechanism occurs, the resistivity vanishes and superconductivity manifests. Before deriving this, it is useful to introduce the mathematics of second quantisation [17] so the functional integral derivation for BCS theory is clear. This technique will be used extensively throughout the thesis, so introducing it now will clarify the mathematical techniques used in chapter 3.

The functional integral technique is a way of rewriting integrals over functions as opposed to just variables. This is a technique in many body physics. Treating such problems in terms of functional integrals gives rise to elegant solutions. For a full derivation of this, see Negele and Orland [17]. The final result gives the partition function, Z given by

$$Z = \int \mathscr{D}[\psi^*_{\mathbf{k}}(\tau), \psi_{\mathbf{k}}(\tau)] \exp\Big(- S(\psi^*_{\mathbf{k}}(\tau), \psi_{\mathbf{k}}(\tau))\Big), \tag{1.11}$$

where $S(\psi^*_{\mathbf{k}}(\tau), \psi_{\mathbf{k}}(\tau))$ is the action, $\mathbf{k}$ is the momentum, τ is imaginary time and is defined as $\tau = -it$, and $\psi_{\mathbf{k}}(\tau)$ represents the wavefunction. The action is defined as

$$S(\psi^*_{\mathbf{k}}(\tau), \psi_{\mathbf{k}}(\tau)) = \int_0^\beta d\tau \sum_{\mathbf{k}} \Big[\psi^*_{\mathbf{k}}(\tau)\partial_\tau \psi_{\mathbf{k}} + \mathcal{H}\big(\psi^*_{\mathbf{k}}(\tau), \psi_{\mathbf{k}}(\tau)\big)\Big], \tag{1.12}$$

where $\beta = 1/T$, with T defined as temperature, and

$$\mathscr{D}[\psi^*_{\mathbf{k}}(\tau), \psi_{\mathbf{k}}(\tau)] = \lim_{M\to\infty} \prod_{k=1}^{M} d\psi^*_{\mathbf{k}}(\tau) d\psi_{\mathbf{k}}(\tau). \tag{1.13}$$

Equations (1.11,1.12,1.13) allow a functional integral representation for any given Hamiltonian $\mathcal{H}$. It can now be seen that any Hamiltonian can be substituted in, and the effective action can be calculated. This is a common technique used in quantum field theory, from condensed matter physics to particle physics. This mathematical formulation can be applied

to BCS superconductivity.

The BCS theory of superconductivity is the most basic formulation of a superconducting system. The system is assumed to be isotropic, and the interaction between the fermions is attractive for a small band of fermions due to phonons. The phonon frequency results in the attractive potential overcoming the repulsive potential from electrons. Consequently a superconducting system can occur. The interacting Hamiltonian of the particles can be written as

$$\mathcal{H} = \sum_s \bar{\psi}_s \epsilon_f \psi_s - J\bar{\psi}_\uparrow \bar{\psi}_\downarrow \psi_\uparrow \psi_\downarrow, \tag{1.14}$$

where $\psi \equiv \psi(\mathbf{r}, \tau)$ is the wavefunction, J is the coupling constant and has no directional dependence since it is an isotropic system, $\epsilon_f \equiv \epsilon_f(\mathbf{r})$ is the Fermi energy, and the arrows and s denote the spins of the particle. This Hamiltonian describes interacting particles, specifically fermions. Equation (1.14) can now be substituted into equations (1.11,1.12,1.13), which results in

$$Z = \int \mathscr{D}[\bar{\psi}, \psi] \exp\Big(- \sum_s \int d\mathbf{r} \int_0^\beta d\tau \bar{\psi}_s (\partial_\tau + \epsilon_f)\psi_s + \int d\mathbf{r} \int_0^\beta d\tau J\bar{\psi}_\uparrow \bar{\psi}_\downarrow \psi_\uparrow \psi_\downarrow \Big). \tag{1.15}$$

Since the quartic term is difficult to compute analytically, a transformation known as the Hubbard-Stratonovich transformation [18] is applied. This changes the quartic term into a quadratic term, by making use of completing the square. Equation (1.15) then becomes

$$\begin{aligned} Z = \int \mathscr{D}[\bar{\psi}, \psi] \exp\Big[&- \sum_s \int d\mathbf{r} \int_0^\beta d\tau \bar{\psi}_s (\partial_\tau + \epsilon_f)\psi_s \\ &- \int d\mathbf{r} \int_0^\beta d\tau \Big(- \frac{|\Delta|^2}{J} + \Delta\bar{\psi}_\uparrow \bar{\psi}_\downarrow + \bar{\Delta}\psi_\uparrow \psi_\downarrow \Big) \Big], \end{aligned} \tag{1.16}$$

where Δ is introduced as a quasiparticle through the transformation and can be thought of as the gap parameter between the bands of energies of the fermions, where it is a constant. It can have directional dependence in more general cases, but for this system it does not as that is one of the assumptions of BCS superconductivity. Equation (1.16) can be rewritten in terms of Nambu vectors as

$$\begin{aligned} Z = \int \mathscr{D}[\bar{\psi}, \psi] \exp\Big(- \int d\mathbf{r} \int_0^\beta d\tau \psi^\dagger A \psi + \int d\mathbf{r} \int_0^\beta d\tau \frac{|\Delta|^2}{J} \Big) \\ = \int \mathscr{D}[\bar{\psi}, \psi] \exp\Big(- (S_1 + S_2) \Big), \end{aligned} \tag{1.17}$$

where $S_1 = \int d\mathbf{r} \int_0^\beta d\tau \psi^\dagger A \psi$, $S_2 = -\int d\mathbf{r} \int_0^\beta d\tau \frac{|\Delta|^2}{J}$ and A is defined as

$$A = \begin{pmatrix} \partial_\tau + \epsilon_f & \bar{\Delta} \\ \Delta & \partial_\tau - \epsilon_f \end{pmatrix}. \tag{1.18}$$

An identity [17] can now be used to make use of A being in matrix form. This is defined as

$$\int \mathscr{D}[\bar{\psi}, \psi] \exp\Big(- \int d\mathbf{r} \int_0^\beta d\tau \psi^\dagger A \psi \Big) = \exp\Big(\text{Tr } \big[\ln\big(\det(A) \big) \big] \Big), \tag{1.19}$$

where ln is the natural logarithm and the trace is now only over the elements of the matrix. Choosing a Fourier basis such that $\Psi(\mathbf{k}, \epsilon) = \int d\tau d\mathbf{r}\, \psi(\mathbf{r}, \tau) e^{-i\epsilon\tau} e^{i\mathbf{k}.\mathbf{r}}$, changes A to give

$$A = \begin{pmatrix} -i\epsilon + E_{\mathbf{k}} & \bar{\Delta} \\ \Delta & -i\epsilon - E_{\mathbf{k}}, \end{pmatrix}. \tag{1.20}$$

where the energy is now dependent on momentum. Using equation (1.20), the eigenvalues are found to be

$$\lambda_\pm = -i\epsilon \pm \sqrt{\Delta^2 + {E_{\mathbf{k}}}^2}, \tag{1.21}$$

which will be substituted into (1.25). Now by integrating out the position, and over all τ for the first term in the action, it is found that

$$S = \frac{V\beta|\Delta|^2}{J} - \sum_{k\epsilon} \text{tr ln} \left[\det \begin{pmatrix} -i\epsilon + E_{\mathbf{k}} & \bar{\Delta} \\ \Delta & -i\epsilon - E_{\mathbf{k}} \end{pmatrix} \right]. \tag{1.22}$$

The trace is now lower case since the sum is now only over a scalar whereas previously the sum was over the vector. Now using two relations, S can be simplified further. The first relation is

$$\sum_{\mathbf{k}} f(\mathbf{k}) = \sum_k \text{tr } f(\mathbf{k}) = V \int \frac{d^d\mathbf{k}}{(2\pi)^d} f(E_{\mathbf{k}}) = V \int dE \rho_D(E) f(E), \tag{1.23}$$

where $\mathbf{k}$ is the momentum, d is the dimension, ρ_D is the density. Since the superconducting state only occurs for a small band of fermions where the attraction energy is greater than the repulsion energy, $\rho_D(E) \to \rho_D$ can be viewed as a constant, and can be taken out of the

integral. The second relation is based upon the Matsubara frequencies [17] and is given by

$$\sum_{\epsilon} f(i\epsilon) = \beta \int_{\gamma} \frac{dz}{4\pi i} \tanh\Big(-\frac{\beta z}{2}\Big) f(-z), \tag{1.24}$$

which is a generic relation that holds as long as the contour integral decays as $1/z^n$ where $n \geq 2$. Now substituting the eigenvalue solutions into S, the result is

$$S = \frac{V\beta|\Delta|^2}{J} - \sum_{k\epsilon} \mathrm{tr}[\ln(\lambda_+\lambda_-)] = \frac{V\beta|\Delta|^2}{J} - \sum_{k\epsilon} \mathrm{tr}\Big[\ln\big[((-i\epsilon)^2 - \Delta^2 - E_{\mathbf{k}}^2)\big]\Big]. \tag{1.25}$$

Combining equation (1.25) with the relations given in (1.23, 1.24), S takes the form

$$S = \frac{V\beta|\Delta|^2}{J} - \left[V\rho_D\beta \int dE \int_{\gamma} \frac{dz}{4\pi i} \tanh\Big(-\frac{\beta z}{2}\Big) \ln[(-z)^2 - \Delta^2 - E^2]\right]. \tag{1.26}$$

To find where the dominant contribution for the superconducting state occurs, the function is minimised and the point at the minimum is the most stable point and subsequently is where the superconducting state occurs. This is done by differentiating S and setting equal to zero to give

$$\frac{\partial S}{\partial \Delta} = 2\frac{V\beta|\Delta|}{J} + \left[V\rho_D\beta \int dE \int_{\gamma} \frac{dz}{4\pi i} \tanh\Big(-\frac{\beta z}{2}\Big) \frac{2\Delta}{z^2 - \Delta^2 - E^2}\right] = 0. \tag{1.27}$$

To evaluate the contour integral, the poles have to be found which forces the integrand $\to \infty$. This occurs for $z = \pm\sqrt{\Delta^2 + E^2}$, and Cauchy's residue theorem is then applied to give

$$\frac{\partial S}{\partial \Delta} = -V\beta\rho_D \int dE \frac{2\pi i}{4\pi i} \tanh\Big(\frac{\beta z}{2}\Big) \frac{2\Delta}{z} + \frac{2V\beta|\Delta|}{J} = 0. \tag{1.28}$$

Substituting the solution for z into equation (1.28) and rearranging gives

$$1 = \rho_D J \int dE \frac{\tanh\left(\frac{\beta\sqrt{\Delta^2+E^2}}{2}\right)}{2\sqrt{\Delta^2 + E^2}}. \tag{1.29}$$

This is known as the BCS gap equation in a self consistency form. To find the temperature at which the superconducting state occurs, Δ is neglected due to the window of particles with that energy being small, and the integration is carried out over the range of the Debye

frequency [19]. Consequently equation (1.29) is approximately evaluated to

$$1 = \rho_D J \int_{-\hbar\omega_D}^{\hbar\omega_D} dE \frac{\tanh\left(\frac{E}{2k_B T_c}\right)}{2E} = \rho_D J \int_0^{\hbar\omega_D} dE \frac{\tanh\left(\frac{E}{2k_B T_c}\right)}{E} \approx \rho_D J \ln\left[\frac{\hbar\omega_D}{k_B T_c}\right], \tag{1.30}$$

where $\hbar$ is Plank's constant divided by 2π and ω_D is the Debye frequency. The limits are 0 and $\hbar\omega_D$, since that is the range of energy for the attractive fermions. Inverting equation (1.30), the critical temperture is evaluated as

$$T_c = \frac{\hbar\omega_D}{k_B} \exp\left(-\frac{1}{\rho_D J}\right). \tag{1.31}$$

This equation describes the critical temperature for a BCS superconducting system. By substituting values for the variables, a value for the temperature can be found. The equation was the first theoretical model for superconductivity and gave a theoretical prediction for the phase transition temperature. This equation only describes the simplest type of superconductivity, known as s-wave superconductivity. For the rest of this thesis, natural units will be used resulting in $\hbar = k_B = c = 1$.

1.2.3 Post 1986 Superconductivity

All superconductivity up to 1986 was thought to be described completely by BCS theory which is completely isotropic and thus has a gap function that has s-wave symmetry. This original theory predicted a maximum critical temperature about $T_c \approx 30K$, and it was believed that superconductivity would not occur above such a temperature. However, this belief was dispelled by the Nobel prize winning work of Bednörz and Müller [7], which showed a superconductor working at approximately $35K$. This led to a flurry of new research both experimentally and theoretically trying to understand this new type of superconductivity. Since this type of superconductivity behaved differently to previous superconducting theory, it was coined "Unconventional Superconductivity", which in the present day is a definition for superconductivity which does not occur through standard s-wave physics. The microscopic description is believed to occur through a variety of different mechanisms, namely spin fluctuations, electron-electron interactions and the interplay between magnetism and electrons. In this state the gap function is no longer isotropic, leading

to potential d-wave, p-wave, or f-wave symmetry. This is one of the signatures of unconventional superconductivity. There is currently no widely agreed microscopic theory for unconventional superconductivity, and it is generally performed macroscopically by using symmetries of the order parameter. The theory will be fully explored in chapter 2.

With the unexpected increase in critical temperature, it gave new impetus to experimentalists and theorists alike, to create room temperature superconductivity. Over the past 30 years, there has been significant progress with the highest known current critical temperature at $250K$ [20], although this experiment was conducted at one million times standard atmospheric pressure. Interestingly, the superconductivity is conventional and is based on BCS with the extension of Eliashberg's theory [21] which includes retardation effects. Formally this was predicted using density functional theory [22], however this is only valid for extreme conditions for the atoms, hence the extremely high pressure.

Current theoretical research is starting to use a variety of different techniques from other fields, such as topology and group theory, to create superconductors that have controllable properties. Fortunately, experimentalists are finding ways of determining the topology of such systems, thus giving the theories verifiable evidence. All the research within this thesis, lies within the label of unconventional superconductivity, due to the non-BCS pairing mechanisms that are used in both chapters 3 and 4. Importantly, the motivation behind chapter 3 is the design of topological superconductors that could eventually be applied to the development of quantum computers, whereas chapter 4 is focused on finding a mechanism for a high critical temperature superconductor by introducing disorder into the system.

1.2.4 Effects of Disorder on Superconductivity

One of the most desirable properties for superconductivity is to be able to control the critical temperature, and thus control the superconducting phase. A useful way of doing this is to introduce disorder into the system, as this is a controllable feature. However, disorder had previously been believed to reduce the critical temperature and in some cases destroy the superconductivity completely [23]. This is because the Cooper pairs are not robust against strong disorder. For weak disorder, the critical temperature remains unchanged, due to Anderson localisation [24]. This is only the case for conventional superconductors. Consequently, this unique feature can be exploited experimentally by using it as a method to determine the difference between unconventional and conventional superconductivity [25].

The negative correlation between disorder and superconductivity was unquestioned, until a revolutionary experiment [3] showed that disorder could enhance the superconducting critical temperature. The most clear graph showing the positive correlation between increasing disorder and critical temperature is shown below.

Graph showing the onset of the critical temperature against disorder

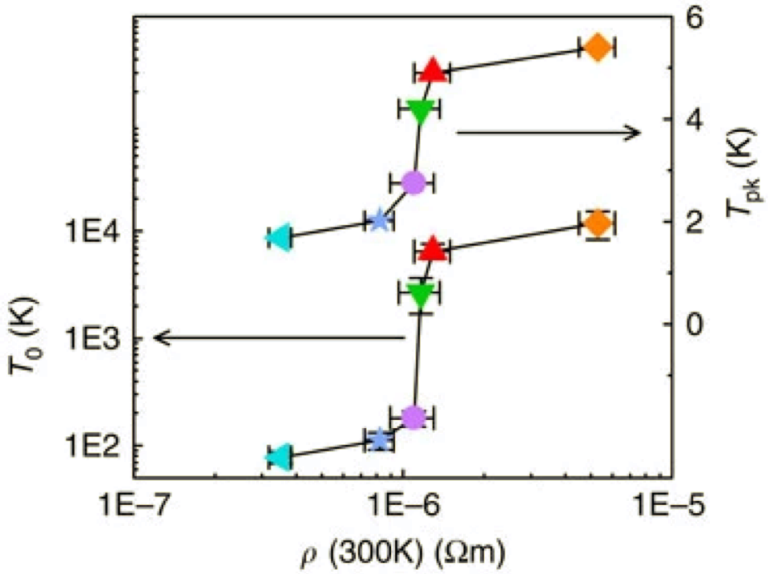

FIGURE 1.1: This graph [3] shows that as disorder is increased the temperature at which superconductivity is about to occur increases. $T_{\text{pk}}(K) \equiv T_{\text{peak}}(K)$ is the onset of superconductivity, and $\rho(300K)$ is the value for the resistivity at $300K$, which experimentally is the method for determining the initial disorder. However, the theory of why this positive correlation occurs is unknown. This graph was taken from the key experiment in reference [3].

The system was a quasi-1D strongly correlated model. This experiment showing that disorder could enhance the critical temperature, had no theoretical model. This is the primary motivation for this thesis. The theory that has been designed to describe this model is discussed extensively in chapter 4. Additionally, there are still many examples where disorder does break superconductivity, so it is not a general phenomenon that disorder increases the critical temperature of superconductivitiy.

1.3 Literature Review of Quasi-1D Superconductors

This section explores some of the theoretical techniques used in current research, and will explore the benefits and negatives of the techniques. There will be particular emphasis on

one dimensional physics, and topological physics as these directly relate to the original content shown in this thesis.

1.3.1 One-Dimensional Physics

One-dimensional physics is an over simplification of a complex world, though recent experiments [26] have shown that on a condensed matter level, the physics not only differs from higher dimensions, but can be incredibly useful and used throughout high performance electronics. However, the mathematical framework for one dimensional systems is distinct to standard Fermi liquid theory [27]. The main cause for this is that Fermi liquid theory breaks down when modelling a one dimensional system due to Peierls instability [28]. The philosophical argument for Peierls instability is based on the belief that if the electrons are primarily localised in Fermi liquid theory, which occurs when the dimensionality of the system is of the order one (or for very low energies), then any perturbation of the electrons is energetically favourable and thus resulting in an instability. Consequently, a new model needed to be developed to explain the physics of the one-dimensional world that removes any instability. The solution was proposed by Tomonaga and Luttinger, in the suitably named Tomonaga-Luttinger liquid theory [29] which will henceforth be known simply as Luttinger liquid theory in this thesis. This is derived in chapter 4 as it will be used extensively within that chapter.

Experimental and Theoretical Development

One-dimensional physics, and the use of Luttinger liquid theory was originally believed to be a theorist's tool, rather than an actual practical theory. This belief changed when experiments [30] were conducted on the Bechgaard salts [31], which showed that in a quasi-1D system, power laws predicted from Luttinger theory were observed in experiment by use of optics and photoemission. This validation led to a flurry of research at the turn of the 21^{st} century up to the present day.

From an experimental perspective, the natural place to study one-dimensional behaviour is by creating coupled one-dimensional wires [32]. This methodology revealed Luttinger liquid behaviour also. Furthermore, similar behaviour was observed when single walled carbon nanotubes were created, providing a useful platform for studying one-dimensional physics. These original results were verified and confirmed later [26]. An additional way

in which one-dimensional systems can be accessed, makes use of the control of lasers by cooling down atoms to form ladders [33]. This allows for a direction to be determined, and therefore the interactions between the atoms would occur along one direction, simulating a one-dimensional system. The most applicable example to the work done throughout this thesis is by studying edge states of condensed matter systems [34], since these are obviously one dimensional, where the main difficulty with these experiments is measuring the edge state accurately.

From a theoretical perspective, this has become a rich research area, due to the curious link between these systems and their topological properties [35]. For an exhaustive review of one dimensional physics, see [27]. This review has particular emphasis on the theory of formulating a 3D system from Luttinger theory in tandem with other models, namely the Hubbard model [36]. This is a useful feature, as the Hubbard model can also be used to describe a one dimensional chain, when used in tandem with the Luttinger model. As an interesting aside, there is an extension of the model known as the t-J model [37] which occurs for strong correlations, and has been used as an attempt to describe high temperature superconductivity. Ultimately, it has not been consistent with experiment [38]. Regardless, without the Luttinger model, the Peierls instability will still occur.

1.3.2 Topological Physics

The field of topological physics, specifically within condensed matter physics has been developing for the past 40 years, however the area has expanded drastically since the turn of the 21^{st} century due to the promising properties that non-trivial topology possesses [39]. The non-triviality arises since there is an added layer of protection for the state due to the topology, typically as the Brillouin zone is deformed thus having a different topology, but the state remains unchanged. The full use of the theory was confirmed by experiment [40]. It is important to understand the benefits that topology yields to condensed matter systems. Primarily, the benefit is that the electronic properties of the edge states are changed such that non trivial physics occurs, which has promising potential in industry. The main discovery which prompted the field within the condensed matter physics community was the discovery that the integer quantum hall effect [40] had topological properties [41]. Consequently,

this revolutionary discovery opened up the potential for a variety of condensed matter systems posessing topological properties. It is curious to note, that the famous Berezinskii-Kosterlitz-Thouless transition [42], is an example of a topological phase transition.

Advantages of Topological Physics

The reason that many researchers in the field today are dedicating their time to topological materials is due to their advantages, namely, robustness against disorder [43, 44], quantum computation [45], and increased communications since backscattering is dramatically reduced [46]. These novel states can behave as insulating in the bulk, and conducting on the edge, which was predicted theoretically [47], and then confirmed experimentally [48].

The robustness against disorder is a particularly useful property as one could envisage a scenario, where precise materials are built and any impurity could destroy the functionality of the material. Using a topological material, allows for some extra protection that would not exist in standard materials. The most useful application of topology within industry is within the development of quantum computers. The theory is dependent on the existence of non-Abelian anyons [49] since Kitaev showed [45] that by using such particles, quantum error correction [50] could be reduced. This is one of the biggest problems in making quantum computing a widespread reality. The existence of non-Abelian anyons is still controversial, there has been the hint of them in an experiment [51] studying the fractional quantum hall effect but this is yet to be fully accepted within the community.

It is important to realise that the practical applications of topological physics are still in their infancy, which is what makes the field so novel and exciting. These reasons are why many research papers within the condensed matter community are studying topological properties of materials that previously were believed to be "topologically trivial".

Interplay of Topology and Superconductivity

The interplay of topology and superconductivity is of particular focus for this thesis, and chapter 3 will be discussing the research that has taken place in this field. Topological insulators [48] were found before topological superconductors, so a large portion of the research in topological physics was studied using insulating systems. Often the developments were applicable to topological superconducting systems.

In 2000, the first theoretical prediction of topological superconductivity was conducted by Read and Green [52] who claimed that a phase transition occured which gave two distinctly different topologies and therefore different topological invariants. This was the first sign that the gap functions of the systems could have non trivial topology, and thus by studying the gap function, the topology of the system could be deduced. This paper was quickly followed by another brilliant paper from Kitaev [53], which showed that Majorana fermions could be hosted along quantum wires thus resulting in a topological state. If a topological system has Majorana fermions on the edge states, this is arguably the best definition for a topological system. A Majorana fermion is a particularly interesting particle [54], since the anti particle is equal to the actual particle. It was first predicted by Ettore Majorana in 1937 as a fundamental particle. As of yet, it has not been discovered fundamentally, however a quasiparticle displaying the same effects has been experimentally verified [55, 56]. Another reason this particle is so sought after, is due to the non-Abelian statistics it posseses, meaning it is another promising candidate for developing quantum computers. Topological superconductivity has been recently verified [57], which further confirms that it is a promising avenue to pursue. Another benefit of topological superconductivity within quantum computers is that the topology protects the quantum nature of the qubit, thus reducing the likelihood of quantum decoherence.

Additonally, due to the protective nature of topology, the mechanism could be used to guard against perturbations which destroy superconductivity. Often, this can break the Cooper pairs which leads to destruction of the superconducting state. If the Cooper pairs were protected by topological properties, this could be a promising avenue for high temperature superconductivity.

An obvious question about these systems, is how to quantify a system as being topological. This is primarily achieved by using topological invariants, thus forming different topological classes of superconductors. However, this is created by the use of symmetries which are introduced in the next section.

1.3.3 Comparing Symmetries in Superconductivity

The use of symmetries within phase transitions is crucial. By considering the symmetries of the gap function and Hamiltonian, much of the physics of the system can be deduced from the symmetries alone. For example, for a superconducting state, spontaneous $U(1)$

symmetry breaking is a signature of superconductivity. This is known as global symmetry breaking. Symmetry breaking can be thought of as adding an impurity to a symmetric molecule. This destroys the rotational and translational symmetry of the system.

Formally, symmetry breaking occurs when a symmetry operator acts upon the state, and the result breaks the symmetry relation given for the Hamiltonian, $\mathcal{H}$. For the example of time reversal symmetry ($\mathcal{T}$-symmetry), a time reversal invariant state is written as

$$\mathcal{T}\mathcal{H}\mathcal{T}^{-1} = \mathcal{H}, \tag{1.32}$$

therefore if the equation is not satisfied, it means $\mathcal{T}$-symmetry has been broken. This can happen both spontaneously and explicitly. In general, it is easy to break $\mathcal{T}$-symmetry by applying a magnetic field to the system, as this gives the system a change in behaviour if time were reversed. The more interesting scenario, is when a system is modelled, and the equations for the system are found, and these break $\mathcal{T}$-symmetry. This is known as spontaneous $\mathcal{T}$-symmetry breaking. A different method is to test if the operator is anti-unitary and does not commute with the Hamiltonian, then this also means the symmetry is broken. If this symmetry is broken, it could suggest topological features of the system, which as discussed have obvious benefits.

It is also important to emphasise the difference between discrete symmetries, and continuous symmetries. Discrete symmetries will be typically used throughout this thesis, and these consist of $\mathcal{T}$-symmetry, chiral symmetry, and particle hole symmetry. Whereas continuous symmetries, namely rotational, translation, and time translational belong to a different group in the context of group theory. These belong to a Lie group, whereas discrete symmetries belong to the finite group. With continuous symmetries, the fundamental Noether's theorem [58] can be used and this has been a pillar of modern physics.

The discrete symmetries can be used to classify topological superconductors and insulators by way of the Altland-Zirnbauer periodic table of topological invariants [59] which began in 1996. Before showing the periodic table, it is beneficial to introduce the chiral, and particle-hole operator. This has been developed in a formal manner in this review [60].The chiral and particle-hole operators vary from the $\mathcal{T}$ operator. The particle-hole operator $\mathcal{C}$ is anti-unitary but anti-commutes with the Hamiltonian. Physically, this means the creation and annihilation operators are symmetries of one another. Mathematically, the relation for

$\mathcal{C}$-symmetry to be conserved is

$$\mathcal{C}\mathcal{H}\mathcal{C}^{-1} = \mathcal{H}. \tag{1.33}$$

Different to the previous symmetries, the chiral operator $\mathcal{S}$ is unitary, however it does anti-commute with the Hamiltonian like the $\mathcal{C}$ operator. Physically, chirality is more complex. The interpretation is that the handedness of the particles are invariant under a transformation. If this is not true, then the chirality is broken. When considering the Hamiltonian, the chiral symmetry, $\mathcal{S}$ is given by

$$\mathcal{S}\mathcal{H}\mathcal{S}^{-1} = \mathcal{H}. \tag{1.34}$$

Chirality is defined as the product of time reversal symmetry and particle-hole symmetry such that

$$\mathcal{S} = \mathcal{T}.\mathcal{C}. \tag{1.35}$$

With this information, the periodic table of topological invariants can be introduced below.

TABLE 1.1: This is the periodic table of topological invariants. It is a useful way of classifying topological superconductors and insulators by the symmetries possessed by the Hamiltonian. The certain symmetries that the systems possess allow this classification, and thus define the nomenclature for the field. As the dimensionality changes, physically certain symmetry relations will then change accordingly.

Class	$\mathcal{T}$	$\mathcal{C}$	$\mathcal{S}$	d =0	1	2	3	4	5	6	7
A	0	0	0	$\mathbb{Z}$	0	$\mathbb{Z}$	0	$\mathbb{Z}$	0	$\mathbb{Z}$	0
AIII	0	0	1	0	$\mathbb{Z}$	0	$\mathbb{Z}$	0	$\mathbb{Z}$	0	$\mathbb{Z}$
AI	$\mathcal{T}^2 = 1$	0	0	$\mathbb{Z}$	0	0	0	$2\mathbb{Z}$	0	$\mathbb{Z}_2$	$\mathbb{Z}_2$
BDI	$\mathcal{T}^2 = 1$	$\mathcal{C}^2 = 1$	1	$\mathbb{Z}_2$	$\mathbb{Z}$	0	0	0	$2\mathbb{Z}$	0	$\mathbb{Z}_2$
D	0	$\mathcal{C}^2 = 1$	0	$\mathbb{Z}_2$	$\mathbb{Z}_2$	$\mathbb{Z}$	0	0	0	$2\mathbb{Z}$	0
D III	$\mathcal{T}^2$ = -1	$\mathcal{C}^2 = 1$	1	0	$\mathbb{Z}_2$	$\mathbb{Z}_2$	$\mathbb{Z}$	0	0	0	$2\mathbb{Z}$
A II	$\mathcal{T}^2$ = -1	0	0	$2\mathbb{Z}$	0	$\mathbb{Z}_2$	$\mathbb{Z}_2$	$\mathbb{Z}$	0	0	0
C II	$\mathcal{T}^2$ = -1	$\mathcal{C}^2$ = -1	1	0	$2\mathbb{Z}$	0	$\mathbb{Z}_2$	$\mathbb{Z}_2$	$\mathbb{Z}$	0	0
C	0	$\mathcal{C}^2$ = -1	0	0	0	$2\mathbb{Z}$	0	$\mathbb{Z}_2$	$\mathbb{Z}_2$	$\mathbb{Z}$	0
C I	$\mathcal{T}^2 = 1$	$\mathcal{C}^2$ = -1	1	0	0	0	$2\mathbb{Z}$	0	$\mathbb{Z}_2$	$\mathbb{Z}_2$	$\mathbb{Z}$

The topological invariants within the table are varieties of $\mathbb{Z}$. The invariants change for different dimensionality denoted by d. It was the $\mathbb{Z}_2$ invariant that was first introduced [47] in the first theoretical topological superconductivity paper. These invariants are entirely categorised by the Chern number [61], C. Note the Chern number, C is not the particle hole operator $\mathcal{C}$. Rigorous calculation of the Chern number will be computed in chapter 3. The $\mathbb{Z}$ invariant implies that C can take any integer value, whereas the $2\mathbb{Z}$ invariant implies that C must take any doubling of an integer value. However, the $\mathbb{Z}_2$ invariant implies that C can only be ± 1, and therefore there are only two states this type of system can exist in.

Whilst table 1.1 is useful for discrete symmetries, it does not show how continous symmetries can be used. For many superconductors, the symmetry of the gap function are used as the way to classify the material. The symmetries that are used are typically rotational, and translational. These operations are applied on the order parameter, and the type of superconductivity is deduced. It is these symmetries, that reveal whether the superconductivity is s, p, or d wave, since the symmetries of the gap function are compared to the symmetries in spherical harmonics, hence the nomenclature. The mathematical formulation for this is shown in chapter 2.

Within this chapter, the historical and mathematical formulation of conventional superconductivity have been discussed, from both a macroscopic, and a microscopic view. Additionally, some of the underlying techniques that will be used throughout this thesis, such as Luttinger liquid theory, and Ginzburg Landau theory have been introduced, for added clarity for the later chapters. A brief introduction to how topology can be classified within condensed matter systems has also been discussed, as these symmetry relations will be used in unconventional superconductivity.

The purpose of this introductory chapter has been to motivate the rest of this thesis by discussing the lack of theoretical progress in creating a theory which correctly describes the interplay between disorder and superconductivity. In addition, the benefits of topology within physics have been introduced, which again promotes the need for research in the field.

Chapter 2 focuses on the mathematical techniques that are used in identifying the symmetries within unconventional superconductivity, and how these mathematical formulations can be used when devising theories.

Chapter 2

Unconventional Superconductivity

This chapter discusses aspects of unconventional superconductivity and the varying types of superconductivity. The theory of unconventional superconductivity is based upon the symmetries of the gap function. As discussed previously, the different classes of superconductivity depend on these symmetries. For example, standard BCS superconductivity has an s-wave symmetry, and is therefore completely isotropic. The unconventionality comes from certain symmetries being broken, which in turn means that unconventional superconductors occur at a lower symmetry group since it has fewer symmetries. Currently, this has only been introduced from a qualitative perspective, however this chapter is dedicated to introducing the techniques for computing the type of superconductivity from a formal perspective. The majority of this chapter has been based on an excellent review [62].

The first evidence that the gap function may be non-isotropic was found in 1972 when it was discovered [63] that superfluidity occurs in helium-3 and this could not be explained by s-wave physics. Superfluidity is analagous to superconductivity, however the difference is since for superfluidity, the vanishing resistance is in the flow of a fluid, rather than the flow of electrons through a solid. This experiment encouraged theorists to look at the symmetries of the gap function and how they can affect the interaction. The symmetries of the gap function, and thus the different types of superconductivity are directly correlated to spherical harmonics that are associated with atomic physics. This is the reason for the nomenclature being s-wave, p-wave, d-wave, and so on.

2.1 d-vector Notation

To consider how a superconductor may be unconventional, first a generic wavefunction for a Cooper pair is defined as

$$\psi^l_{s,s'}(\mathbf{r},\mathbf{r}') = \chi_{s,s'} f_l(\mathbf{r}-\mathbf{r}'), \tag{2.1}$$

where $\chi_{s,s'}$ controls the spin part of the wavefunction and $f_l(\mathbf{r}-\mathbf{r}')$ is the translationally invariant spin independent part of the wavefunction. Equation (2.1) is decomposed to

$$\psi^l_{s,s'}(\mathbf{r},\mathbf{r}') = \chi_{s,s'} \sum_{\mathbf{k}} a_l(\mathbf{k}) e^{i\mathbf{k}.(\mathbf{r}-\mathbf{r}')}, \tag{2.2}$$

where $a_l(\mathbf{k})$ can be expanded in terms of spherical harmonics. It is this term that generates the definitions of the different types of superconductivity. Expanding this term results in

$$a_l(\mathbf{k}) = \sum_{m=-l}^{l} \Delta^l_m \mathrm{Y}_{lm}(\mathbf{k}), \tag{2.3}$$

where $\mathrm{Y}_{lm}(\mathbf{k})$ are the spherical harmonics, and l is the angular momentum, and m is the magnetic number.

Since the wavefunction must be anti-symmetric when the fermions are swapped, this implies that

$$\psi^l_{s,s'}(\mathbf{r},\mathbf{r}') = -\psi^l_{s',s}(\mathbf{r}',\mathbf{r}) = \chi_{s',s} f_l(-(\mathbf{r}-\mathbf{r}')), \tag{2.4}$$

which implies that $\chi_{s,s'} = -\chi_{s',s}$ for $f_l(\mathbf{r}-\mathbf{r}') = f_l(-(\mathbf{r}-\mathbf{r}'))$. Whereas, $\chi_{s,s'} = \chi_{s',s}$ for $f_l(-(\mathbf{r}-\mathbf{r}')) = -f_l(\mathbf{r}'-\mathbf{r})$. The two results for this show that the spin part of the wavefunction depends on the parity, which is denoted by $(-1)^l$. Thus for different values of l, the wavefunction takes a different form. For even parity, the spin part is anti symmetric, but for odd parity, the spin part is symmetric, and the orbital part is anti symmetric. Again, this is a hint as to how the superconductivity changes according to l and hence spherical harmonics. From this defintion, $l = 0$ results in an s-wave superconductor, and any $l > 0$ is the definition for an unconventional superconductor. When the orbital part of the wavefunction remains symmetric, namely for when $l = 2n$, where n is an integer, the total spin of the system takes the value $S = 1$, however when $l = 2n+1$, the system has total spin $S = 0$.

When $S = 0$, the singlet state must be defined as

$$|singlet\rangle = |\uparrow\downarrow\rangle - |\downarrow\uparrow\rangle\,, \tag{2.5}$$

which is related to the spin part of the wavefunction by

$$\chi^{singlet}_{s,s'} = \langle s|\,\langle s'|\,\big(\,|\uparrow\downarrow\rangle - |\downarrow\uparrow\rangle\,\big), \tag{2.6}$$

which when written in matrix form becomes

$$\chi^{singlet}_{s,s'} = \begin{pmatrix} \langle\uparrow\uparrow|\,\big(\,|\uparrow\downarrow\rangle - |\downarrow\uparrow\rangle\,\big) & \langle\uparrow\downarrow|\,\big(\,|\uparrow\downarrow\rangle - |\downarrow\uparrow\rangle\,\big) \\ \langle\downarrow\uparrow|\,\big(\,|\uparrow\downarrow\rangle - |\downarrow\uparrow\rangle\,\big) & \langle\downarrow\downarrow|\,\big(\,|\uparrow\downarrow\rangle - |\downarrow\uparrow\rangle\,\big) \end{pmatrix} = \begin{pmatrix} 0 & 1 \\ -1 & 0 \end{pmatrix} = i\sigma_y, \tag{2.7}$$

where σ_y is one of the Pauli matrices. From this, different values of l can be taken to get the superconducting wavefunction. Namely, for $l = 0$ the equation in momentum representation yields

$$\psi^0_{\uparrow,\downarrow}(\mathbf{k}) = i\sigma_y\Delta^0_0\mathrm{Y}_{00}(\mathbf{k}). \tag{2.8}$$

By then finding the spherical harmonics for these values for l and m, the result is

$$\psi^0_{\uparrow,\downarrow} = i\sigma_y\Delta\frac{1}{2\pi^2}, \tag{2.9}$$

which gives only a single bare order parameter Δ, and the wavefunction is independent of momentum, thus resulting in isotropy. The system becomes more interesting when taking the total spin to be $S = 1$, since there are three different combinations for the spin to occur this way. They are given by

$$|triplet\rangle = \begin{cases} |T1\rangle = |\uparrow\uparrow\rangle = |1\rangle\,, \\ |T2\rangle = |\uparrow\downarrow\rangle + |\downarrow\uparrow\rangle = |0\rangle\,, \\ |T3\rangle = |\downarrow\downarrow\rangle = |-1\rangle\,, \end{cases} \tag{2.10}$$

using this, the spin part of the wavefunction in matrix form is calculated to be

$$\chi^{\eta}_{s,s'} = \begin{cases} \chi^{1}_{\uparrow,\uparrow} = \begin{pmatrix} 1 & 0 \\ 0 & 0 \end{pmatrix}, \\ \chi^{0}_{\uparrow,\downarrow} = \begin{pmatrix} 0 & 1 \\ 1 & 0 \end{pmatrix}, \\ \chi^{-1}_{\downarrow,\downarrow} = \begin{pmatrix} 0 & 0 \\ 0 & 1 \end{pmatrix}, \end{cases} \tag{2.11}$$

where η is the projection of the spin onto the z axis and corresponds to each component of the spin triplet state. Using this definition, the wavefunction can be succinctly written as

$$\psi^{l}_{s,s'}(\mathbf{k}) = \sum_{\eta=-1}^{1} a^{\eta}_{l}(\mathbf{k})\chi^{\eta}_{s,s'}, \tag{2.12}$$

which when using the matrices above, allows the wavefunction to be written explicitly as a matrix given by

$$\hat{\psi}^{l}(\mathbf{k}) = \begin{pmatrix} \psi^{l}_{\uparrow,\uparrow}(\mathbf{k}) & \psi^{l}_{\uparrow,\downarrow}(\mathbf{k}) \\ \psi^{l}_{\uparrow,\downarrow}(\mathbf{k}) & \psi_{\downarrow,\downarrow}(\mathbf{k}) \end{pmatrix} = \begin{pmatrix} a^{1}_{l}(\mathbf{k}) & a^{0}_{l}(\mathbf{k}) \\ a^{0}_{l}(\mathbf{k}) & a^{-1}_{l}(\mathbf{k}) \end{pmatrix}. \tag{2.13}$$

Note for a gap function in the form of a matrix, due to the anti-symmetry for the odd parity the matrix must obey

$$\psi^{l}_{s,s'}(\mathbf{k}) = -\psi^{l}_{s',s}(-\mathbf{k}). \tag{2.14}$$

To see how these components are related, the time reversal operator, $\mathcal{T}$ can be applied on each component separately and equation (2.14) can be used. For the first component of the matrix, the result is

$$\mathcal{T}\psi^{l}_{\uparrow,\uparrow}(\mathbf{k})\mathcal{T}^{-1} = (\psi^{l}_{\downarrow,\downarrow}(-\mathbf{k}))^{*} = -(\psi^{l}_{\downarrow,\downarrow}(\mathbf{k}))^{*}, \tag{2.15}$$

which implies the diagonal elements of the matrix are related to each other by taking the complex conjugate and multiplying by -1. For the off-diagonal elements, application of the

$\mathcal{T}$ operator yields

$$\mathcal{T}\psi^l_{\uparrow,\downarrow}(\mathbf{k})\mathcal{T}^{-1} = -(\psi^l_{\downarrow,\uparrow}(-\mathbf{k}))^* = (\psi^l_{\downarrow,\uparrow}(\mathbf{k}))^*. \tag{2.16}$$

This implies that the off diagonal terms are equal to each other. Consequently, a new convention can be introduced to reduce the number of variables. This is known as d-vector notation, by defining

$$\begin{aligned}\hat{\psi}^l(\mathbf{k}) &= \begin{pmatrix} -d_x(\mathbf{k}) + id_y(\mathbf{k}) & d_z(\mathbf{k}) \\ d_z(\mathbf{k}) & d_x(\mathbf{k}) + id_y(\mathbf{k}) \end{pmatrix} \\ &= (d_x(\mathbf{k})\sigma_x + d_y(\mathbf{k})\sigma_y + d_z(\mathbf{k})\sigma_z)i\sigma_y = i(\mathbf{d}(\mathbf{k})\boldsymbol{\sigma})\sigma_y,\end{aligned} \tag{2.17}$$

where

$$\mathbf{d}(\mathbf{k}) = \sum_{m=-l}^{l} \Delta^l_m \mathrm{Y}_{lm}(\mathbf{k}), \tag{2.18}$$

and σ are the Pauli matrices. By using this expression, different forms of the wavefunction can be found for different order parameters depending on the choice of quantum numbers. The difference between spin singlet, and spin triplet superconductivity is emphasised by how many more order parameters there are in the spin triplet case.

2.2 Generalised BCS Theory

Generalised BCS theory is different to standard BCS theory as it has a generalised potential, so allows for more scenarios and thus has potential for more symmetries. The Hamiltonian is written as

$$\mathcal{H} = \sum_{\mathbf{k},s} \xi_{\mathbf{k}} \bar{\psi}_{\mathbf{k},s}\psi_{\mathbf{k},s} + \frac{1}{2}\sum_{\mathbf{k},\mathbf{k}'}\sum_{s,s',s_1,s'_1} V_{\mathbf{k},\mathbf{k}',s,s',s_1,s'_1}\bar{\psi}_{\mathbf{k},s}\bar{\psi}_{-\mathbf{k},s'}\psi_{\mathbf{k},s_1}\psi_{-\mathbf{k},s'_1}, \tag{2.19}$$

where the potential $V_{\mathbf{k},\mathbf{k}',s,s',s_1,s'_1}$ must obey standard fermion anti commutation laws. The interaction can then be assumed to be weak coupling up to some energy cutoff due the system being described by Fermi liquid theory. From this, a mean field Hamiltonian can be written as

$$\begin{aligned}\mathcal{H} = \sum_{\mathbf{k},s} \xi_{\mathbf{k}} \bar{\psi}_{\mathbf{k},s}\psi_{\mathbf{k},s} + \frac{1}{2}\sum_{\mathbf{k},\mathbf{k}'}\sum_{s,s',s_1,s'_1} \Big(&\bar{\Delta}_{\mathbf{k},s,s'}\psi_{-\mathbf{k},s}\psi_{\mathbf{k},s'} + \Delta_{\mathbf{k},s,s'}\bar{\psi}_{\mathbf{k},s}\bar{\psi}_{-\mathbf{k},s'} \\ &- \Delta_{\mathbf{k},s,s'}\langle\bar{\psi}_{\mathbf{k},s}\bar{\psi}_{-\mathbf{k},s'}\rangle\Big).\end{aligned} \tag{2.20}$$

From this equation, the gap functions are then defined as

$$\Delta_{\mathbf{k},s,s'} = \sum_{\mathbf{k}',s_1,s_1'} V_{\mathbf{k},\mathbf{k}',s,s',s_1,s_1'} \langle \psi_{-\mathbf{k},s_1} \psi_{\mathbf{k},s_1'} \rangle, \tag{2.21}$$

and the conjugate of this yields

$$\bar{\Delta}_{\mathbf{k},s_1,s_1'} = \sum_{\mathbf{k}',s,s'} V_{\mathbf{k}',\mathbf{k},s,s',s_1',s_1} \langle \bar{\psi}_{\mathbf{k},s} \bar{\psi}_{-\mathbf{k},s'} \rangle. \tag{2.22}$$

Since the spins can only take two values, this allows the gap function to be written as a matrix such that

$$\hat{\Delta}_{\mathbf{k}} = \begin{pmatrix} \Delta_{\mathbf{k},\uparrow,\uparrow} & \Delta_{\mathbf{k},\uparrow,\downarrow} \\ \Delta_{\mathbf{k},\downarrow,\uparrow} & \Delta_{\mathbf{k},\downarrow,\downarrow} \end{pmatrix}. \tag{2.23}$$

The direct comparisons with equation (2.13) can be seen. For example, for spin singlet pairing, for any even integer l, the gap function is

$$\hat{\Delta}_{\mathbf{k}} = i a_l(\mathbf{k}) \sigma_y, \tag{2.24}$$

similar to the Cooper pair wavefunction. Therefore, extending this for the spin triplet case, the gap function takes the form

$$\hat{\Delta}_{\mathbf{k}} = i(\mathbf{d}(\mathbf{k})\boldsymbol{\sigma})\sigma_y. \tag{2.25}$$

It is this analogy, that allows the gap function to be thought of as similar to the Cooper pair wavefunction. By considering only the gap function, this is a common method for determining the type of superconductivity within a system. It is important to note, this is a phenomenological approach, and does not give an accurate account of the microscopic features of the system. To confirm that this theory still holds true for standard BCS theory, consider equation (2.24), and choose $l = 0$. For this scenario, equation (2.9) is recovered.

2.3 Symmetries of the Gap Function

Studying the different symmetries of the gap function allows many physical properties to be deduced about the superconductivity. As previously discussed, certain symmetry breaking can lead to non trivial topological properties, and probing the gap function is a useful tool

for a theorist. The $\mathcal{T}$-symmetry operator has already been applied to a generic gap function, as that was used to derive the d-vector notation. However, there are still many other symmetry operators that can be used as devices to demystify some of the properties of the superconductivity.

Firstly, consider a variety of different symmetry operators. Time reversal symmetry, particle hole symmetry, and chiral symmetry have already been introduced, but many others exist. The next symmetry operators to be introduced are inversion, spin rotation, orbital rotation, and the $U(1)$ gauge symmetry. The inversion operator is defined as

$$\mathcal{I}\hat{\Delta}_{\mathbf{k}} = \pm\hat{\Delta}_{-\mathbf{k}}, \tag{2.26}$$

where the $+$ sign is the case for spin singlet superconductivity, and the $-$ sign is for spin triplet superconductivity. The spin rotation operator is defined by

$$\mathcal{G}\hat{\Delta}_{\mathbf{k}} = e^{-i\mathbf{S}.\boldsymbol{\phi}_R}\hat{\Delta}_{\mathbf{k}}e^{i\mathbf{S}.\boldsymbol{\phi}_R}, \tag{2.27}$$

where $\boldsymbol{\phi}_R$ is the projection of the rotation of the spin, and $\mathbf{S}$ is the total spin. When $\mathbf{S} = 0$, as is the case for spin singlet superconductivity, the spin rotation operator has no effect. For orbital rotation, the operator is given as

$$g\hat{\Delta}_{\mathbf{k}} = \hat{\Delta}_{R(g)\mathbf{k}}, \tag{2.28}$$

where $R(g)$ is a rotation matrix which rotates the momentum. The final symmetry to be introduced is $U(1)$ gauge symmetry,

$$\mathcal{U}\hat{\Delta}_{\mathbf{k}} = e^{i\phi}\hat{\Delta}_{\mathbf{k}}, \tag{2.29}$$

where ϕ is the phase of the gap function. This is an important symmetry, and will be crucial to the research that takes place in chapter 3 since it is the breaking of $\mathcal{U}(1)$ symmetry which defines superconductivity. All of these results, and the effects they have on both the spin singlet, and spin triplet state can be summarised neatly in the table shown below [62]

TABLE 2.1: This table shows how the different gap functions act under varying symmetry operators. It is important to notice how they can vary depending on whether superconductivity is spin singlet, or spin triplet.

Operator	Spin Singlet State	Spin Triplet State
Fermion Exchange	$\hat{\Delta}_{\mathbf{k}} = \hat{\Delta}_{-\mathbf{k}}$	$\hat{\Delta}_{\mathbf{k}} = -\hat{\Delta}_{-\mathbf{k}}$
$\mathcal{T}$-symmetry	$\mathcal{T}\hat{\Delta}_{\mathbf{k}} = (\hat{\Delta}_{-\mathbf{k}})^*$	$\mathcal{T}\hat{\Delta}_{\mathbf{k}} = -(\hat{\Delta}_{-\mathbf{k}})^*$
Spin Rotation	$\mathcal{G}\hat{\Delta}_{\mathbf{k}} = \hat{\Delta}_{\mathbf{k}}$	$\mathcal{G}\hat{\Delta}_{\mathbf{k}} = e^{-i\mathbf{S}.\boldsymbol{\phi}_R}\hat{\Delta}_{\mathbf{k}}e^{i\mathbf{S}.\boldsymbol{\phi}_R}$
Orbital Rotation	$g\hat{\Delta}_{\mathbf{k}} = \hat{\Delta}_{R(g)\mathbf{k}}$	$g\hat{\Delta}_{\mathbf{k}} = \hat{\Delta}_{R(g)\mathbf{k}}$
$U(1)$ Gauge Symmetry	$\mathcal{U}\hat{\Delta}_{\mathbf{k}} = e^{i\phi}\hat{\Delta}_{\mathbf{k}}$	$\mathcal{U}\hat{\Delta}_{\mathbf{k}} = e^{i\phi}\hat{\Delta}_{\mathbf{k}}$

Conventionally in the literature, the spin singlet state is denoted by $\psi_{\mathbf{k}}$, and the spin triplet state is denoted by $\mathbf{d}_{\mathbf{k}}$.

The different symmetry groups are crucial to the development of the standard model of particle physics, since it is these symmetries which predict the existence of certain particles. Whilst the application here is limited to condensed matter physics, the use of symmetries, and symmetry breaking is a key concept throughout theoretical physics.

2.3.1 Examples of Unconventional Superconductivity

It is beneficial to see how the mathematical formulation that has been previously developed can be used in practice. Knowing that the gap function represents a quasiparticle, and approximately corresponds to the Cooper pair wavefunction. To get the quasiparticle spectrum, the absolute value squared must be taken, such that

$$|\Delta_{\mathbf{k}}|^2 = \frac{1}{2}tr\left(\hat{\Delta}_{\mathbf{k}}^{\dagger}\hat{\Delta}_{\mathbf{k}}\right). \tag{2.30}$$

This equation will be used throughout this section for different types of superconductivity.

p-wave Superconductivity

The first example of superfluidity discovered, was helium-3. This has been identified as a p-wave superconductor, so the equations developed next apply to this system. For a p-wave system, the angular momentum is $l = 1$, and $m = \pm 1$ which when using equation (2.18)

gives

$$d(\mathbf{k}) = \frac{\Delta_0}{k_F}(k_x \pm ik_y)\hat{z}, \tag{2.31}$$

where k_F is the Fermi momentum, and Δ_0 is the weighting of the gap function. These parameters account for the constants. The quasiparticle spectrum is obtained as

$$|\Delta_{\mathbf{k}}|^2 = |\Delta_0|^2 \frac{k_x^2 + k_y^2}{k_F^2}. \tag{2.32}$$

From equation (2.31), it can be seen that there are gap nodes along the z direction at ± 1. This implies that the angular momentum is conserved since the nodes do not occur within the x, y directions. Due to this conservation, chirality occurs in the system. Consequently, this type of spectrum is known as chiral p-wave superconductivity. However, since there are different choices for m corresponding to a given l, the different choices for m can yield different phases for the superconductor. The phase derived above is known as the A phase [63]. This is not the only superconducting phase in helium-3. A similar type of interaction can occur, but only along one of the spin channels such that the interaction takes place for $|\uparrow\uparrow\rangle$. This is known as the A_1 phase. Importantly, since the interaction occurs in one element of the matrix, rather than for all of the spin channels in the matrix, this results in a type of superconductivity known as non-unitary. For non-unitary superconductivity, the quasiparticle spectrum is given by

$$|\Delta_{\pm\mathbf{k}}|^2 = |\mathbf{d}(\mathbf{k})|^2 \pm |\mathbf{d}^*(\mathbf{k}) \times \mathbf{d}(\mathbf{k})|. \tag{2.33}$$

This equation can be used to find the A_1 phase. By considering a solution for $l = 1$ which only couples along the $|\uparrow\uparrow\rangle$ spin channel, this implies that the first element of the gap function matrix is taken in d-vector form such that $-d_x + id_y$ corresponds to $-k_x + ik_y$, and then the spherical harmonics are found for such a system. Since the coupling is along the spin up channel, the only combination is for $l = 1$ and $m = 1$. Writing the d-vector in directional components yields

$$\mathbf{d}(\mathbf{k}) = \frac{\Delta_0}{k_F}\Big(k_x + ik_y, ik_x - k_y, 0\Big). \tag{2.34}$$

The dependence on space can be found by taking the last term in (2.33) and computing it. Noting that $k_z^2 = k_x^2 + k_y^2$, the result is approximately

$$|\mathbf{d}^*(\mathbf{k}) \times \mathbf{d}(\mathbf{k})| = \frac{\Delta_0^2}{k_F^2} k_z^2. \tag{2.35}$$

This type of superconductivity is therefore anisotropic as it depends on the sign of the momentum from equation (2.33), and thus does not have a conventional quasiparticle spectrum. There is experimental evidence [64] that this phase exists, and occurs primarily in ferromagnets, so is particularly susceptible to an applied magnetic field.

Another phase for superfluid helium, is the B phase. This occurs in all the spin channels, but each spin channel corresponds to a different coupling. This is a unique phase, in the sense that despite the unconventional superconductivity of the p-wave pairing, the quasiparticle spectrum is found to be isotropic. Therefore, the gap function matrix has the same symmetries as the constructed matrix from the wavefunction, such that

$$\hat{\Delta}_{\mathbf{k}} = \frac{\Delta_0}{k_F} \begin{pmatrix} -k_x + ik_y & k_z \\ k_z & k_x + ik_y \end{pmatrix}, \tag{2.36}$$

which implies that

$$d_v = k_v, \tag{2.37}$$

where $v = x, y, z$ from the previous notation. It can be seen the gap function is isotropic, and the quasiparticle spectrum is given by

$$|\hat{\Delta}_{\mathbf{k}}|^2 = \frac{\Delta_0^2}{k_F^2}(k_x^2 + k_y^2 + k_z^2) = \frac{\Delta_0^2}{k_F^2}|\mathbf{k}|^2 = \Delta_0^2. \tag{2.38}$$

This result shows that the quasiparticle spectrum is entirely dependent on the magnitude of the gap, and has no $\mathbf{k}$ dependence, similar to BCS. To determine the difference between this superconductivity and standard BCS, a calculation for spin susceptibility was made [65] due to the sensitivity of the spin to applied magnetic fields. This difference allows for experimental verification of which type of superconductivity occurs.

There are different phases for spin triplet superconductors, as there are many different solutions for each l, due to m. There are many more variations for which each mechanism can affect which spin channel, however only experimentally observed phases for He-3 have

been discussed. Sr_2Ru0_4 is another famous example [66], which has similar behaviour to what has been described, except the physics is specifically for superconductivity rather than the general superfluidity which has been discussed here.

d-wave Superconductivity

The most promising pairing symmetry for the majority of the high temperature superconductors is d-wave superconductivity, particularly $d_{x^2-y^2}$. This signature has been observed in a variety of materials [67, 68], primarily due to the point nodes on the diagonals. To formulate this mathematically, d-wave pairing occurs for $l = 2$ which gives a total spin, $S = 0$. Therefore equation (2.24) must be used. The quantum numbers are chosen to be $l = 2$ and $m = 2$. There are many different combinations of l and m, so this is not the only pairing mechanism for d-wave superconductivity, however it is the most commonly observed one. Using these choices of l and m, the gap function becomes

$$\mathbf{d}(\mathbf{k}) = \frac{\Delta_0}{k_f}(k_x + ik_y). \tag{2.39}$$

This can be approximately written as

$$|\Delta_{\mathbf{k}}|^2 \propto (k_x^2 - k_y^2), \tag{2.40}$$

which is where the term $d_{x^2-y^2}$ originates from.

All the pairing symmetries for higher values for l can all be derived by similar methods. Whilst it is relatively easy to suggest a pairing mechanism by adjusting the quantum numbers, and choosing which spin channel the symmetry occurs along, this is only theory. Finding experimental verification for these pairing symmetries is a difficult task and often requires many indicators before the community accepts a certain symmetry. It is this reason why there is still some debate about the type of symmetry in high temperature superconductivity.

Crystal Superconductors

Everything discussed so far about the mathematical formulation for unconventional superconductivity has required the models to be isotropic. This is required for the Cooper pairs

to be described by the angular momentum. There are materials which do not adhere to isotropy, and thus require a different mathematical description based upon point group symmetries. By using point group symmetry, and a given l, the gap function can be written in a basis of irreducible representations of the point group. There are 7 members of the crystal family for the Bravais lattice, totalling in 32 point group symmetries and 230 space groups [69]. Therefore, there are many different combinations which can be used, which can not be covered within the timeframe of this thesis.

A typical point group symmetry that occurs regularly in high temperature superconductors is tetragonal symmetry [70]. There are different types of tetragonal symmetry, but the one that corresponds to the high temperature superconductors is

$$\mathcal{R} = D_4\mathcal{I} = D_{4h}, \tag{2.41}$$

where D_4 describes the rotations for a body centred cubic Bravais lattice, and $\mathcal{I}$ describes the inversion symmetry of such a system. D_4 can be broken down into more symmetries, which are given as C_2, C_3, C_4, and C_6, which denote rotations along the $\hat{z}$ axis. Additionally, there are symmetries along the $\hat{x}$ axis denoted by U_n.

These symmetries can be used to determine the gap functions, however the mathematical grounding of this is beyond the scope of this thesis.

2.4 Microscopic Theories

This section explores the speculative theories for the microscopic mechanism of unconventional superconductivity. It is important to stress that these theories are not widely accepted within the community, though there is still mathematical foundations behind these theories.

The typical belief is that the microscopic mechanism is dominated by strong electron correlations, rather than the standard electron-phonon interaction used in BCS theory. This is where the main question lies; how do the electrons interact in such a way that forms a strong attractive interaction.

2.4.1 Spin Fluctuation Theory

Spin fluctuation theory [71] is a commonly used explanation for unconventional superconductivity due to the intuitive logic, and relative experimental success. The theory is based upon the magnetic fields that are generated by the alignment of the spins in the quasiparticle which represents the spin excitations of the electrons. This is commonly referred to as a magnon. Consequently, different types of magnetism correspond to different types of superconductivity. For example, ferromagnetic spin fluctuations typically correspond to p-wave superconductivity, whereas anti-ferromagnetic fluctuations typically correspond to d-wave.

The theory can be thought of from a phenomenological perspective where an effective interaction occurs. The interaction results in a spin susceptibility which is directly proportional to the correlation length of the spin fluctuation squared, when the system is near the magnetic instability. Intuitively, for spin fluctuations to induce superconductivity, the correlation length must be large. This results in a large spin susceptibility thus giving a magnetic instability which introduces the superconducting mechanism. This is the case for the weak coupling theory. Much like Ginzburg Landau theory, the phenomenological aspect of this approach to spin fluctuation theory allows generality, and thus is not restricted by microscopic details. This leads to an incomplete understanding of the mechanism.

Weak Coupling Theory

Firstly, spin fluctuations can lead to different forms of interactions which is the origin of weak/strong coupling theory. For weak coupling theory the interaction is due to the magnetic instability [67]. Formally, this is due to antiferromagnetic paramagnons, which is a quasiparticle that contains all the information about the spin part of the wavefunction. Once these quasiparticles are found, a weak coupling is introduced which occurs through a slight magnetic field. By finding the spin susceptibility it can be shown that the interaction between these antiferromagnetic paramagnons enable a superconducting state to occur.

Strong Coupling Theory

Unlike weak coupling theory, strong coupling theory is not dependent on the magnetic instabilities. The attraction between the quasiparticles is a result of scattering of the quasiparticles in certain channels [71]. Additionally, the depairing effects are accounted for due to

the scattering. To compute this, Green's functions and the self energy are calculated, and the quasiparticle spectrum is revealed. From this, superconducting properties can be deduced.

Both the weak and strong coupling theory are determined as a result of spin fluctuations, but there is no accepted consistent theory which unites these two theories. At the time of writing, FLEX theory [72] may provide a consistent theory.

FLEX (Fluctuation Exchange) Approximation

In order to describe this microscopic theory for spin fluctuations, the main theory that is used is the FLEX approximation [73]. The FLEX approximation is based upon a pertubation theory expansion where the result is taken at one loop level, and then the spin fluctuation is renormalised. The theory takes the dressed one particle Green's function, which contains the renormalised mass and energy, and then uses it to calculate the spin susceptibility. From this, the region where spin fluctuations dominate is known, and therefore in weak coupling, the magnetic instability reveals the superconducting coupling, whereas in strong coupling, the theory shows the important scattering effects.

It should be clear, that FLEX is a mathematical tool for deriving the physics for spin fluctuation exchange, and it is not a complete theory.

Whilst the theory of spin fluctuation induced superconductivity has only been introduced from a philosophical viewpoint, such that the motivation behind the theory can be explained, to understand it fully a mathematically rigorous technique has to be introduced. For the purposes of this thesis, the mathematical formulation will not be derived, however this is done here [74, 75].

2.4.2 Interlayer Coupling [76] and Resonance Valence Bond Theory [77]

These two theories are linked since Anderson derived both of them in the same year, and then used Resonance Valence Bond theory to explain interlayer coupling. Interlayer coupling is not exclusively performed this way and can be a weak coupling theory, whereas Resonance Valence Bond theory is a strong coupling theory.

Interlayer Coupling

Interlayer coupling is a theory [76] that states there is an increased coupling in the particle-particle channel between layers, when the layer is sufficiently small. Consequently, this tunnelling allows for superconductivity to emerge, thus stabilising the superconductor, and allows the system to reach a higher critical temperature. The coupling between the layers essentially acts as a method for Josephson tunnelling. Therefore it is natural to assume that interlayer coupling would help the superconducting state.

The contribution of this extra tunnelling manifests itself as a correction to the self energy, thus the interlayer coupling can be thought of as another avenue which allows a superconducting current to flow. Additionally, the intralayer effects can change how the interlayer coupling affects the superconductivity, so this also needs to be considered when constructing the model.

Whilst this theory has some theoretical and experimental success, it does not have the same support within the community as spin fluctuation theory.

Resonance Valence Bond Theory

Anderson [77] first proposed Resonance Valence Bond (RVB) theory in 1987, only a year after the discovery of high temperature superconductivity by Bednorz and Müller. RVB is a strongly correlated theory based on Cooper pairs having a singlet state which is bound, but when the system is doped these spin singlet states are attracted to each other forming a superconducting state. This is an example of how disorder can form a superconducting state, however introducing further disorder does not raise the critical temperature.

The underlying theory behind the model relies on Mott insulators [78], as the phase transition is claimed to be a Mott insulator-superconductor transition. Accepting that the theory is based upon a Mott insulator immediately implies this theory is strongly correlated, and that Fermi liquid theory is not relevant for RVB theory. The doping is crucial to the underlying mechanism, as the doping creates an electron hole pair, which in turn results in an attraction between the Cooper pairs.

From a technical perspective, the system is derived from the t-J model [79], which is a logical step as the model describes strongly correlated systems. Since this model has a familiar form of the Hamiltonian, known techniques can be used to find the valence bond

wavefunction. The RVB analysis can then be extended to a mean field level, which allows a solution for the gap function to be found, which yields the type of superconductivity.

This theory is not as popular as spin fluctuation theory. It does suggest that high temperature superconductivity could be linked to strongly correlated systems, in a similar way that spin fluctuation theory does. Whilst these theories are fundamentally different, the underlying importance of spin is common.

All the theories discussed are not widely accepted within the whole community, either experimentally or theoretically. The reason they have been introduced is to extend what possible mechanisms could explain the underlying microscopic physics of unconventional superconductivity.

The purpose of this chapter was to introduce the different theories of unconventional superconductivity, both from a macroscopic and microscopic perspective. Within both of these areas, only the essential features have been covered. For example, within macroscopic unconventional superconductivity if the system can not be described by the quantum number l, point group symmetries have to be used. The microscopic part has been intentionally introduced at a peripheral level, since there is no widely agreed consensus within the community. However, it is still informative to gain an understanding into what research is being performed in the field.

The next chapter begins the research section of this thesis, and will focus on topological superconductivity.

Chapter 3

Topological Superconductors

This chapter provides an analytical framework extending the model in the paper by Karnaukhov [1] which shows that non-trivial topology occurs spontaneously in a superconductor. The mathematical derivation is similar to the one introduced for BCS theory, and it will be written in terms of Green's functions, for which a brief introduction will be given. Once the gap function is derived, the Chern number will be formally introduced and used to calculate the topology of the system. If the Chern number is found to be non-zero then the system is said to have a non-trivial topology.

The claim of the Karnaukhov paper is that non-trivial topology arises spontaneously in a superconductor, with no external perturbation. However, all the results in that paper are based on numerical simulations. Within this thesis, the derivation of the ground state, and subsequently the derivation of the gap function have been performed analytically using justifiable assumptions. From this, the energy states are derived, and the minimum solution for the system is found. The minimum energy is the favourable energy state. Since the gap function is found using a saddle-point approach, the second equation in this approach imposes an extra condition which means the solution for the gap function is dependent on the phase of the gap function. This phase can take two values, and the value which minimises the ground state energy is the favourable solution. From this favourable solution, the topology of the system can be deduced.

An assumption by Karnaukhov was the gap function was homogenous, thus implying the system was momentum ($\mathbf{q}$) independent. The assumption was due to the system exhibiting translational invariance. After performing the analytical results for $\mathbf{q} = 0$, this assumption will be checked. The method for this is by finding the solutions for the first superconducting instability which occurs at the lowest energy eigenvalue. At that point,

the value of $\mathbf{q}$ will determine the $\mathbf{q}$ dependence for the first superconducting Cooper pair. This is done for varying values of chemical potential. If $\mathbf{q} \neq 0$ for the first superconducting instability, this implies the assumptions are not justified. Moreover, if it is shown that homogeneity in translational invariant systems can not necessarily be assumed, this could shape the way in which future research is conducted.

3.1 Model

The model is a 2D spinless square lattice with attraction between the sites. It is not assumed that the attractions in the x and y direction are the same, therefore homogeneity is not assumed. The model can be shown graphically in figure 3.1.

Spinless square lattice with attraction between the sites

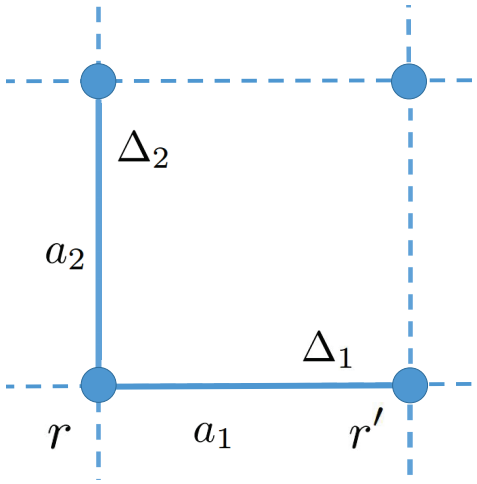

FIGURE 3.1: The diagram shows how each direction yields a different coupling. The distance between the sites is the same but the coupling and translation vectors are not, hence the difference in labelling.

From this model, a generic Hamiltonian for the system can be written, the gap function can be found and any assumptions about the model can be imposed on the gap function. This will be explained in detail in the next section.

3.1.1 Derivation of Gap Function

A generic Hamiltonian can be written as

$$\hat{\mathcal{H}} = \sum_{\mathbf{r}\mathbf{r}'} \Big(\hat{\psi}^\dagger_{\mathbf{r}} \xi_{\mathbf{r}\mathbf{r}'} \hat{\psi}_{\mathbf{r}'} - J_{\mathbf{r}\mathbf{r}'} \hat{\psi}^\dagger_{\mathbf{r}} \hat{\psi}^\dagger_{\mathbf{r}'} \hat{\psi}_{\mathbf{r}'} \hat{\psi}_{\mathbf{r}} \Big), \tag{3.1}$$

where the sum over $\mathbf{r}, \mathbf{r}'$ is over all the lattice sites. At this stage, the Hamiltonian does not yet have the full restrictions of the model above. These restrictions are imposed using the gap function. Equation (3.1) can be used to write the action in terms of fermionic fields, where imaginary time is used such that

$$S = \sum_{\mathbf{r}\mathbf{r}'} \Big(\sum_{\tau} \bar{\psi}_{\mathbf{r}} (\partial_\tau + \xi_{\mathbf{r},\mathbf{r}'}) \psi_{\mathbf{r}'} - J_{\mathbf{r}\mathbf{r}'} \bar{\psi}_{\mathbf{r}} \bar{\psi}_{\mathbf{r}'} \psi_{\mathbf{r}'} \psi_{\mathbf{r}} \Big). \tag{3.2}$$

In a similar way to what has been done previously, to introduce the gap function, a Hubbard Stratonovich transformation is chosen such that the gap field decouples the quartic interaction term. Therefore the action becomes

$$S = \sum_{\mathbf{r}\mathbf{r}'} \left(\frac{|\Delta_{\mathbf{r}\mathbf{r}'}|^2}{4J_{\mathbf{r}\mathbf{r}'}} + \sum_{\tau} \bar{\psi}_{\mathbf{r}} (\partial_\tau + \xi_{\mathbf{r},\mathbf{r}'}) \psi_{\mathbf{r}'} + \frac{1}{2} (\Delta_{\mathbf{r}\mathbf{r}'} \bar{\psi}_{\mathbf{r}} \bar{\psi}_{\mathbf{r}'} + \bar{\Delta}_{\mathbf{r}\mathbf{r}'} \psi_{\mathbf{r}'} \psi_{\mathbf{r}}) \right). \tag{3.3}$$

Using the property that the gap field is anti-symmetric due to the parity and the bosonic statistics it possesses, allows the action to be written as

$$S = \sum_{\mathbf{r}\mathbf{r}'} \frac{|\Delta_{\mathbf{r}\mathbf{r}'}|^2}{4J_{\mathbf{r}\mathbf{r}'}} + \sum_{\tau} \psi^\dagger (\partial_\tau + \hat{\xi}) \psi + \frac{1}{2} (\psi^\dagger \hat{\Delta} \bar{\psi} + \psi^T \hat{\Delta}^\dagger \psi). \tag{3.4}$$

Before writing the action in a full matrix form as before, the Fermi fields can be written in Nambu notation. To do this, the non interacting part of the Hamiltonian must use the relation that

$$\psi^\dagger (\partial_\tau + \hat{\xi}) \psi = -\psi^T (\partial_\tau + \hat{\xi})^T \bar{\psi}. \tag{3.5}$$

Another important relation to note, is that $\partial_\tau^T = -\partial_\tau$ which occurs because the conjugate of imaginary time produces a minus sign. Defining the Nambu vectors as $\mathbf{\Psi}^\dagger = (\psi^\dagger, \psi^T)$, the action becomes

$$S = \sum_{\mathbf{r}\mathbf{r}'} \frac{|\Delta_{\mathbf{r}\mathbf{r}'}|^2}{4J_{\mathbf{r}\mathbf{r}'}} + \frac{1}{2} \sum_{\tau} \mathbf{\Psi}^\dagger \begin{pmatrix} \partial_\tau + \hat{\xi} & \hat{\Delta} \\ \hat{\Delta}^\dagger & \partial_\tau - \hat{\xi}^T \end{pmatrix} \mathbf{\Psi}. \tag{3.6}$$

This can now be written in terms of Green's functions. To do this, the motive for using Green's functions will now be introduced.

Green's functions are formal solutions to differential equations, and the link between them and the correlation function has been exploited over the past 60 years. They are particularly useful when considering many-body physics. There are many different types of Green's functions, namely greater, lesser, imaginary, advanced, and retarded [17]. These are related to the direction of time, and the physical space that they occupy. For the rest of this chapter, imaginary time Green's functions will be used, since they contain all of the thermal information within the system. Importantly, imaginary time Green's functions are valid for τ going from $0 \rightarrow \beta$. To understand the origin of Green's functions, consider

$$\mathcal{L}(\mathbf{r})G(\mathbf{r},\mathbf{r}') = \delta(\mathbf{r}-\mathbf{r}'), \tag{3.7}$$

where $\mathcal{L}(\mathbf{r})$ is the Lagrangian, and $G(\mathbf{r},\mathbf{r}')$ is the Green's function. Using this, and noting the Schrödinger equation, an analagous equation can be written as

$$(\partial_\tau + \mathcal{H})G(\mathbf{r},\mathbf{r}';\tau,\tau') = \delta(\mathbf{r}-\mathbf{r}')\delta(\tau-\tau'), \tag{3.8}$$

where the equation has been written in imaginary time. By then taking a Fourier transform such that the Green's function is in momentum and frequency space, this yields

$$G(\mathbf{k},\epsilon) = \frac{1}{-i\epsilon + E_{\mathbf{k}}}, \tag{3.9}$$

which for a non interacting system gives

$$G(\mathbf{k},\epsilon) = \frac{1}{-i\epsilon + \xi_{\mathbf{k}}}. \tag{3.10}$$

This is known as the non interacting Green's function. To transform the Green's function to position and imaginary time, take the inverse Fourier transform and assume translational invariance to get

$$G(\mathbf{r},\mathbf{r}';\tau,\tau') = \frac{1}{\beta}\sum_{\epsilon}\int d\mathbf{k}G(\mathbf{k},\epsilon)e^{i(\mathbf{r}-\mathbf{r}').\mathbf{k}-i(\tau-\tau')\epsilon}. \tag{3.11}$$

Green's functions are directly related to correlation functions, which yields

$$G(\mathbf{r},\mathbf{r}';\tau,\tau') = \langle \psi^\dagger(\mathbf{r}',\tau')\psi(\mathbf{r},\tau)\rangle. \tag{3.12}$$

where $\langle \dots \rangle = (1/Z)\,\mathrm{Tr}(\dots)$ is the thermal average of the system and is known as the correlation function. The operators inside the brackets are normal ordered. Since this is the thermal average, this result is known as the thermal Green's function. The information contained within this can be used to solve a range of problems. The non-interacting Green's function can be used to find solutions for interacting systems. This is done by defining a Green's function for a system of many particles such that

$$G^n(\mathbf{r}_1,\tau_1\dots\mathbf{r}_n,\tau_n;\mathbf{r}_1',\tau_1'\dots\mathbf{r}_n',\tau_n') = \langle \psi^\dagger(\mathbf{r}_1',\tau_1')\dots\psi^\dagger(\mathbf{r}_n',\tau_n')\psi(\mathbf{r}_n,\tau_n)\dots\psi(\mathbf{r}_1,\tau_1)\rangle, \tag{3.13}$$

To write this in a form of non-interacting Green's functions consider

$$G(\mathbf{r},\tau,\mathbf{r}_1,\tau_1;\mathbf{r}',\tau',\mathbf{r}_1'\tau_1') = \langle \psi^\dagger(\mathbf{r}_1',\tau_1')\psi^\dagger(\mathbf{r}',\tau')\psi(\mathbf{r},\tau)\psi(\mathbf{r}_1,\tau_1)\rangle, \tag{3.14}$$

which can be rewritten using Wick's theorem [17] as

$$\begin{aligned} G(\mathbf{r},\tau,\mathbf{r}_1,\tau_1;\mathbf{r}',\tau',\mathbf{r}_1'\tau_1') = {} & \langle \psi^\dagger(\mathbf{r}',\tau')\psi(\mathbf{r},\tau)\rangle\langle \psi^\dagger(\mathbf{r}_1',\tau_1')\psi(\mathbf{r}_1,\tau_1)\rangle \\ & -\langle \psi^\dagger(\mathbf{r}_1',\tau_1')\psi(\mathbf{r},\tau)\rangle\langle \psi^\dagger(\mathbf{r}',\tau')\psi(\mathbf{r}_1,\tau_1)\rangle. \end{aligned} \tag{3.15}$$

Consequently, it can be seen that this many particle Green's function has been reduced to four non-interacting Green's functions, which have already been calculated. It is useful to know that once one type of Green function has been calculated, the other types can be derived using known techniques.

Using this understanding, equation (3.6) can be written in terms of Green's functions such that

$$S = \sum_{\mathbf{r}\mathbf{r}'} \frac{|\Delta_{\mathbf{r}\mathbf{r}'}|^2}{4J_{\mathbf{r}\mathbf{r}'}} + \frac{1}{2}\sum_\tau \mathbf{\Psi}^\dagger \hat{G}^{-1}\mathbf{\Psi}, \tag{3.16}$$

where

$$\hat{G}^{-1} = \begin{pmatrix} \partial_\tau + \hat{\xi} & \hat{\Delta} \\ \hat{\Delta}^\dagger & -(\partial_\tau + \hat{\xi})^T. \end{pmatrix} = \hat{G}_0^{-1} + \hat{\mathbf{\Delta}}. \tag{3.17}$$

This inverse is due to $\hat{G}_0^{-1}$ being the non interacting inverse Green function, and consequently $\hat{G}_0$ is defined as

$$\hat{G}_0 = \begin{pmatrix} \hat{g} & 0 \\ 0 & -\hat{g}^T \end{pmatrix}, \tag{3.18}$$

where $\hat{g} = (\partial_\tau + \hat{\xi})^{-1}$. The gap field matrix is

$$\hat{\mathbf{\Delta}} = \begin{pmatrix} 0 & \hat{\Delta} \\ \hat{\Delta}^\dagger & 0 \end{pmatrix}, \tag{3.19}$$

with $\hat{\Delta} = -\hat{\Delta}^T$. Therefore, as previously derived, the Fermi fields can be integrated out to give

$$S = \sum_{\mathbf{r}\mathbf{r}'} \frac{|\Delta_{\mathbf{r}\mathbf{r}'}|^2}{4J_{\mathbf{r}\mathbf{r}'}} - \frac{1}{2}\operatorname{Tr}\ln\hat{G}^{-1}. \tag{3.20}$$

Now the structure of the gap fields must be understood. Since the system is translationally invariant and modelled on sites and links between these sites, it is convenient to reparameterise $\mathbf{r}$ and $\mathbf{r}'$. This allows for a choice to be made such that

$$\Delta_{\mathbf{r}\mathbf{r}'} = \Delta_{\mathbf{r}-\mathbf{r}'}\Big(\frac{\mathbf{r}+\mathbf{r}'}{2}\Big) = \Delta_{\mathbf{l}}(\mathbf{R}), \tag{3.21}$$

where $\mathbf{r} = \mathbf{R} + \mathbf{l}/2$ and $\mathbf{r}' = \mathbf{R} - \mathbf{l}/2$. The $\mathbf{R}$ can be thought of as the centre of mass of the Cooper pair, and $\mathbf{l}$ is the link between each site. With this new parameterisation, $\mathbf{R}$ only has relevance if the system is inhomogenous, however $\mathbf{l}$ will have relevance as the links between sites can be different even if the system is translationally invariant. These gap field equations can be extended to momentum representation which yields

$$\Delta_{\mathbf{k}\mathbf{k}'} = \Delta_{\mathbf{k}-\mathbf{k}'}\Big(\frac{\mathbf{k}+\mathbf{k}'}{2}\Big) = \Delta_{\boldsymbol{\kappa}}(\mathbf{q}), \tag{3.22}$$

where $\mathbf{k} = \mathbf{q} + \boldsymbol{\kappa}/2$ and $\mathbf{k} = \mathbf{q} - \boldsymbol{\kappa}/2$. Rewriting equation (3.22) as

$$\Delta_{\boldsymbol{\kappa}}(\mathbf{q}) = \sum_{\mathbf{l}} \Delta_{\mathbf{l}}(\mathbf{q}) e^{i\phi(\boldsymbol{\kappa}.\mathbf{l})}, \tag{3.23}$$

allows a further simplification. This simplification yields

$$\Delta_{\boldsymbol{\kappa}}(\mathbf{q}) = -i\sum_{\mathbf{l}} \Delta_{\mathbf{l}}(\mathbf{q}) \sin(\boldsymbol{\kappa}.\mathbf{l}), \tag{3.24}$$

since the gap field is anti-symmetric due to parity. This is as a result of the bosonic statistics the gap field possesses. Therefore this solution respects the anti-symmetry required. Thus in an homogenous situation, the gap field becomes

$$\Delta_{\mathbf{k}} = -i\sum_{\mathbf{l}} \Delta_{\mathbf{l}} \sin(\mathbf{k}.\mathbf{l}). \tag{3.25}$$

In the paper [1] which inspired this research, there was an ansatz that $\Delta_{\mathbf{k}} = |\Delta| e^{i\phi_{\mathbf{k}}}$ which was justified by a translational gap field. However this assumption will be checked in section 3.3. Consequently, the structure of the gap function must be investigated. This is calculated by performing a Ginzburg-Landau analysis on the gap function in the action such that

$$S = \sum_{\mathbf{Rl}} \frac{|\Delta_{\mathbf{l}}(\mathbf{R})|^2}{4J_{\mathbf{l}}} + \frac{1}{4} Tr\big(\hat{G}_0 \hat{\mathbf{\Delta}}\big)^2 + \frac{1}{8} Tr\big(\hat{G}_0 \hat{\mathbf{\Delta}}\big)^4, \tag{3.26}$$

which can be reduced to

$$S = \sum_{\mathbf{Rl}} \frac{|\Delta_{\mathbf{l}}(\mathbf{R})|^2}{4J_{\mathbf{l}}} - \frac{1}{2} tr\big(\hat{\Delta}^\dagger \hat{g} \hat{\Delta} \hat{g}^T\big) + \frac{1}{4} tr\big(\hat{\Delta}^\dagger \hat{g} \hat{\Delta} \hat{g}^T\big)^2. \tag{3.27}$$

At this stage, time independence is imposed upon the system and the action is reduced to the free energy since $S = \beta F$. This allows the quadratic part of the free energy to be written as

$$F_2 = \sum_{\mathbf{ql}} \frac{|\Delta_{\mathbf{l}}(\mathbf{q})|^2}{4J_{\mathbf{l}}} - \frac{1}{2} \sum_{\epsilon \mathbf{qk}} g^{\epsilon}_{\mathbf{k}+\mathbf{q}/2} g^{-\epsilon}_{-\mathbf{k}+\mathbf{q}/2} |\Delta_{\mathbf{k}}(\mathbf{q})|^2. \tag{3.28}$$

Using the definition for $\Delta_{\mathbf{k}} = -i\sum_{\mathbf{l}} \Delta_{\mathbf{l}} \sin(\mathbf{k}.\mathbf{l})$, gives the quadratic free energy taking the form

$$F_2 = \sum_{\mathbf{qll'}} \frac{|\Delta_{\mathbf{l}}(\mathbf{q})|^2}{4J_{\mathbf{l}}} - \frac{1}{2} \bar{\Delta}_{\mathbf{l}}(\mathbf{q}) \Pi_{\mathbf{ll'}}(\mathbf{q}) \Delta_{\mathbf{l'}}(\mathbf{q}), \tag{3.29}$$

where

$$\Pi_{\mathbf{ll'}}(\mathbf{q}) = \sum_{\epsilon \mathbf{k}} g^{\epsilon}_{\mathbf{k}+\mathbf{q}/2} g^{-\epsilon}_{-\mathbf{k}+\mathbf{q}/2} \sin(\mathbf{k}.\mathbf{l}) \sin\big(\mathbf{k}.\mathbf{l}'\big), \tag{3.30}$$

and is the kernel that dictates the superconducting instability. Since the system that is being considered is a square lattice, it is believed to be homogenous which implies that $\mathbf{q} = 0$. Therefore, this new quadratic free energy becomes

$$F_2 = \sum_{\mathbf{ll'}} \frac{|\Delta_{\mathbf{l}}|^2}{4J_{\mathbf{l}}} - \frac{1}{2} \bar{\Delta}_{\mathbf{l}} \Pi_{\mathbf{ll'}} \Delta_{\mathbf{l'}}, \tag{3.31}$$

with

$$\Pi_{\mathbf{l}\mathbf{l}'} = \sum_{\epsilon\mathbf{k}} g^{\epsilon}_{\mathbf{k}} g^{-\epsilon}_{-\mathbf{k}} \sin(\mathbf{k}.\mathbf{l}) \sin(\mathbf{k}.\mathbf{l}'). \tag{3.32}$$

Since the solution for $\Delta_{\mathbf{l}}$ is still not known, the fourth order term in the free energy needs to be considered. The quartic term of the free energy can be written as

$$F_4 = \frac{1}{4} \sum_{\epsilon\mathbf{k}} \left(g^{\epsilon}_{\mathbf{k}} g^{-\epsilon}_{-\mathbf{k}}\right)^2 |\Delta_{\mathbf{k}}|^4 = \sum_{\mathbf{k}} h_{\mathbf{k}} |\Delta_{\mathbf{k}}|^4, \tag{3.33}$$

where $h_{\mathbf{k}} = \frac{1}{4} \sum_{\epsilon} \left(g^{\epsilon}_{\mathbf{k}} g^{-\epsilon}_{-\mathbf{k}}\right)^2$. This can be written as

$$F_4 = \sum_{\mathbf{k}\mathbf{l}\mathbf{l}'} h_{\mathbf{k}} \left[\left(\Delta_{\mathbf{l}} s_{\mathbf{k}\mathbf{l}} + \Delta_{\mathbf{l}'} s_{\mathbf{k}\mathbf{l}'}\right) \left(\bar{\Delta}_{\mathbf{l}} s_{\mathbf{k}\mathbf{l}} + \bar{\Delta}_{\mathbf{l}'} s_{\mathbf{k}\mathbf{l}'}\right) \right]^2, \tag{3.34}$$

where $s_{\mathbf{k}\mathbf{l}} = \sin(\mathbf{k}.\mathbf{l}) \equiv s_1$, and $s_{\mathbf{k}\mathbf{l}'} = \sin(\mathbf{k}.\mathbf{l}') \equiv s_2$, $\Delta_{\mathbf{l}} \equiv \Delta_1$, and $\Delta_{\mathbf{l}'} \equiv \Delta_2$. This can be expanded to give

$$F_4 = \sum_{\mathbf{k}\eta} h_{\mathbf{k}} \left[|\Delta_1|^4 s_1^4 + |\Delta_2|^4 s_2^4 + 2|\Delta_1|^2 |\Delta_2|^2 s_1^2 s_2^2 + s_1^2 s_2^2 (\Delta_1 \bar{\Delta}_2 + \bar{\Delta}_1 \Delta_2)^2 \right], \tag{3.35}$$

where $\eta = 1, 2$. Terms with odd sin terms are neglected due to their anti-symmetry, in addition to terms which only contain momentum that does not correspond the field, namely $\Delta_1 s_2$ since they are weakly coupled so are negligible. Therefore the quartic free energy can be further simplified to

$$F_4 = \sum_{\mathbf{k}\eta} h_{\mathbf{k}} \Big[b(|\Delta_1|^4 + |\Delta_2|^4) + c\left[2|\Delta_1|^2 |\Delta_2|^2 + (\Delta_1 \bar{\Delta}_2 + \bar{\Delta}_1 \Delta_2)^2\right] \Big], \tag{3.36}$$

where $b = s_1^4 + s_2^4$ and $c = s_1^2 s_2^2$. The quartic free energy can now be minimised such that

$$\frac{\partial F_4}{\partial |\Delta_1|} = 4b|\Delta_1|^3 + 4c|\Delta_1||\Delta_2|^2 = 0, \tag{3.37}$$

which admits solutions $|\Delta_1| = -|\Delta_2|$ at $\phi = \pm\pi/2$. The solution for ϕ comes from a dot product within the argument of s_1 and s_2 which allows $b = c$, and therefore allows this choice for the minimisation of the function. Since it has been shown that the solution to the gap function depends on the modulus and an angle, it justifies the ansatz that $\Delta_{\mathbf{k}} = |\Delta| e^{i\phi_{\mathbf{k}}}$. Interestingly, the relation for the gap function shows a solution $\Delta_1 \pm i\Delta_2$ suggesting $p_x \pm ip_y$ superconductivity, which has been introduced previously as p-wave superconductivity.

To determine how the topology occurs, the symmetries of the gap function can be studied. Since the gap function ansatz is $\Delta_{\mathbf{k}} = |\Delta| e^{i\phi_{\mathbf{k}}}$, the symmetry relations can be found. When these are computed it is found that the non-trivial topological state is spontaneously broken due to $\mathcal{T}$-symmetry, when the solution for $\phi = \pm\pi/2$, whereas, the symmetry is preserved for $\phi = n\pi$, where n is an integer.

3.2 Derivation of the Ground State For Zero Net Momentum

The ground state for a zero net momentum ($\mathbf{q} = 0$) Cooper pair will now be derived. Imposing translational invariance on equation (3.6) and therefore changing to momentum representation gives

$$S = N \sum_{\mathbf{l}} \frac{|\Delta_{\mathbf{l}}|^2}{4J_{\mathbf{l}}} + \frac{1}{2} \sum_{\mathbf{k},\tau} \Psi^{\dagger}_{\mathbf{k}} \begin{pmatrix} \partial_\tau + \xi_{\mathbf{k}} & \boldsymbol{\Delta}_{\mathbf{k}} \\ \bar{\Delta}_{\mathbf{k}} & \partial_\tau - \xi_{-\mathbf{k}} \end{pmatrix} \Psi_{\mathbf{k}}. \tag{3.38}$$

Integrating out the fermions as was done in the general case, allows a solution to be written as

$$S = N\beta \sum_{\Gamma} \frac{|\Delta_\Gamma|^2}{4J_\Gamma} - \frac{1}{2} \sum_{k,\tau} \mathrm{tr} \ln \left[(-i\epsilon)^2 - E^2_{\mathbf{k}} \right], \tag{3.39}$$

where $E_{\mathbf{k}} = \sqrt{\xi^2_{\mathbf{k}} + |\Delta_{\mathbf{k}}|^2}$. Transforming to Matsubara frequencies to perform a complex integral results in

$$S = N\beta \sum_{\Gamma} \frac{|\Delta_\Gamma|^2}{4J_\Gamma} - \frac{1}{2} \sum_{k} \mathrm{tr} \ln \left[\cosh\left(\frac{\beta E_{\mathbf{k}}}{2} \right) \right]. \tag{3.40}$$

From this, the difference between the interacting action, and the non-interacting action can be found such that

$$\delta S = S - S(\Delta_\Gamma = 0) = N\beta \sum_{\Gamma} \frac{|\Delta_\Gamma|^2}{4J_\Gamma} - \sum_{\mathbf{k}} \ln \left[\left(\frac{\cosh\left(\frac{\beta E_{\mathbf{k}}}{2} \right)}{\cosh\left(\frac{\beta \xi_{\mathbf{k}}}{2} \right)} \right) \right]. \tag{3.41}$$

In an attempt to find the lowest ground state, the limit as $T \to 0$ or $\beta \to \infty$ is taken, which results in $\cosh(\beta E_{\mathbf{k}}/2) \to (1/2)\exp((\beta E_{\mathbf{k}})/2)$. This result implies

$$2\delta F(T = 0) = \frac{|\Delta|^2}{J} - \int d\mathbf{k} (E_{\mathbf{k}} - \xi_{\mathbf{k}}). \tag{3.42}$$

To find the ground state energy, a saddle point approximation needs to be used such that the minimum of the energy is found with respect to the gap function and the angle. These give the gap equations. Before finding these equations, recall the definition that $\xi_{\mathbf{k}} = -t/2[\cos(k_x) + \cos(k_y)] - \mu$, where the $1/2$ is applied to stop overcounting of sites and μ is the chemical potential. Throughout this derivation t will be normalised to 1. Additionally, using the assumption that $\Delta_{k_x,k_y} = |\Delta|e^{i\phi}$, where $\phi \equiv \phi_{\mathbf{k}} = \phi_{k_x} - \phi_{k_y}$. The gap function can be written as $|\Delta_{\mathbf{k}}|^2 = |\Delta|^2 g_{\mathbf{k}}(\phi)$ where $g_{\mathbf{k}}(\phi) = \sin^2(k_x) + \sin^2(k_y) + 2\cos(\phi)\sin(k_x)\sin(k_y)$. Consequently, these gap equations are found by

$$\frac{\partial \delta F(|\Delta|, \phi)}{\partial \alpha} = 0, \tag{3.43}$$

where $\alpha = |\Delta|^2, \phi$. These equations are found as

$$\frac{\partial \delta F(|\Delta|, \phi)}{\partial |\Delta|^2} = \frac{1}{J} - \frac{\partial E(|\Delta, \phi|)}{\partial |\Delta|^2} = 0, \tag{3.44}$$

which implies

$$\frac{\partial E(|\Delta, \phi|)}{\partial |\Delta|^2} = \frac{1}{J}. \tag{3.45}$$

The other gap equation is

$$\frac{\partial \delta F(|\Delta|, \phi)}{\partial \phi} = \frac{\partial E(|\Delta|, \phi)}{\partial \phi} = 0, \tag{3.46}$$

which can be further analysed to

$$\frac{\partial E(|\Delta|, \phi)}{\partial \phi} = -\frac{1}{2}\int d\mathbf{k} \frac{\sin(\phi)\sin(k_x)\sin(k_y)|\Delta|^2}{\sqrt{\xi_{\mathbf{k}}^2 + |\Delta|^2\big(\sin^2(k_x) + \sin^2(k_y) + 2\cos(\phi)\sin(k_x)\sin(k_y)\big)}} = 0. \tag{3.47}$$

This has trivial solutions for $\phi = n\pi$. If $\phi = \pm\pi/2$, then this yields a new solution for the integrand. When this integral is computed, the result is zero, subsequently resulting in $\phi = \pm\pi/2$ also being solutions to the gap equation. The non-triviality of the $\phi = \pm\pi/2$ solutions is due to the fact that these solutions break $\mathcal{T}$-symmetry. Since solutions have been found for one of the gap equations, it is then important to analyse the other gap equation such that the minimum energy can be found. Therefore equation (3.45) can be written as

$$\frac{1}{J} = \int d\mathbf{k} \frac{g_{\mathbf{k}}(\phi)}{\sqrt{\xi_{\mathbf{k}}^2 + |\Delta|^2 g_{\mathbf{k}}(\phi)}}, \tag{3.48}$$

where the $1/2$ has been cancelled since the sum over the links gives 2. To find the ground state energy for the system, the solution for energy must be found when the gap function is evaluated at $1/J$ such that $E(\Delta = \Delta(g)) \equiv E(g)$, where $g \equiv 1/J = E'(|\Delta|^2)$. The prime in this case represents the derivative with respect to $|\Delta|^2$. To calculate the minimum energy at $\Delta = \Delta(g)$, the energy must be minimised with respect to g such that

$$\frac{dE(g)}{dg} = \frac{dE(|\Delta|^2)}{d(|\Delta|^2)}\bigg|_{|\Delta|=|\Delta(g)|} \frac{d|\Delta(g)|^2}{dg} = g\frac{d|\Delta(g)|^2}{dg}. \tag{3.49}$$

From this, $E(g)$ can be found to give

$$E(g) = -\int_g^\infty dg' \frac{dE(g')}{dg'} = -\int_g^\infty dg' g' \frac{d|\Delta(g')|^2}{dg'} = g|\Delta(g)|^2 + \int_g^\infty dg' |\Delta(g)|^2. \tag{3.50}$$

Since the absolute ground state energy, is the smallest amount of energy possible, therefore

$$E_{GS} = \frac{1}{2}[g|\Delta(g)|^2 - E(g)] = -\frac{1}{2}\int_g^\infty dg' |\Delta(g')|^2. \tag{3.51}$$

By then calculating this ground state energy for both solutions of ϕ will show which solution is the favourable solution. To make use of the equation for the ground state energy, the solution for the integral needs to be found to allow the gap function to be derived. The integral is non-analytic and therefore approximations have to be made before a solution can be found.

3.2.1 Edge of the Band

To find the most favourable solution for ϕ, the ground state energy must be calculated for each value of ϕ. To do this analytically, assumptions must be made. By splitting the gap function into two regions; one at the edge of the band, and one at the middle of the band, relevant assumptions can be made and the ground state energy can be found in both circumstances. Since it is logical to assume, that if the ground state energy is minimised for the same value of ϕ at both the edge and middle of the band, then it can be assumed which value of ϕ would be the most favourable value, and thus the topology of the system can be deduced.

To find an analytical solution at the edge of the band, certain assumptions must be made.

Since the momenta at the edge of the band is small, this allows a Taylor expansion to be performed on the momentum dependent functions. The fact the Fermi surface is spherical at the edge of the band also allows the choice of polar coordinates. This can be seen visually in figure 3.2.

The Fermi surface of $\xi_{\mathbf{k}}$ in the 2D plane for $\mu = 0$

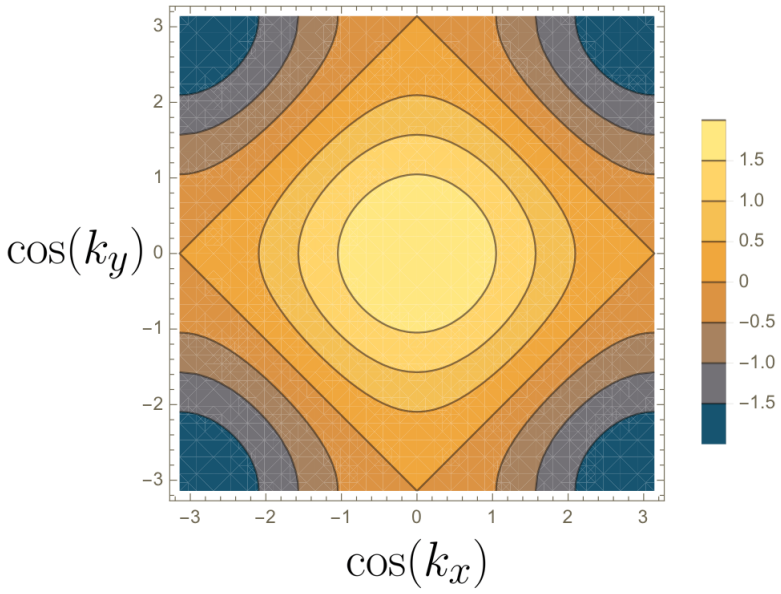

FIGURE 3.2: This Fermi surface clearly shows that at the edge of the band, the surface is spherical, and therefore allowing small momenta is a valid choice. Near the middle of the band, this approximation is no longer valid and the momentum distribution is approximately square.

Using this approximation results in equation (3.48) taking the form

$$g = \frac{1}{J} = \int d\mathbf{k} \frac{k_x^2 + k_y^2 + 2\cos(\phi)k_x k_y}{\sqrt{\left(-2 + \frac{k_x^2+k_y^2}{2} - \mu\right)^2 + |\Delta|^2\left(k_x^2 + k_y^2 + 2\cos(\phi)k_x k_y\right)}}, \tag{3.52}$$

This is now in the form where changing to polar coordinates is appropriate. Therefore $k_x = k\cos\theta$ and $k_y = k\sin\theta$, and the integral changes from $\int d\mathbf{k} = \int dk_x dk_y \to \int dk d\theta k$. The integral becomes

$$g = \int_0^{2\pi} \frac{d\theta}{2\pi^2} \int dk \frac{k(k^2 + 2k^2\cos(\phi)\sin(\theta)\cos(\theta))}{\sqrt{\left(-2 + \frac{k^2}{2} - \mu\right)^2 + |\Delta|^2(k^2 + 2k^2\cos(\phi)\sin(\theta)\cos(\theta))}}, \tag{3.53}$$

which yields

$$g = \int_0^{2\pi} \frac{d\theta}{2\pi^2} \int dk \frac{k^3(1+\cos(\phi)\sin(2\theta))}{\sqrt{\left(\frac{k^2}{2}-\delta\mu\right)^2 + |\Delta|^2 k^2 (1+\cos(\phi)\sin(2\theta))}}, \tag{3.54}$$

where $\delta\mu = \mu + 2$. Since small momentum is being considered, this allows $\xi = k^2/2$ where the integration has limits from $\delta\mu - \omega_0 \leq \xi \leq \delta\mu + \omega_0$ which is the window of superconducting electrons. Using these bounds, the integral becomes

$$\frac{1}{J} = \frac{2}{\pi} \int_0^{2\pi} \frac{d\theta}{2\pi} f(\theta) \int_{-\omega_0}^{\omega_0} d\xi \frac{\xi + \delta\mu}{\sqrt{\xi^2 + 2(\xi+\delta\mu)|\Delta|^2 f(\theta)}}, \tag{3.55}$$

where $f(\phi,\theta) \equiv f(\theta) = 1 + \cos(\phi)\sin(2\theta)$. Now this integral can be evaluated, by completing the square in the denominator such that

$$\frac{1}{J} = \frac{2}{\pi} \int_0^{2\pi} \frac{d\theta}{2\pi} f(\theta) \int_{-\omega_0}^{\omega_0} d\xi \frac{\xi + \delta\mu}{\sqrt{\left(\xi + |\Delta|^2 f(\theta)\right)^2 + a^2}}, \tag{3.56}$$

where $a^2 = -|\Delta|^2 f(\theta)(|\Delta|^2 f(\theta) - 2\delta\mu)$. Then let $\xi + |\Delta|^2 f(\theta) = a\sinh(s) \Rightarrow \operatorname{arcsinh}((\xi + |\Delta|^2 f(\theta))/a) = s$. Also, $d\xi = a\cosh(s)$, which yields

$$\frac{1}{J} = \frac{2}{\pi} \int_0^{2\pi} \frac{d\theta}{2\pi} f(\theta) \int_{-\operatorname{arcsinh}\left(\frac{\omega_0 + |\Delta|^2 f(\theta)}{a}\right)}^{\operatorname{arcsinh}\left(\frac{\omega_0 + |\Delta|^2 f(\theta)}{a}\right)} ds \frac{a\cosh(s)\left(a\sinh(s) - |\Delta|^2 f(\theta) + \delta\mu\right)}{\sqrt{a^2\left(\sinh^2(s)+1\right)}}. \tag{3.57}$$

This integral evaluated becomes

$$\frac{1}{J} = \frac{2}{\pi} \int_0^{2\pi} \frac{d\theta}{2\pi} f(\theta) \Big(a\cosh(s) - |\Delta|^2 f(\theta) s + \delta\mu s\Big) \Bigg|_{-\operatorname{arcsinh}\left(\frac{\omega_0 + |\Delta|^2 f(\theta)}{a}\right)}^{\operatorname{arcsinh}\left(\frac{\omega_0 + |\Delta|^2 f(\theta)}{a}\right)}. \tag{3.58}$$

Since the vicinity of interest is the phase transition, the approximation $|\Delta| \to 0$ can be made at the integration bounds such that

$$\operatorname{arcsinh}\left(\frac{\omega_0 + |\Delta|^2 f(\theta)}{a}\right) \approx \operatorname{arcsinh}\left(\frac{\omega_0}{a}\right). \tag{3.59}$$

Then using the fact that $\cosh(-x) = \cosh(x)$, the integral approximately becomes

$$\frac{1}{J} \approx \frac{2}{\pi} \int_0^{2\pi} \frac{d\theta}{2\pi} f(\theta) \operatorname{arcsinh}\left(\frac{\omega_0}{a}\right) \left[2\delta\mu - 2|\Delta|^2 f(\theta)\right]. \tag{3.60}$$

Recalling a and using the identity $\operatorname{arcsinh}(x) = \ln\left(x + \sqrt{x^2+1}\right)$, the result can be further simplified. By also noting

$$\frac{\omega_0^2}{\sqrt{|\Delta|^2 f(\theta)(-|\Delta|^2 f(\theta) - 2\delta\mu)}} \gg 1, \tag{3.61}$$

this implies that $\operatorname{arcsinh}(x) = \ln\left(x + \sqrt{x^2+1}\right) \to \ln(2x)$, and therefore

$$\frac{1}{J} \approx \frac{2}{\pi} \int_0^{2\pi} \frac{d\theta}{2\pi} f(\theta) \ln\left[\frac{2\omega_0}{\sqrt{-|\Delta|^2 f(\theta)(|\Delta|^2 f(\theta) - 2\delta\mu)}}\right] \left[2\delta\mu - 2|\Delta|^2 f(\theta)\right]. \tag{3.62}$$

Since the $|\Delta|^4$ term in the denominator is small, this can be ignored, and therefore

$$\frac{1}{J} \approx \frac{2}{\pi} \int_0^{2\pi} \frac{d\theta}{2\pi} f(\theta) \ln\left[\frac{2\omega_0}{\sqrt{2\delta\mu|\Delta|^2 f(\theta)}}\right] \left[2\delta\mu - 2|\Delta|^2 f(\theta)\right]. \tag{3.63}$$

Due to the $\delta\mu$ term being more dominant than the $|\Delta|^2$ term, the equation is approximated to

$$\frac{1}{J} \approx \int_0^{2\pi} \frac{d\theta}{\pi^2} f(\theta) 2\delta\mu \ln\left[\frac{\sqrt{2}\omega_0}{\sqrt{\delta\mu}|\Delta|}\right] - \frac{1}{2} \int_0^{2\pi} \frac{d\theta}{\pi^2} 2\delta\mu f(\theta) \ln\big(f(\theta)\big). \tag{3.64}$$

This is then at a point where the gap function can be written. Since

$$\frac{\pi}{4\delta\mu J} = \ln\frac{\Omega}{|\Delta|} - \gamma(\phi), \tag{3.65}$$

where $\Omega = \sqrt{2}\omega_0/\sqrt{\delta\mu}$, and $\gamma(\phi) = \frac{1}{4}\int_0^{2\pi} \frac{d\theta}{\pi} f(\theta,\phi) \ln\big(f(\theta,\phi)\big)$. From this,

$$\left|\Delta_\phi\right| = \Omega e^{-\gamma(\phi)} e^{-g}, \tag{3.66}$$

where $g = \pi/4\delta\mu J$. Since $g \gg 1$, this implies that the main contribution to the gap function comes from the dependence on ϕ. By then substituting this into the equation for the ground

state energy, the result becomes

$$E_{GS} = -\frac{1}{2}\frac{2\delta\mu}{\pi}\left|\Delta_\phi\right|^2 = -\frac{\delta\mu}{\pi}\left|\Delta_\phi\right|^2. \tag{3.67}$$

Now to evaluate which value for ϕ gives a lower energy. By remembering that $f(\theta) = 1 + \cos(\phi)\sin(2\theta) \equiv f(\phi,\theta)$, allows the values for ϕ that were found previously to be substituted in. When $\phi = \pm\pi/2$, since cos is an even function, implies $\cos(\pi/2) = \cos(-\pi/2) = 0$, and $f(\pm\pi/2,\theta) = 1$. Therefore $f(\pi/2,\theta)\ln(f(\pi/2,\theta)) = 1\ln(1) = 0$. When this is substituted into the ground state energy, the result is

$$E_{GS}^{\pm\frac{\pi}{2}} = -\frac{\delta\mu}{\pi}\left|\Omega e^0 e^{-g}\right|^2 = -\frac{\delta\mu}{\pi}\left|\Omega e^{-g}\right|^2. \tag{3.68}$$

for $\phi = \pi/2$. Now considering $\phi = n\pi$, implies that $f(0,\theta) = 1 + \sin(2\theta)$. Since there is typically a sign change between $\cos(0) = 1$, and $\cos(\pi) = -1$, this requires more analysis. However, the sign change can be removed, if the momentum is flipped, since the choice of the direction of momentum is not absolute. For a flipping of momentum, $f(0,\theta) = 1 + \sin(2\theta) = f(\pi,\theta)$. It can be seen that the integral of $f(n\pi,\theta)\ln(f(n\pi,\theta))$ is non-analytic. To determine the result, two inexact approaches are used. The first is to plot the integrand, and study whether the integral will be positive or negative based upon the graph. Since, it is being compared with $E_{GS}^{\pm\frac{\pi}{2}}$, by determining whether $\gamma(n\pi)$ is positive or negative, determines which ground state energy is lower. The second method, is to compute the integral numerically, and focus on the sign of the result. When looking at the plot of the integrand shown in figure (3.3), it is clear that on average, the integrand is positive.

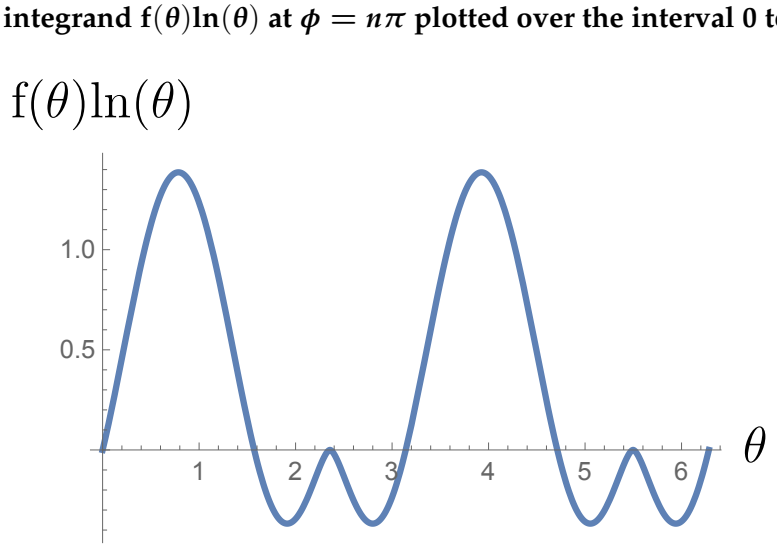

FIGURE 3.3: The figure clearly shows that the average of the integrand is positive, as there is only a small amount of the graph which becomes negative. Therefore the integral is positive.

The first method suggests that $\phi = n\pi$ yields a positive integral, which would result in a less negative ground state energy than the solution for $\phi = \pm\pi/2$ since $e^{-\gamma(n\pi)} < 1$. Consequently, the non trivial $\phi = \pm\pi/2$ appears to be the favourable solution. This is further confirmed, since the numerical solution for the integral in Mathematica gave a solution $\gamma(0,\pi) = 1.92801$, which again is clearly positive. When considering $E_{GS}^{n\pi}$, and in particular, $e^{-\gamma(n\pi)}$ implies that for $\gamma(n\pi)$ being positive yields $e^{-\gamma(n\pi)} < 1$, resulting in $E_{GS}^{n\pi} > E_{GS}^{\pm\pi/2}$. Since the lowest energy is the most favourable state, this allows a favourable solution for ϕ to be found. Using these two methods, it can be said that the non trivial solution for ϕ at $\phi = \pm\pi/2$ is the favourable solution for the edge of the band, suggesting a non trivial topology. The results need to be checked for the middle of the band.

3.2.2 Middle of the Band

To calculate the gap function for the middle of the band requires different methods as the approximations used for the edge of the band can no longer be applied. By consulting figure 3.2, at the middle of the band, the Fermi surface appears square-like, therefore applying a small momentum approximation, and writing only in terms of the angle is no longer valid.

For this scenario, new parameterisation needs to be performed such that

$$k_{\pm} = \frac{1}{2}(k_x \pm k_y), \tag{3.69}$$

which then implies

$$\epsilon_{\mathbf{k}} = -\frac{1}{2}\big(\cos(k_x) + \cos\big(k_y\big)\big) = -\cos(k_+)\cos(k_-), \tag{3.70}$$

and

$$g_k(\phi) = \sin^2(k_x) + \sin^2(k_y) + 2\cos(\phi)\sin(k_x)\sin\big(k_y\big) = 2\big[v^2 + \cos(\phi)(v_+^2 - v_-^2)\big], \tag{3.71}$$

where

$$v^2 = v_+^2 + v_-^2, \tag{3.72}$$

$$v_\pm = \frac{\partial \epsilon_{\mathbf{k}}}{\partial k_\pm}. \tag{3.73}$$

The integration range for this problem is between $-\omega_0$ and ω_0. Since, new variables have been introduced, the variables in the integration must be changed too, such that

$$dk_x dk_y = 2dk_+ dk_-, \tag{3.74}$$

where

$$dk_+ dk_- = d\epsilon_{\mathbf{k}} \frac{dk_-}{v_+} = d\epsilon_{\mathbf{k}} \frac{dk_+}{v_-} = d\epsilon_{\mathbf{k}} \frac{dl}{v}, \tag{3.75}$$

where l is a length parameter. Explicitly, the velocities are given by

$$\frac{\partial \epsilon_{\mathbf{k}}}{\partial k_\pm} = \sin(k_\pm)\cos(k_\mp) = v_\pm. \tag{3.76}$$

Using all of this information, the integral above can be written as

$$\frac{1}{J} = 2\int_{-\omega_0}^{\omega_0} \frac{dk_+ dk_-}{2\pi^2} \frac{g_{\mathbf{k}_\pm(\phi)}}{\sqrt{\xi_{\mathbf{k}_\pm}^2 + |\Delta|^2 g_{\mathbf{k}_\pm}(\phi)}}. \tag{3.77}$$

From this, the result can be calculated for each of the results for ϕ, and the most favourable solution can be found.

By again considering the Fermi surface, whilst the system cannot be transformed into k where the change is denoted by an angle, the system can be broken up into four quarters. Since these quarters are symmetric and even, only one of these quarters needs to be evaluated in the integral, and the integral can be multiplied by 4 to give the final result.

Additionally, since only one of the quarters needs to be integrated, the limits for the integral range from 0 to $\pi/2$. To now transform $g_{\mathbf{k}}(\phi)$ in terms of these defined variables above, it is useful to evaluate $g_{\mathbf{k}}(\phi)$ at $\phi = n\pi$ and $\phi = \pm\pi/2$. By evaluating $g_{\mathbf{k}}(\phi = 0)$, the solution becomes

$$\begin{aligned} g_{\mathbf{k}}(\phi = 0) &= \sin^2(k_x) + \sin^2(k_y) + 2\sin(k_x)\sin(k_y) = \big[\sin(k_x) + \sin(k_y)\big]^2 \\ &= \Big[2\sin\big(\frac{k_x + k_y}{2}\big)\cos\big(\frac{k_x - k_y}{2}\big)\Big]^2 = \big[2\sin(k_+)\cos(k_-)\big]^2 = 4v_+^2, \end{aligned} \tag{3.78}$$

similarly, $g_{\mathbf{k}}(\phi = \pi)$ becomes

$$\begin{aligned} g_{\mathbf{k}}(\phi = \pi) &= \sin^2(k_x) + \sin^2(k_y) = 2\sin(k_x)\sin(k_y) = \big[\sin(k_x) - \sin(k_y)\big]^2 \\ &= \Big[2\sin\Big(\frac{k_x - k_y}{2}\Big)\cos\Big(\frac{k_x + k_y}{2}\Big)\Big]^2 = \big[2\sin(k_-)\cos(k_+)\big]^2 = 4v_-^2. \end{aligned} \tag{3.79}$$

For $g_{\mathbf{k}}(\phi = \pm\pi/2)$, the calculation is

$$\begin{aligned} g_{\mathbf{k}}(\phi = \pm\pi/2) &= \sin^2(k_x) + \sin^2(k_y) = \frac{1}{2}\big[2\sin^2(k_x) + 2\sin^2(k_y)\big] \\ &= \frac{1}{2}\big[\sin^2(k_x) + \sin^2(k_y) + 2\sin(k_x)\sin(k_y) \\ &\quad + \sin^2(k_x) + \sin^2(k_y) - 2\sin(k_x)\sin(k_y)\big], \end{aligned} \tag{3.80}$$

which by using the above formulae, allows

$$\begin{aligned} g_{\mathbf{k}}(\phi = \pm\pi/2) &= 2\Big[\Big(\frac{1}{2}(\sin(k_x) + \sin(k_y))\Big)^2 + \Big(\frac{1}{2}(\sin(k_x) - \sin(k_y))\Big)^2\Big] \\ &= 2\big[(\sin(k_+)\cos(k_-))^2 + (\sin(k_-)\cos(k_+))^2\big] = 2(v_+^2 + v_-^2). \end{aligned} \tag{3.81}$$

Now, the two integrals can be written for both $\phi = n\pi$, and $\phi = \pm\pi/2$. Since, only one of the momenta needs to be integrated over, dk_+dk_- becomes $d\epsilon_{\mathbf{k}}dk_-/v_+$ by using equation (3.76). Therefore for $\phi = n\pi$ the integral is

$$\frac{1}{J} = \frac{8}{\pi^2}\int_{-\omega_0}^{\omega_0} d\epsilon_{\mathbf{k}} \int_0^{\arccos|\epsilon|} \frac{dk_-}{v_+} \frac{v_+}{\sqrt{(\epsilon_{\mathbf{k}} - \mu)^2 + 4|\Delta|^2 v_+^2}}, \tag{3.82}$$

where the limits come from $\epsilon_{\mathbf{k}} = -\cos(k_+)\cos(k_-)$, and at $\mathbf{k} = 0 \Rightarrow k_x = k_y = 0$, and consequently $k_- = 0$. Also, for $\mathbf{k} = \pi/2$, this means the maximum of $\cos(k_+) = 1$, and

$\epsilon_{\mathbf{k}} = -\cos(k_-) \Rightarrow k_- = \arccos|\epsilon_{\mathbf{k}}|$. For the $\phi = \pm\pi/2$ integral, the result is

$$\frac{1}{J} = \frac{2}{\pi^2}\int_{-\omega_0}^{\omega_0} d\epsilon_{\mathbf{k}} \int_0^{\arccos|\epsilon|} \frac{dk_-}{v_+} \frac{2(v_+^2 + v_-^2)}{\sqrt{(\epsilon_{\mathbf{k}} - \mu)^2 + 2|\Delta|^2(v_+^2 + v_-^2)}}. \tag{3.83}$$

As has previously been discussed, the signs of the momenta are interchangeable by symmetry, this then implies that the numerator in the integral results in $4v_+^2$. This does not occur in the square root in the denominator as this is not even. Consequently, the integral becomes

$$\frac{1}{J} = \frac{16}{\pi^2}\int_0^{\omega_0} d\epsilon_{\mathbf{k}} \int_0^{\arccos|\epsilon|} \frac{dk_-}{v_+} \frac{v_+^2}{\sqrt{(\epsilon_{\mathbf{k}} - \mu)^2 + 2|\Delta|^2(v_+^2 + v_-^2)}}. \tag{3.84}$$

To write v_+ and v_- in terms of k_- and $\epsilon_{\mathbf{k}}$, equation (3.70) must be used. From this,

$$\begin{aligned} \epsilon_{\mathbf{k}}^2 = \cos^2(k_+)\cos^2(k_-) = \cos^2(k_-) - \cos^2(k_-)\sin^2(k_+) = \cos^2(k_-) - v_+^2 \\ \Rightarrow v_+ = \sqrt{\cos^2(k_-) - \epsilon_{\mathbf{k}}^2}. \end{aligned} \tag{3.85}$$

To find v_-, use $\epsilon_{\mathbf{k}}^2 = \cos^2(k_+)\cos^2(k_-)$ and also $v_- = \sin^2(k_-)\cos^2(k_+)$, which can be combined to give

$$\begin{aligned} \cos^2(k_+) = \frac{\epsilon_{\mathbf{k}}^2}{\cos^2(k_-)} = \frac{v_-}{\sin^2(k_-)} \\ \Rightarrow v_- = \epsilon_{\mathbf{k}}^2 \tan^2(k_-). \end{aligned} \tag{3.86}$$

As can be seen, even with this parameterisation, the integrals are still non-analytic, however there are some assumptions that can be made at the middle of the band. Since $|\epsilon_{\mathbf{k}}| \ll 1$ at the middle of the band, this implies that $v_+ \approx \cos(k_-) \gg v_-$ almost everywhere, except for near $\cos(\pi/2) \approx \pi/2 - k_- \leq |\epsilon_{\mathbf{k}}|$ where the Fermi surface starts to curve. By neglecting this small contribution, the upper limit of the integral can be set to $\pi/2$. Using these assumptions, the integrals can then be written as

$$I(\phi = n\pi) = \frac{16}{\pi^2}\int_0^{\omega_0} d\xi \int_0^{\frac{\pi}{2}} dk \frac{\cos(k)}{\sqrt{\xi^2 + 4|\Delta|^2\cos^2(k)}}, \tag{3.87}$$

$$I(\phi = \pm\frac{\pi}{2}) = \frac{16}{\pi^2}\int_0^{\omega_0} d\xi \int_0^{\frac{\pi}{2}} dk \frac{\cos(k)}{\sqrt{\xi^2 + 2|\Delta|^2\cos^2(k)}}, \tag{3.88}$$

where $k = k_-$. Since the only difference between these integrals is a factor of 2 in the square

root in the denominator, the integral for $\phi = n\pi$ will be computed, and then the other result will be deduced. The k integral is an exact integral and gives

$$I(\phi = n\pi) = \frac{16}{\pi^2}\int_0^{\omega_0} d\xi \frac{\arctan\left(\frac{2\Delta}{\xi}\right)}{2\Delta}. \tag{3.89}$$

The integral over the spectrum can be computed to give

$$I(\phi = n\pi) = \frac{8}{\Delta\pi^2}\Big[\omega_0 \arctan\left(\frac{2\Delta}{\omega_0}\right) + \Delta \ln\left(4\Delta^2 + \omega_0^2\right) - \Delta \ln\left(4\Delta^2\right)\Big]. \tag{3.90}$$

Since the calculation is taking place near the phase transition, the dominant terms in the integral occur as $\Delta \to 0$. Therefore, by only considering these terms, the result is

$$I(\phi = n\pi) = \frac{8}{\pi^2}\Big[\ln\left(\frac{4\Delta^2 + \omega_0^2}{4\Delta^2}\right)\Big] = \frac{8}{\pi^2}\Big[\ln\left(\frac{4\Delta^2 + \omega_0^2}{\Delta^2}\right) - \ln(4)\Big], \tag{3.91}$$

and since $\omega_0/\Delta \gg 4$, the result simplifies to

$$I(\phi = n\pi) = \frac{16}{\pi^2}\Big[\ln\left(\frac{\omega_0}{\Delta}\right) - \ln(2)\Big] = \frac{1}{J}. \tag{3.92}$$

By now letting $-\ln(2) = \gamma$, the gap function can be solved to yield

$$\Delta = \omega_0 e^{\gamma} e^{-\frac{\pi^2}{16J}} = \omega_0 e^{\gamma} e^{-g} = \Delta(\phi = n\pi). \tag{3.93}$$

For the case when $\phi = \pm\pi/2$, the integral is

$$I(\phi = \pm\frac{\pi}{2}) = \frac{8}{\pi^2}\Big[\ln\left(\frac{2\Delta^2 + \omega_0^2}{2\Delta^2}\right)\Big] = \frac{8}{\pi^2}\Big[\ln\left(\frac{4\Delta^2 + 2\omega_0^2}{\Delta^2}\right) - \ln(4)\Big], \tag{3.94}$$

which by similar cancellation of terms gives

$$I(\phi = \pm\frac{\pi}{2}) = \frac{16}{\pi^2}\Big[\ln\left(\frac{\sqrt{2}\omega_0}{\Delta}\right) - \ln(2)\Big] = \frac{1}{J}. \tag{3.95}$$

For the solution, the gap function can be found to give

$$\Delta = \sqrt{2}\omega_0 e^{\gamma} e^{-\frac{\pi^2}{16J}} = \sqrt{2}\omega_0 e^{\gamma} e^{-g} = \Delta\Big(\phi = \pm\frac{\pi}{2}\Big). \tag{3.96}$$

Using these equations, this implies that

$$\Delta(\phi = \pm\frac{\pi}{2}) = \sqrt{2}\Delta(\phi = n\pi). \tag{3.97}$$

Since the equations are only different by a factor of $\sqrt{2}$, this means the integrals do not need to be calculated explicitly, and only computed in terms of $\Delta(\phi = n\pi)$. By computing the integrals, it is clear to see that $|\Delta(\phi = \pm\pi/2)|^2 = 2|\Delta(\phi = n\pi)|^2$, and therefore

$$\begin{aligned} E_{GS}(\phi = n\pi) &= -\frac{1}{4}|\Delta(\phi = n\pi)|^2 > E_{GS}(\phi = \pm\pi/2) \\ &= -\frac{1}{4}|\Delta(\phi = \pm\pi/2)|^2 = -\frac{1}{2}|\Delta(\phi = n\pi)|^2. \end{aligned} \tag{3.98}$$

Consequently, it can be seen that the non trivial solution for ϕ is again most negative, and is the favourable solution. Since this occurs at both the middle and edge of the band, it can be claimed that the non trivial solution is the most favourable, thus implying a $p_x + ip_y$ topological superconductor due to symmetries of the gap function, as shown earlier.

3.2.3 Calculation of Chern Number

The symmetries of the gap function for $\mathbf{q} = 0$ imply a non trivial topology for $\phi = \pm\pi/2$, since the minimum of the free energy had a solution for $\Delta_1 \pm i\Delta_2 = 0$ which in this square lattice system corresponds to $\Delta_x \pm i\Delta_y = 0$. However, there are other methods of determining non trivial topology which have previously been mentioned in this thesis. The method that will be used in this section is the calculation of the Chern number.

The full mathematical understanding of the Chern number is quite complex, so for the purpose of this thesis, it will be introduced at a surface level. To understand the concept, studying the Berry phase and Berry curvature introduces the foundational principles. The important aspect to note, is that a non-zero Chern number implies non trivial topology, and a zero Chern number implies a topologically trivial system. Physically, a non-zero Chern number implies a protected edge state, since the closed curvature of the edge state can be traversed more than once. However, if the Chern number is zero, this implies that the curvature of the edge state can only be traversed once. This is intrinsically linked to the Winding number [80], which is related to the Chern number.

The formal definition of the Chern number is given as

$$C_{\pm} = \frac{1}{4\pi}\int_{BZ} dk_x dk_y\, \hat{\mathbf{n}}_{\mathbf{k}}.(\partial_{k_x}\hat{\mathbf{n}}_{\mathbf{k}} \times \partial_{k_y}\hat{\mathbf{n}}_{\mathbf{k}}), \tag{3.99}$$

where $\hat{\mathbf{n}}_{\mathbf{k}}$ is the unit Bloch vector from the Bloch sphere. $\hat{\mathbf{n}}_{\mathbf{k}}$ is the unit vector $\mathbf{n}_{\mathbf{k}}/|\mathbf{n}_{\mathbf{k}}|$, where $\mathbf{n}_{\mathbf{k}}$ can be thought of as resolving the components of the Hamiltonian into x, y, z components. Therefore, for the system that is being studied $\mathbf{n}_{\mathbf{k}}$ becomes

$$\mathbf{n}_{\mathbf{k}} = \big(|\Delta|\sin(k_x), |\Delta|\sin\big(k_y\big), \xi_{\mathbf{k}}\big), \tag{3.100}$$

where $\xi_{\mathbf{k}}$ is defined as before. The result for the integrand is given by

$$\begin{aligned}
\hat{\mathbf{n}}_{\mathbf{k}}.\big(\partial_{k_x}\hat{\mathbf{n}}_{\mathbf{k}} \times \partial_{k_y}\hat{\mathbf{n}}_{\mathbf{k}}\big) &= \frac{\mathbf{n}_{\mathbf{k}}.(\partial_{k_x}\mathbf{n}_{\mathbf{k}} \times \partial_{k_y}\mathbf{n}_{\mathbf{k}})}{|\mathbf{n}_{\mathbf{k}}|^3} \\
&= -\frac{|\Delta|^2\big(\cos(k_x) + \cos\big(k_y\big) + \mu\cos(k_x)\cos\big(k_y\big)\big)}{\big|\big(|\Delta|\sin(k_x), |\Delta|\sin\big(k_y\big), \xi_{\mathbf{k}}\big)\big|^3} \\
&= -\frac{|\Delta|^2\big(\cos(k_x) + \cos\big(k_y\big) + \mu\cos(k_x)\cos\big(k_y\big)\big)}{\Big(\sqrt{|\Delta|^2(\sin^2(k_x) + \sin^2(k_y)) + \xi_{\mathbf{k}}^2}\Big)^3}.
\end{aligned} \tag{3.101}$$

The Chern number is

$$C_{\pm} = -\frac{1}{4\pi}\int_{BZ} dk_x dk_y \frac{|\Delta|^2\big(\cos(k_x) + \cos\big(k_y\big) + \mu\cos(k_x)\cos\big(k_y\big)\big)}{\Big(\sqrt{|\Delta|^2(\sin^2(k_x) + \sin^2(k_y)) + \xi_{\mathbf{k}}^2}\Big)^3}, \tag{3.102}$$

which can not be solved using standard analytical techniques. Numerical simulations have to be performed in Mathematica to determine the Chern number and are shown below.

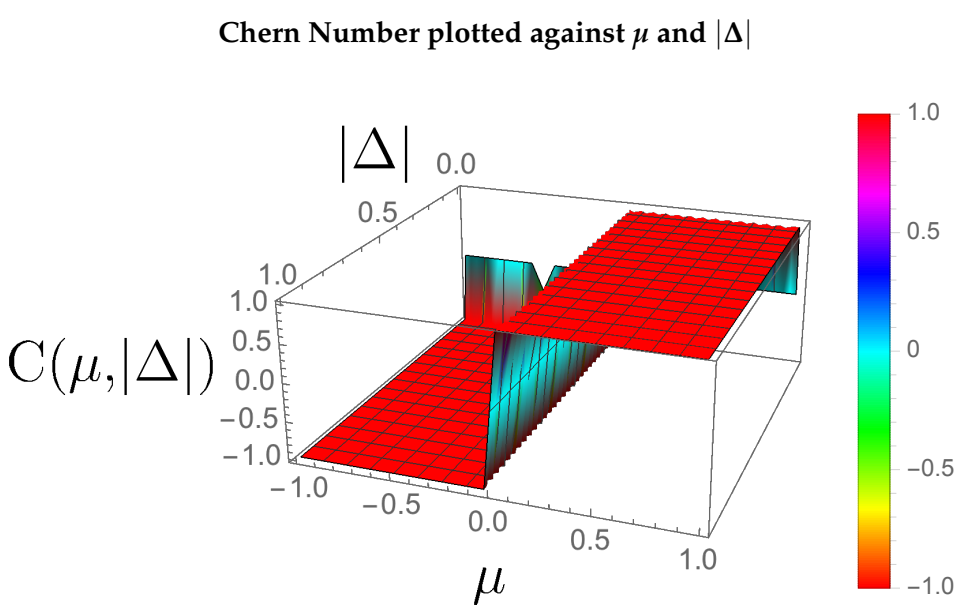

FIGURE 3.4: This plot shows how the Chern number goes from -1 to 1 as the sign of the chemical potential changes. However, the fact that the Chern number is at ± 1 further confirms that this is a topological superconductor. The anomalies in this plot occur at $|\Delta| = 0$, and this is because it is not in the superconducting phase.

The calculation of the Chern number provides further evidence that the system has non trivial topology when the phase is $\phi = \pm\pi/2$, and the change in sign of the Chern number as the chemical potential goes from negative to positive also reveals a new type of topological phase transition in the system.

Figure (3.4) implies that at $\mu = 0$, there is not a topological phase, since the Chern number is zero. Whether this is due to the system being in a different type of phase is a question that requires addressing and is considered in the next section.

3.3 Superconducting Instability For Non Zero Net Momentum

The previous section regarding the ground state energy demonstrated a non trivial solution for the gap function resulting in non trivial topology, and thus a topological superconductor was created for $\mathbf{q} = 0$. This was because analysis of the fourth order term in the free energy was analytically difficult, and therefore the simplification of $\mathbf{q} = 0$ was made. The benefit of studying the fourth order term, allows information about the gap function to be deduced. However, whilst $\mathbf{q} \neq 0$ does not allow a solution for the gap function to be found from the

fourth order term, information about the superconducting transition can still be found from the second order term. For example, what is the most favourable solution for $\mathbf{q}$ when the minimum of the energy is found. The purpose of this section is to study information about the phase transition itself.

By referring to equation (3.31), this shows the scenario before the assumption of $\mathbf{q} = 0$ was made. At this stage, the fact that the model is a square lattice can be imposed by setting $\mathbf{l} = \mathbf{a}_\mu$ and $\mathbf{l}' = \mathbf{a}_\nu$. Therefore the quadratic term becomes

$$F_2 = \sum_{\mathbf{q},\mu,\nu} \Delta^\dagger_\mu(\mathbf{q}) \Big[\frac{1}{2J} - \frac{1}{2}\Pi_{\mu\nu}(\mathbf{q}) \Big] \Delta_\nu(\mathbf{q}), \tag{3.103}$$

where $\Pi_{\mu\nu}(\mathbf{q}) = \sum_{\epsilon,\mathbf{k}} g^{\epsilon}_{\mathbf{k}+\mathbf{q}/2} g^{-\epsilon}_{-\mathbf{k}+\mathbf{q}/2} \sin\big(\mathbf{k}.\mathbf{a}_\mu\big) \sin(\mathbf{k}.\mathbf{a}_\nu)$. Note that J no longer has directional dependence as it only occurs for nearest neighbour coupling, hence why a factor of 2 was introduced. Now the lattice spacing $|a|$ can be set to 1. From this, the kernel in F_2 can be written in matrix form as

$$\hat{\Pi}(T,\mu) = \frac{1}{2} \sum_{\mathbf{q}} \begin{pmatrix} \frac{1}{J} - \Pi_{11} & -\Pi_{12} \\ -\Pi_{21} & \frac{1}{J} - \Pi_{22} \end{pmatrix}, \tag{3.104}$$

where

$$\Pi_{\pm}(\mathbf{q};T,\mu) = \frac{1}{2}\big(\Pi_{11} \pm \Pi_{22}\big) = \frac{1}{2} \int_{-\pi}^{\pi} \frac{d\mathbf{k}}{2\pi^2} \pi_{\mathbf{k}}(\mathbf{q};T,\mu) \big[\sin^2(k_x) \pm \sin^2(k_y) \big], \tag{3.105}$$

$$\Pi_{\perp}(\mathbf{q};T,\mu) = \Pi_{12} = \Pi_{21} = \int_{-\pi}^{\pi} \frac{d\mathbf{k}}{2\pi^2} \pi_{\mathbf{k}}(\mathbf{q};T,\mu) \sin(k_x) \sin\big(k_y\big), \tag{3.106}$$

$$\pi_{\mathbf{k}}(\mathbf{q};T,\mu) = \frac{\tanh\left(\frac{\xi_{\mathbf{k}+\frac{\mathbf{q}}{2}}}{2T}\right) + \tanh\left(\frac{\xi_{-\mathbf{k}+\frac{\mathbf{q}}{2}}}{2T}\right)}{\xi_{\mathbf{k}+\frac{\mathbf{q}}{2}} + \xi_{-\mathbf{k}+\frac{\mathbf{q}}{2}}} = g^{\epsilon}_{\mathbf{k}+\frac{\mathbf{q}}{2}} g^{-\epsilon}_{-\mathbf{k}+\frac{\mathbf{q}}{2}}. \tag{3.107}$$

The calculation for the Green's functions is the same as the one that has been used previously, hence the tanh functions. Additionally remember that $\xi_{\mathbf{k}} = \cos(k_x) - \cos\big(k_y\big) - \mu$. The superconducting instability occurs when the energy eigenvalue first reaches zero, and the point at which this occurs reveals the most favourable choice for $\mathbf{q}$. To find this, the eigenvalues of this matrix need to be found as

$$E(\mathbf{q};T,\mu) = \frac{1}{J} - \Pi_{+}(\mathbf{q};T,\mu) - \sqrt{\Pi^2_{-}(\mathbf{q};T,\mu) + \Pi^2_{\perp}(\mathbf{q};T,\mu)} = \frac{1}{J} + \mathrm{E}_{-}(\mathbf{q};T,\mu), \tag{3.108}$$

where $\mathrm{E}_{-}(\mathbf{q};T,\mu)$ is given by

$$\mathrm{E}_{-}(\mathbf{q};T,\mu) = -\Pi_{+}(\mathbf{q};T,\mu) - \sqrt{\Pi_{-}^{2}(\mathbf{q};T,\mu) + \Pi_{\perp}^{2}(\mathbf{q};T,\mu)}. \tag{3.109}$$

By plotting $\mathrm{E}_{-}(\mathbf{q};T,\mu)$ and finding the minimum of this, deductions can be made about $\mathbf{q}$. Different plots will be made for different values of μ. If the minimum for the energy is at $\mathbf{q} = 0$ for any choice of μ, then the simplification that $\mathbf{q} = 0$ is justified, and the previous analysis holds in all cases.

Since the integrals in $\Pi_{\pm}(\mathbf{q},T,\mu)$ and $\Pi_{\perp}(\mathbf{q},T,\mu)$ are not analytically tractable without any assumptions, the integrals will consequently be calculated numerically. Once the integrals have been computed numerically, this allows for a plot of $\mathrm{E}_{-}(\mathbf{q},T,\mu)$ to be shown. The expectation from these plots is that the minima will always be $\mathbf{q} = 0$ regardless of the choice of μ and T. First the plot for $\mu = -1$ and $T = 1$ is shown in figure 3.5.

$\mathrm{E}_{-}(\mathbf{q},\mathbf{T},\mu)$ plotted at $\mathbf{T} = \mathbf{1}$ and $\mu = -\mathbf{1}$

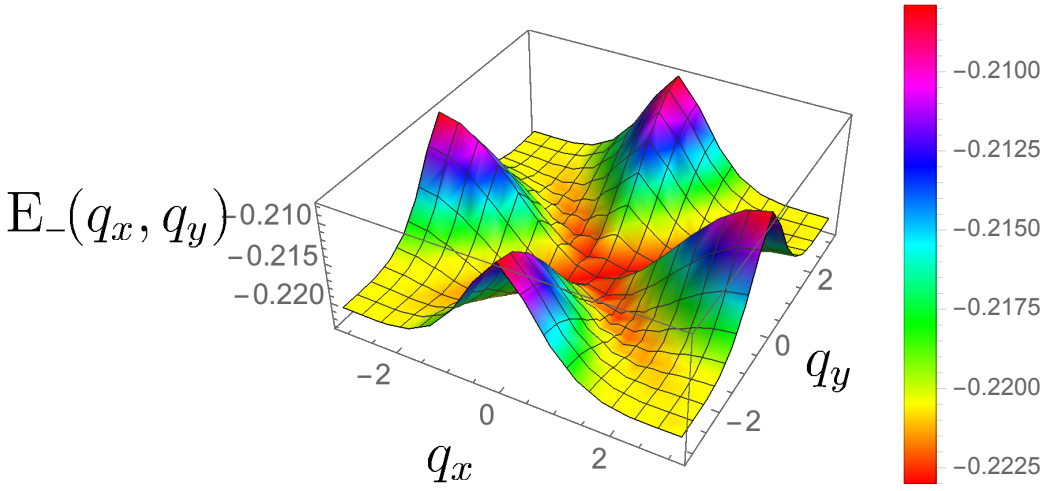

FIGURE 3.5: This plot shows the expected behaviour, where the minimum of the energy appears to be at $\mathbf{q} = 0$. The diagonals are much lower than the off diagonals, and further investigation is needed as to why this occurs.

This plot shows that for certain values, the assumption that the gap function is independent of the momentum is a valid one. To further illustrate this conclusion, the minimum of the energy being $\mathbf{q} = 0$, a clearer plot is the density of the energy. This is shown below in figure 3.6.

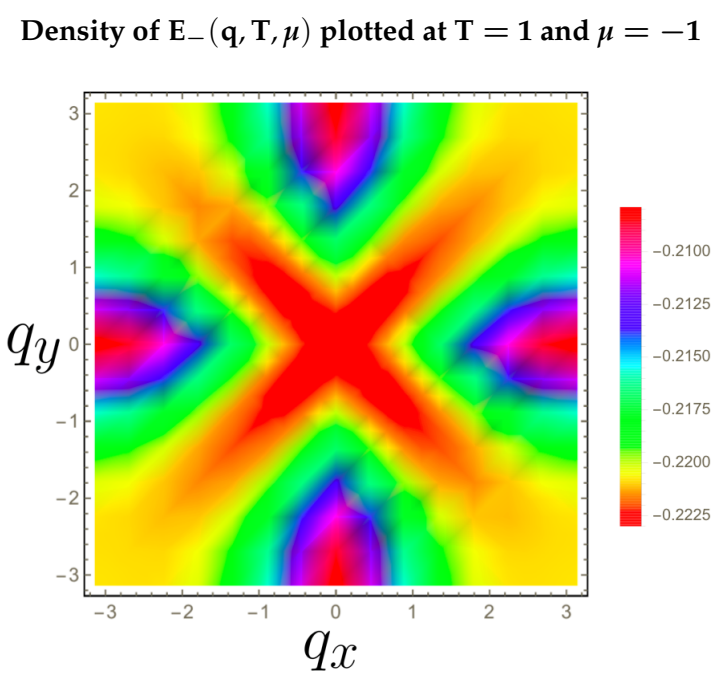

FIGURE 3.6: This density plot confirms the behaviour in figure 3.5. This is since the darkest red is clearly focused at $\mathbf{q} = 0$, whereas the areas around the minimum appear only slightly above.

This further confirms that the gap function is momentum independent for a non zero chemical potential. At this point, it is beneficial to vary the chemical potential to see how this affects the plots, and whether the minimum of the energy is changed.

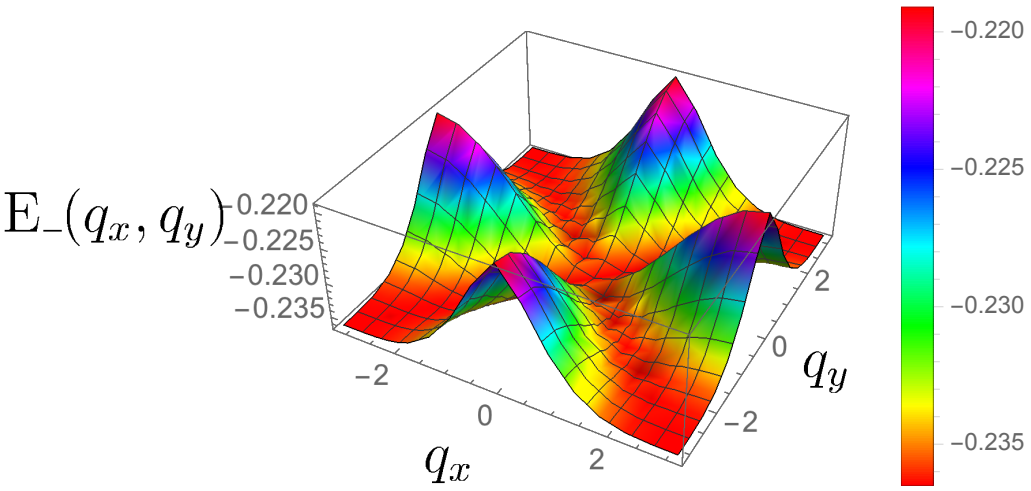

FIGURE 3.7: The plot shows that at half filling ($\mu = 0$), there appears to be minima which goes along the diagonals of the energy at $q_x = \pm q_y$. Outside of these diagonals, the energy increases as **q** increases, which is the expected behaviour.

It is important to emphasise that the minima along the diagonals was not expected as it is widely assumed that in a translational invariant system $\mathbf{q} = 0$ is the favourable solution. However, this graph appears to indicate differently. Interestingly, there appears to be a continuum of ground state energies along the diagonals. This suggests any point along these diagonals is equally likely to be a favourable solution. As a confirmation check, it is useful to continue to plot the 2D profile of the height as a density plot. This is shown in figure 3.8.

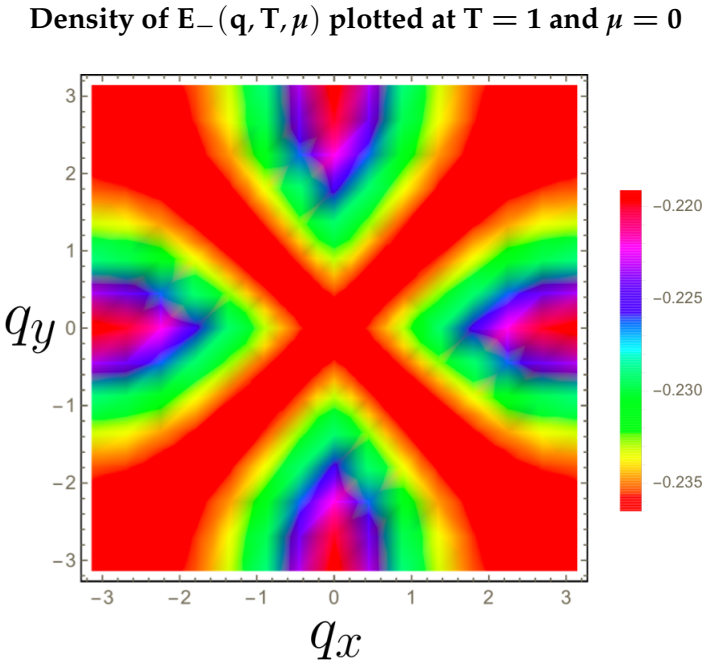

FIGURE 3.8: This density plot clearly shows that along the diagonals of the energy at $k_x = \pm k_y$, the energy is minimised. This is unexpected as it is generally assumed $\mathbf{q} = 0$ for a translationally invariant system. However the minimum for $\mathbf{q}$ is dependent on the chemical potential.

Since it is clear that there is a dependence on μ for the minima of the energy, ideally a plot will be able to show whether the minima of $\mathbf{q}$ form a continuum of points, or a single point for varying values for μ. The energy generally appears to increase as $|\mathbf{q}|$ is increased. This allows a useful graph to be plotted where $\mathrm{E}_-(\pi, \pi, 1, \mu) - \mathrm{E}_-(0, 0, 1, \mu) = \delta\mathrm{E}(\mu)$ which will reveal whether the minimum of the energy is exactly along the diagonals. Since at $\mu = 0$, this difference should be zero if there are a continuum of Cooper pairs, the graph will provide confirmation for this, in addition to determining whether this occurs for any other values of μ.

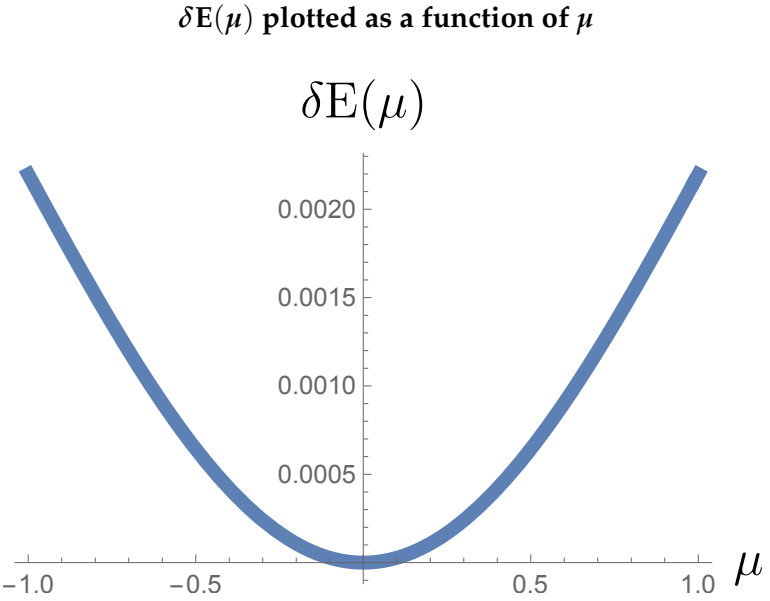

FIGURE 3.9: The change in energy from $(k_x, k_y) = (\pi, \pi)$ to $(k_x, k_y) = (0, 0)$ shows that as $\mu = 0$ the result is zero, thus confirming the belief that there is a continuum of Cooper pairs along the diagonals at $\mu = 0$. However, this plot also reveals that $\mu = 0$ is the only point at which this happens.

Figures 3.7, 3.8, 3.9 show that at half filling, this superconductor has a continuum of Cooper pairs along the diagonals of the Brillouin zone, when the superconducting state first condenses, implying the widely used assumption that $\Delta(\mathbf{q} = 0)$ for translationally invariant systems may be limited. It has been shown that there is a dependence on this critical value for $\mathbf{q}$ and the chemical potential μ.

3.4 Discussion

This chapter has provided a theoretical and numerical analysis for investigating non-trivial topology in a 2D spinless square lattice. The main features are that non-trivial topology spontaneously occurs due to $\mathcal{T}$-symmetry breaking, but only when the chemical potential is non-zero. This is due to the assumption that the gap field being homogeneous is only valid for a non-zero chemical potential, as was shown in section 3.3. This analysis revealed that a continuum of ground states could occur along the diagonals of the Brillouin zone for the gap field, resulting in a inhomogeneous gap field at half filling.

It is worth considering how this system may be achieved experimentally. To determine whether the predictions that are made within this chapter are valid, more calculation still

needs to be performed. This is because a suitable method to determine the non-trivial topology, and especially the non-zero nature of the Cooper pairs at half filling is to compute the specific heat, since a jump in specific heat could imply these particular conditions. This is scope for future work resulting from the research in this chapter, and is an opportunity for collaboration between theorists and experimentalists.

The model which has been considered is a simple and highly symmetric system. Therefore, this type of analysis can be extended for a system which is 3D as opposed to 2D. It would be expected that the conclusions would be the same due to symmetry arguments of the gap function, but this should still be investigated to confirm this belief. A benefit of studying the system in 3D is that a solution for critical temperature could be found. The reason the critical temperature was not found in the 2D scenario, is due to the gap function being an inaccurate way to determine the critical temperature. Additionally, the square system could be changed to a different type of lattice, namely a hexagonal lattice. The methodology used in this chapter would still apply, the difference would be absorbed in the gap function. A similar approach was performed numerically for a hexagonal lattice in the paper by Karnaukhov [1].

The results of this chapter have contributed to original research in the field. The analytical method for showing a non trivial superconductor has not been performed previously. Additionally, the analyticity of the method is rigorous in determining that the topological phase is preferred over the normal superconducting phase. Moreover, by showing that translationally invariant systems might be dependent on $\mathbf{q}$, the way in which future research will be conducted should change. It has been shown that $\mathbf{q} = 0$ is a poor assumption in certain cases as it may depend on μ, and should not be widely used.

The next chapter provides the framework for disorder induced superconductivity which is the main focus of this thesis.

Chapter 4

Disorder Induced Superconductors

This chapter focuses on the main inspiration for the thesis which was a result of an experiment [3] which showed that disorder could enhance superconductivity. This was previously believed to be physically unrealisable. The understanding of this phenomenon from a theoretical aspect is the focus of the chapter. Luttinger liquids are rigorously introduced, then using this framework, a quasi one-dimensional model is designed such that there is Josephson coupling between the Luttinger liquid wires. Once an action for this is written, disorder is added, and the physics of the system is studied.

The analysis of this chapter, is a mixture of analytical and numerical work, where renormalisation group (RG) [81] is introduced such that the RG equations for the system can be written. This results in a system of coupled linear first order differential equations. To determine how the parameters of the system affect each other, this system of equations is solved numerically, and the results of this are shown graphically. From this analysis, conclusions may be drawn.

4.1 Model

4.1.1 Luttinger Liquid Derivation

Since the basis of the model is a set of coupled Luttinger liquid wires, the mathematical framework of Luttinger liquids is introduced. To derive the model [81] the initial assumption is that the dispersion law can be linearised to give

$$\xi_q = \frac{q^2}{2m} - \mu = \frac{(q-q_f)(q+q_f)}{2m} \approx \begin{cases} v_f(q-q_f) & \text{near } q = q_f \\ -v_f(q+q_f) & \text{near } q = -q_f \end{cases}, \tag{4.1}$$

where q is the momentum, q_f is the Fermi momentum, and v_f is the Fermi velocity, ξ_q is the dispersion law, and μ is the chemical potential. This approximation is valid for $|E - E_F| \approx E_F$ since the expansion is about the Fermi level, due to all long wave excitations being well described by linearisation. This linearising means the dispersion relation can be written as

$$\xi_q = \eta v_f q, \tag{4.2}$$

where $\eta = R, L = \pm 1$ to describe left moving and right moving particles respectively.

To derive the Luttinger liquid (LL) Hamiltonian, the most generic Hamiltonian needs to be considered such as

$$\mathcal{H} = \sum_{\eta=R,L} \mathcal{H}_{0\eta} + \mathcal{H}_{int}, \tag{4.3}$$

where

$$\mathcal{H}_{int} = \frac{1}{2} \int \rho_D(x) V(x - x') \rho_D(x') dx dx', \tag{4.4}$$

and $\rho_D(x)$ is the density matrix. Using this generic Hamiltonian, the aim is to write the Hamiltonian in a bosonic form since for electron-hole pairs, when the number of particles are conserved, the excitations are bosonic. This step is known as bosonisation [82] and is crucial as it allows for condensates to form. The first step is to write the action as quadratic in terms of density fields. Write the general expression for the non interacting action as

$$S_0 = \int \mathcal{L}_0 dx dt, \tag{4.5}$$

where

$$\mathcal{L}_0 = \bar{\psi}(x,t)[i\partial_t - \mathcal{H}_0]\psi(x,t), \tag{4.6}$$

where the non interacting Lagrangian can be split into right and left moving particles from the linearisation. The linear dispersion can be written as $v_f q$, meaning the non-interacting Hamiltonian is

$$\mathcal{H}_0 = \sum_\eta \eta v_f q \rightarrow -\sum_\eta \eta v_f i\partial_x, \tag{4.7}$$

consequently the directional action is

$$S_{0\eta} = \int dx dt\, \bar{\psi}_\eta(x,t)[i\partial_t + i\eta v_f \partial_x]\psi_\eta(x,t) \equiv \int dx dt\, \bar{\psi}_\eta(x,t) i\partial_\eta \psi_\eta, \tag{4.8}$$

where $\partial_\eta = \partial_t + \eta v_f \partial_x$, which implies $\partial_\pm = \partial_t \pm v_f \partial_x$. The wavefunction for both the left and right moving particles can be written as

$$\begin{aligned}\psi(x,t) = \exp\big(iq_f x\big) \int_{q>0} dq \exp\big(i(q-q_f)x - i\omega t\big) \\ + \exp\big(-iq_f x\big) \int_{q<0} dq \exp\big(i(q+q_f)x - i\omega t\big).\end{aligned} \tag{4.9}$$

In the vicinities of $\pm q_F$, the wavefunction becomes

$$\psi(x,t) \approx \exp\big(iq_f x\big)\psi_R(x,t) + \exp\big(-iq_f x\big)\psi_L(x,t), \tag{4.10}$$

and therefore $\rho_D(x,t) = \bar{\psi}(x,t)\psi(x,t) = \rho_{D,R} + \rho_{D,L}$ since the cross terms do not contribute when integrating over the fields in the action. Before calculating the action, the first step in bosonising the Fermi fields needs to take place by writing

$$\psi_\eta(x,t) = \chi_\eta \exp\big(i\theta_\eta(x,t)\big), \tag{4.11}$$

where $\theta_\eta(x,t)$ is a bosonic field which describes the left and right moving particles, and χ_η is a Majorana field which is required to preserve the Fermi statistics and is spatially independent. Importantly, the Majorana field has the property that the particle and anti particle are equivalent, given by $\bar{\chi} = \chi$. If this new field is substituted into the directional action, the result is

$$S'_{0\eta} = \int dx dt \chi_\eta [i\partial_\eta - \alpha_\eta]\chi_\eta, \tag{4.12}$$

where $\alpha_\eta = \partial_\eta \theta_\eta$. Since this new variable has been introduced, a gauge transformation must be considered where

$$\psi_\eta(x,t) = \psi'_\eta \exp\big(i\theta_\eta(x,t)\big), \tag{4.13}$$

such that $\psi'_\eta = \chi_\eta \exp\Big(i\theta'_\eta(x,t)\Big)$. Later in the thesis (see Appendix B) it will be beneficial to calculate current-current and density-density correlation functions, subsequently it is useful to write in terms of the partition function. The functional integral for this system becomes

$$Z_\eta = \int \mathcal{D}\bar{\psi}\mathcal{D}\psi \exp\big(iS_{0\eta}\big) = J(\alpha_\eta) \int \mathcal{D}\bar{\psi}'\mathcal{D}\psi' \exp\Big(iS'_{0\eta}\Big) = J(\alpha_\eta) Z'_\eta. \tag{4.14}$$

The Jacobian for this gauge transformation must be calculated since this also contributes to the action. Consequently, the Jacobian is found to be (see appendix A)

$$J(\alpha) = J(\theta_R, \theta_L) = J_+ J_- = \exp\Big[-\sum_\eta \frac{i\eta}{4\pi} \operatorname{Tr}\Big(\partial_\eta \theta_\eta \partial_x \theta_\eta\Big)\Big], \tag{4.15}$$

and therefore the entire action is due to the contribution from the Jacobian. Using this, the action can be written as

$$S_{0\eta} = -i \ln\big(J(\alpha_\eta)\big) = -\frac{\eta}{4\pi} \operatorname{Tr}\Big(\partial_\eta \theta_\eta \partial_x \theta_\eta\Big). \tag{4.16}$$

To write the action in a more convenient form, new variables are introduced in the form of

$$\phi = \frac{1}{2}(\theta_R - \theta_L), \tag{4.17}$$

and

$$\theta = \frac{1}{2}(\theta_R + \theta_L). \tag{4.18}$$

When these new variables are substituted into $-\sum_\eta \frac{\eta}{4\pi} \operatorname{Tr}\big(\partial_\eta \theta_\eta \partial_x \theta_\eta\big)$, the action becomes

$$S_0 = \sum_\eta S_{0\eta} = \frac{1}{2\pi} \int dx dt \big(-\partial_t \phi \partial_x \theta - \partial_t \theta \partial_x \phi - v_f [(\partial_x \phi)^2 + (\partial_x \theta)^2]\big). \tag{4.19}$$

The first two terms in the integral can be integrated by parts which yields a generalised coordinate $\partial_x \phi$, and a generalised momentum $\partial_x \theta$, which then implies that

$$\mathcal{H}_0 = \frac{v_f}{2\pi} \int dx dt [(\partial_x \phi)^2 + (\partial_x \theta)^2], \tag{4.20}$$

since the terms resemble the general expression for the Lagrangian, $\mathcal{L} = p\dot{q} - \mathcal{H}_0$. Before the interaction term is added, the density field needs to be rigorously defined. If it is treated as normally known, $\rho_{D,\eta}(x,t) = \bar{\psi}_\eta(x,t)\psi_\eta(x,t)$, then a quantum field theory anomaly occurs. Therefore, to ensure a contribution occurs from the density, it needs to be introduced via a source field, h_η such that

$$S_0(h) = S_0 - i\sum_\eta \bar{\psi}_\eta h_\eta \psi_\eta = i \sum_\eta \int dx dt \bar{\psi}_\eta (\partial_\eta - h_\eta)\psi_\eta. \tag{4.21}$$

Consequently to calculate any correlation function involving the density, the Jacobian needs to be calculated by using similar functional integral techniques and using the Green's function without the source field due to no contribution from the density field and dividing it by the Green's function which includes the source field. After manipulation, this yields

$$J_\eta(h) = \exp\left[iS_0 - \frac{i\eta}{2\pi}\int dxdt\, h_\eta \partial_x \theta_\eta\right]. \tag{4.22}$$

The calculation is performed in a similar way as shown in appendix A. Now since the density can be explicitly obtained by taking the derivative of the non-interacting action with respect to the source field, which implies

$$\rho_{D,\eta} = -i\frac{\partial \ln Z_{0\eta}(h)}{\partial h_\eta} = -\frac{\eta}{2\pi}\partial_x \theta_\eta, \tag{4.23}$$

and therefore the full density is

$$\rho_D = \sum_\eta \rho_{D,\eta} = \rho_{D,R} + \rho_{D,L} = -\frac{1}{\pi}\partial_x \phi. \tag{4.24}$$

Now the density has been defined, the interaction term can be added to the Hamiltonian. A typical interaction is the density-density interaction, and the interaction can be defined to be a contact interaction, this results in

$$\begin{aligned}\mathcal{H}_{int} &= \int_{\text{Contact}} dxdx' \bar{\psi}(x)\bar{\psi}(x')V(x,x')\psi(x)\psi(x') \\ &\to V\int dx \rho_D^2(x) = V\int dx\big(-\frac{1}{\pi}\partial_x\phi\big)^2.\end{aligned} \tag{4.25}$$

However, this potential V does not take into account the different interactions between the different moving particles, namely R-R, L-L and R-L interactions. Terminology is introduced to define these types of interactions such that the R-L interaction is defined as g_2 interaction, and the R-R and L-L interactions are defined as g_4. The diagram in figure 4.1 shows the g_4 interaction. The solid lines represent a right moving fermion, and the dashed lines represent a left moving fermion. The arrows represent time.

The g_4 interaction for two fermions on the same side of Fermi surface

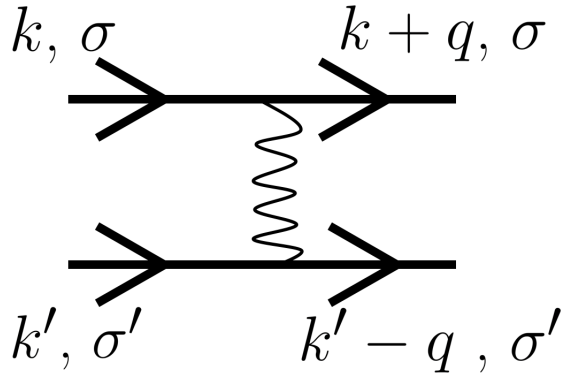

FIGURE 4.1: This diagram shows the g_4 interaction. This is a coupling interaction for fermions on the same side of the linearised Fermi spectrum. Both fermions are right moving, and the interaction maintains the directionality.

The next diagram shows the mechanism for the g_2 interaction.

The g_2 interaction for two fermions on opposite sides of the Fermi surface

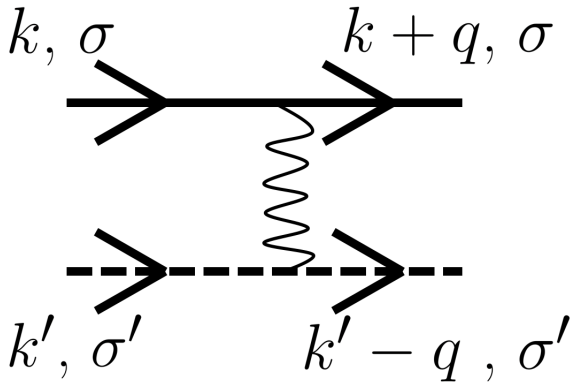

FIGURE 4.2: This diagram shows the g_2 interaction. This is a coupling interaction for a left moving fermion and a right moving fermion on opposite sides of the linearised Fermi spectrum. This does not change the directionality of the fermions. Hence the fermions remain on their original side of the linearised Fermi spectrum, this represents forward scattering.

There is also the possibility for backscattering interactions but these are known as g_1 and g_3 interactions and will not be discussed here as currently we have not taken spin into account. The interacting Hamiltonian can be written as

$$\mathcal{H}_{int} = \int dx \big(\frac{g_4}{2}\sum_{\eta}\rho^2_{D,\eta} + g_2\rho_{D,R}\rho_{D,L}\big), \tag{4.26}$$

and $\mathcal{H}_0$ is given by

$$\mathcal{H}_0 = \frac{v_f}{2\pi} \int dxdt[(\partial_x\phi)^2 + (\partial_x\theta)^2]. \tag{4.27}$$

The full Hamiltonian is

$$\begin{aligned}\mathcal{H} = \mathcal{H}_0 + \mathcal{H}_{int} = \frac{1}{4\pi^2}\Big[(2\pi v_f + g_4) \int dxdt[(\partial_x\phi)^2 + (\partial_x\theta)^2] \\ -g_2 \int dxdt\big(\partial_x\theta_L \partial_x\theta_R\big)\Big],\end{aligned} \tag{4.28}$$

which becomes

$$\begin{aligned}\mathcal{H} = \mathcal{H}_0 + \mathcal{H}_{int} = \frac{1}{4\pi^2}\Big[(2\pi v_f + g_4) \int dxdt[(\partial_x\phi)^2 + (\partial_x\theta)^2] \\ -g_2 \int dxdt[(\partial_x\theta)^2 - (\partial_x\phi)^2]\Big].\end{aligned} \tag{4.29}$$

After algebraic manipulation, this can be simplified to the standard well known Luttinger liquid Hamiltonian given by

$$\mathcal{H} = \frac{u}{2\pi}\Big[\frac{1}{K}(\partial_x\phi)^2 + K(\partial_x\theta)^2\Big], \tag{4.30}$$

where $u = v_f K$, K is the Luttinger parameter and is defined by

$$K = \sqrt{\frac{2\pi v_f + g_4 - g_2}{2\pi v_f + g_4 + g_2}}. \tag{4.31}$$

A different derivation is found in [81]. A major benefit of this theory is that the Hamiltonian is quadratic and thus is exactly solvable which allows for completely analytic solutions.

Using this Luttinger Hamiltonian, the action can be written as

$$S = \int dxdt\Big\{\frac{1}{\pi}\nabla\theta\partial_t\big(\partial_x\phi\big) - \frac{u}{2\pi}\Big[\frac{1}{K}(\partial_x\phi)^2 + K(\partial_x\theta)^2\Big]\Big\}, \tag{4.32}$$

where one of the fields can be integrated out [81] to give

$$S = \int dxdt\frac{K}{2\pi}\Big[\frac{1}{u}\big(\partial_t\theta\big)^2 - u\big(\partial_x\theta\big)^2\Big], \tag{4.33}$$

or

$$S = \int dxdt\frac{1}{2\pi K}\Big[\frac{1}{u}\big(\partial_t\phi\big)^2 - u\big(\partial_x\phi\big)^2\Big]. \tag{4.34}$$

This total action contains everything that is expected in the standard Luttinger liquid theory. However to reproduce the experiment, more terms must be added to the total action. The main terms that need to be studied are the Josephson coupling as it represents superconductivity, the disorder term, and an extra spin interaction which included backscattering. To explain the experiment, a positive correlation must be found between the Josephson coupling and disorder. With this action, the model for the system can be constructed.

4.1.2 Full Action for Model

Now the Luttinger liquid theory has been rigorously introduced, an attempt to construct a model which reproduces the experiment [3] can be performed. The action that is used is essentially the same as one in the book by Giamarchi [81], except weak Josephson coupling is allowed between the wires. It is based upon taking the standard action that has been derived previously, and allowing for this action to have spin and charge parts, such that

$$S = \sum_{\eta} \int dx d\tau \frac{1}{2\pi K_\eta} \Big[\frac{1}{u_\eta} \big(\partial_\tau \phi_\eta\big)^2 + u_\eta \big(\partial_x \phi_\eta\big)^2 \Big]. \tag{4.35}$$

where $\eta = \rho, \sigma$, where ρ and σ are the charge and spin degrees of freedom respectively. Also, the fields have been changed to imaginary time. Since spin has been introduced, another type of interaction can occur known as g_1 which is when backscattering occurs for one type of interaction given by the term $\bar{R}_\uparrow \bar{L}_\downarrow R_\downarrow L_\uparrow$. Diagrammatically, this is given as

The $g_{1\perp}$ interaction for two fermions on opposite sides of the Fermi surface

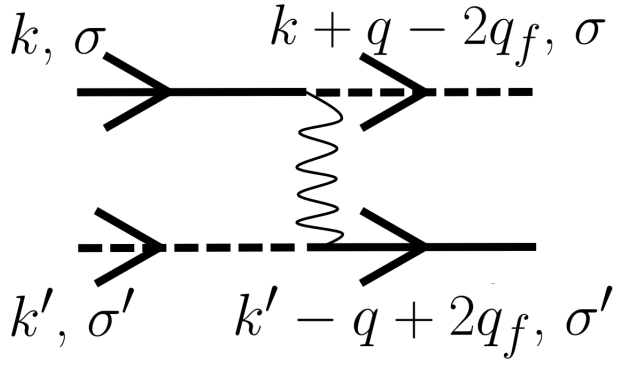

FIGURE 4.3: This diagram shows the $g_{1\perp}$ interaction. The interaction couples fermions on opposite sides of the linearised Fermi spectrum, and then changes the direction of each fermion. Therefore the left moving fermion becomes right moving, and vice versa. $g_{1\perp}$ is a backscattering interaction in which the interaction results in the fermions changing sides.

Consequently, this term has to be added to the action, and is defined as

$$S_{\perp} = -\frac{2g_{1\perp}}{(2\pi\alpha)^2}\int dx \cos\left(\sqrt{8}\phi_{\sigma}\right), \tag{4.36}$$

where α is a small parameter cutoff and $g_{1\perp}$ only occurs in the perpendicular direction. With this new $g_{1\perp}$ term, the Luttinger parameter K is modified such that it contains the $g_{1\perp}$ terms in the numerator and denominator of the square root, with the same sign as g_2. Since this experiment requires a disorder term, this is added by defining

$$S_{dis} = -\frac{D_b}{(2\pi\alpha)^2}\sum_{s}\int dx d\tau d\tau' \cos\Big[2\big(\phi_s(x,\tau) - \phi_s(x,\tau')\big)\Big], \tag{4.37}$$

where D_b is the bare disorder parameter, and $s = \uparrow, \downarrow$. To add the superconducting term, use the Josephson coupling definition which is given by

$$S_J = -J\sum_{i,j}\int dx d\tau \cos\left[\sqrt{2}\big(\phi_{\rho}^{i}(x,\tau) - \theta_{\sigma}^{i}(x,\tau) - (\phi_{\rho}^{j}(x,\tau) - \theta_{\sigma}^{j}(x,\tau))\big)\right], \tag{4.38}$$

where i, j denote the wires and J is the superconducting coupling. Using all of this, the total action is given by

$$\mathcal{S} = S_{\rho} + S_{\sigma} + S_{\perp} + S_{dis} + S_J. \tag{4.39}$$

From this action, renormalisation group equations can be written for the system to give a description of the physics at the energy scales in condensed matter physics.

4.1.3 Renormalisation Group (RG) Analysis

Renormalisation Group theory [83] is one of the pillars of modern theoretical physics. The whole of the standard model in particle physics relies on the theory, and it is widely applied in condensed matter physics. The RG implemented within this thesis is Wilson RG [84]. The general approach is to split the modes into fast modes and slow modes, and then to integrate one of the modes out so the action is dependent on one of the modes only. At this point the action can be rescaled and renormalised. From this, the RG equations can be extracted, which will then describe the physics at either the slow or fast mode scenario. In condensed matter physics, since low energies are generally dealt with, the fast modes

are integrated out in this scenario, such that the action is dependent on slow modes which correspond to low energies.

By performing Giamarchi-Schulz RG analysis [85], see Appendix B for full derivation of one of the equations, the equations derived from the action (4.39), are given by

$$\begin{aligned}
\tilde{y}' &= -2(\tilde{K}_\sigma - 1)\tilde{y} - D, \\
\tilde{K}_\sigma' &= -\frac{1}{2}\tilde{K}_\sigma^2\tilde{y}^2 - \frac{1}{2}\tilde{K}_\sigma^2 D, \\
\tilde{K}_\rho' &= -\frac{1}{2}\tilde{K}_\rho^2\frac{u_\rho}{u_\sigma}D, \\
D' &= -(\tilde{K}_\sigma + \tilde{K}_\rho + \tilde{y} - 3)D, \\
J' &= \Big(2 - \tilde{K}_\sigma - \frac{1}{\tilde{K}_\rho}\Big)J, \\
\tilde{u}_\rho' &= -\frac{\tilde{u}_\rho^2}{2\tilde{u}_\sigma}\tilde{K}_\rho D, \\
\tilde{u}_\sigma' &= -\frac{\tilde{u}_\sigma\tilde{K}_\sigma}{2}D.
\end{aligned} \tag{4.40}$$

where $y = g_{1\perp}/\pi$, $D = \Big((2D_b\alpha)/(\pi u_\sigma^2)\Big)\Big(u_\sigma/u_\rho\Big)^{K_\rho}$, and the differentiation is with respect to $-\ln T \equiv l$. The tilded variables are defined in equation (4.43). Note that J and D are not tilded. The tilded variables result from introducing a low energy cutoff in the integral such that $|\tau - \tau'| < \alpha$, which leads to separating the integral into two terms for different times [85, 86]. Since one of the terms can be absorbed into the standard Luttinger liquid, and it is coupled to the $g_{1\perp}$ term, this leads to the re-definition of $\tilde{g}_{1\perp}$ given by

$$\tilde{g}_{1\perp}(l) = g_{1\perp}(l) - \frac{2D_b\alpha}{u_\sigma}. \tag{4.41}$$

Therefore the remaining terms are re-defined due to the $g_{1\perp}$ interaction. To solve the RG equations, it is mathematically convenient to solve the equations in the tilde form, then substitute in the bare parameters after. By considering equation (4.40), it can be shown that $\tilde{u}_\rho/\tilde{K}_\rho$ is constant, which implies that $\tilde{u}_\rho$ can be removed by letting

$$\tilde{u}_\rho = \Big(\frac{\tilde{u}_\rho}{\tilde{K}_\rho}\Big)\tilde{K}_\rho = \Big(\frac{\tilde{u}_\rho^{(0)}}{\tilde{K}_\rho^{(0)}}\Big)\tilde{K}_\rho. \tag{4.42}$$

The bare parameters can be found by substitution and expansion for small D, such that

$$\begin{aligned}
\tilde{g}_1^{\perp} &= g_1^{\perp} - \pi u_\sigma D\Big(\frac{u_\rho^{(0)}K_\rho}{K_\rho^{(0)}u_\sigma}\Big)^{K_\rho},\\
\tilde{K}_\rho &= K_\rho - \frac{K_\rho^2+1}{4}D\Big(\frac{u_\rho^{(0)}K_\rho}{K_\rho^{(0)}u_\sigma}\Big)^{K_\rho},\\
\tilde{K}_\sigma &= K_\sigma - \frac{K_\sigma^2+1}{4}D\Big(\frac{u_\rho^{(0)}K_\rho}{K_\rho^{(0)}u_\sigma}\Big)^{K_\rho},\\
\tilde{y} &= y - D\Big(\frac{u_\rho^{(0)}K_\rho}{K_\rho^{(0)}u_\sigma}\Big)^{K_\rho},\\
\tilde{u}_\sigma &= u_\sigma + \frac{K_\sigma^2-1}{4K_\sigma}u_\sigma D\Big(\frac{u_\rho^{(0)}K_\rho}{K_\rho^{(0)}u_\sigma}\Big)^{K_\rho},
\end{aligned} \tag{4.43}$$

where (0) represents the initial conditions. With these relations between the bare parameters and the tilded parameters, the RG equations can be written purely in terms of the bare parameters to yield

$$\frac{dK_\rho}{dl} = -\frac{1}{4}\big(K_\rho^2+1\big)\big(K_\rho+K_\sigma+y-3\big)D\Big(\frac{u_\rho^{(0)}K_\rho}{K_\rho^{(0)}u_\sigma}\Big)^{K_\rho} - \frac{1}{2}\frac{u_\rho^{(0)}K_\rho^3}{K_\rho^{(0)}u_\sigma}D, \tag{4.44}$$

$$\frac{dK_\sigma}{dl} = -\frac{1}{2}K_\sigma^2 y^2 - \Big[\frac{1}{4}\Big(K_\sigma^2+1\Big)\Big(K_\rho+K_\sigma+y-3\Big) - yK_\sigma^2\Big]D\Big(\frac{u_\rho^{(0)}K_\rho}{K_\rho^{(0)}u_\sigma}\Big)^{K_\rho} - \frac{1}{2}K_\sigma^2 D, \tag{4.45}$$

$$\frac{dy}{dl} = 2(1-K_\sigma)y + \Big[1+K_\sigma-K_\rho+\frac{y}{2}\Big(K_\sigma^2-1\Big)\Big]D\Big(\frac{u_\rho^{(0)}K_\rho}{K_\rho^{(0)}u_\sigma}\Big)^{K_\rho} - D, \tag{4.46}$$

$$\frac{dD}{dl} = -(K_\rho+K_\sigma+y-3)D, \tag{4.47}$$

$$\frac{du_\sigma}{dl} = \frac{K_\sigma^2-1}{4K_\sigma}\Big(K_\sigma+K_\rho+y-3\Big)u_\sigma D\Big(\frac{u_\rho^{(0)}K_\rho}{K_\rho^{(0)}u_\sigma}\Big)^{K_\rho} - \frac{u_\sigma K_\sigma}{2}D, \tag{4.48}$$

$$\frac{dJ}{dl} = \Big(2-K_\sigma-\frac{1}{K_\rho}\Big)J. \tag{4.49}$$

Now these coupled differential equations must be solved, and the dependency on the superconducting onset temperature and the bare value of disorder must be studied.

4.2 Disorder Induced Superconductivity

The coupled differential equations derived above represent all the necessary physics contained within the system. Before solving them numerically, an attempt to understand any

analytical properties can be made. Since in the experiment [3], the measurable is resistivity, one needs to extract resistivity from the equations. which is given by [85]

$$\rho(l) = D(l)\exp(-l), \tag{4.50}$$

from which

$$\rho(T) = D(T)T. \tag{4.51}$$

This equation for resistivity is used because the system is far into the localisation phase [81]. To reproduce the experiment, one of the main signatures is a large jump in the minimum of resistivity at a specific value for a small increase in disorder. This is shown in figure 4.4 [3].

The temperature at which the minimum of the resistivity occured against the initial value of disorder.

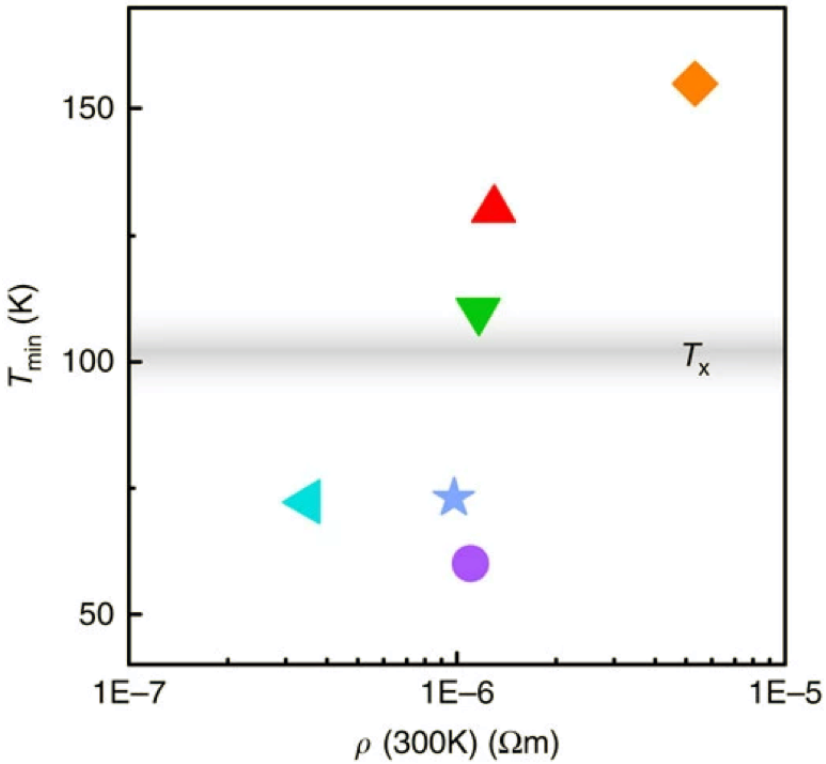

FIGURE 4.4: This graph was taken from the experimental paper [3] and shows how there is a sudden jump in the temperature at the minimum of resistivity for a slight increase in disorder. This is a clear signature of the experiment.

The minimum in resistivity must be found from the derived equations. By substituting equation (4.47) into (4.50) and minimising, it is found that

$$\rho'(l) = -\big(K_\rho + K_\sigma + y - 2\big) D \exp(-l) = 0, \tag{4.52}$$

which means the minimum will occur when $K_\rho + K_\sigma + y - 2 = 0$. Consequently, this will be one of the measurables that will be plotted in the numerical analysis. $K_\rho + K_\sigma + y$ is known as the scaling dimension of disorder and is denoted by $[D(l)]$. From this, the jump in resistivity should be found accurately as finding the point where the scaling dimension of disorder minus two $\big([D(l)] - 2\big)$ crosses zero defines the minimum. To reproduce the experiment, this must produce large differences for small change in disorder.

Another important feature to be extracted comes from equation (4.49), since this fundamentally denotes the superconductivity in the system. It is imperative that it is always increasing, especially with increasing disorder. The RG equation for J' can be solved as

$$J(l) = J_0 \exp\Big[\int_0^{l_c} dl \Big(2 - K_\sigma - \frac{1}{K_\rho}\Big)\Big]. \tag{4.53}$$

Therefore, to get an increasing superconducting coupling constant, $2 - K_\sigma - \frac{1}{K_\rho} > 0$, and henceforth $K_\sigma + \frac{1}{K_\rho} < 2$. This is another key measurable that will be evaluated. Similarly, $K_\sigma + \frac{1}{K_\rho}$ is known as the scaling dimension of superconductivity and is denoted by $[J(l)]$.

Another important aspect is the use of RG within this model. RG is only valid for small interaction parameters due to the rescaling in the theory, so when a parameter becomes of order one, then the evolution of the system with respect to temperature must be stopped as the physics becomes invalid. The physical implications for this are emphasised later in 4.2.1.

4.2.1 Numerical Results

With a problem of this nature, the choices for initial conditions are important. Since there are six initial conditions that need to reflect the experiment, the choice for these cannot be arbitrary. Since the focus of this theory is to determine how disorder changes the system, it is beneficial to start without disorder, and examine how the system evolves under increasing disorder. This is achieved by taking equations (4.44-4.49), and taking $D = 0$. From this the separatrix of the system can be found. When disorder is ignored, only $\tilde{y}$ and $\tilde{K}_\sigma$ vary. A

solution for $\tilde{y}$ can be found as

$$\tilde{y}^2 = 8\Big(\frac{1}{\tilde{K}_\sigma} + \ln \tilde{K}_\sigma - C\Big), \tag{4.54}$$

where $C = 1$. Consequently, the RG trajectories without disorder will flow according to equation (4.54). This is shown in figure 4.5.

The RG flow for the disorderless system

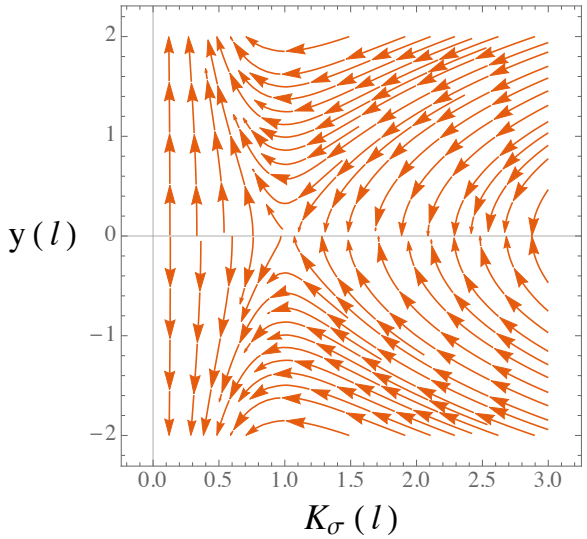

FIGURE 4.5: This graph shows the how the trajectories for initial points will flow in the disorderless case. By studying this graph for the disordered case, it can be deduced how disorder affects the system.

The numerical plot is computed in terms of the bare disorderless parameters. Therefore increasing disorder will change how the trajectories flow, and thus will change the way the system behaves. By varying the strength of the disorder, the amount by which the system changes can be studied specifically in figures (4.9, 4.23).

The numerical results have been solved using Mathematica, where the solutions to the coupled differential equations have been found, and then these results have been plotted. The main plot that is considered depicts y against K_σ, as it is known how the RG flow develops without disorder. Introducing disorder signifies how certain phase transitions are induced by disorder. Once trajectories and values of disorder have been decided, then physical measurables are shown, namely resistivity and when superconducting order emerges.

The first numerical analysis experiment reveals whether the model predicts disorder induced superconductivity. For this, both T_{min} and T_{peak} will be studied. Recall T_{peak} from

figure 1.1. However, for the purposes of the experiment, it is especially important that T_{peak} happens at higher temperatures for higher values of disorder.

After some exploration in selecting the initial conditions, disorder induced superconductivity was numerically observed. This is found by choosing $K_\sigma^{(0)} = 1.4$, $y^{(0)} = -0.563$, $K_\rho^{(0)} = 2.16$, $u_\sigma^{(0)} = 0.6$, $u_\rho^{(0)} = 0.7$, $J^{(0)} = 0.45$. Using a disorder range which varies as $D^{(0)} = 0.09, 0.11, 0.13, 0.15$, the impact of disorder on the system is shown in figures (4.6 - 4.19)

The graphs for the important features, in addition to the graphs of the parameters are shown below.

Resistivity for varying disorders

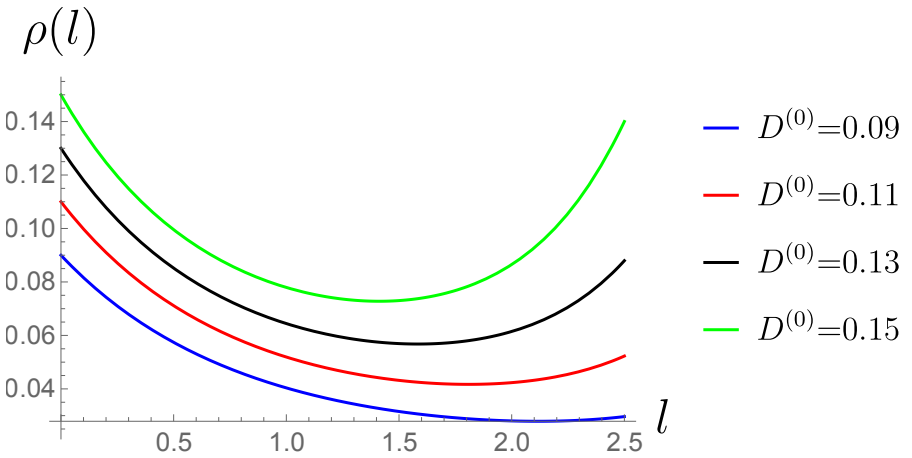

FIGURE 4.6: The plot shows clear minimum for three values of disorder. It is useful to consult the scaling dimension of disorder to check whether the sign of the solution is changed from negative to positive as a confirmation in the minimum of resistivity.

Scaling dimension of disorder - 2 for varying disorders

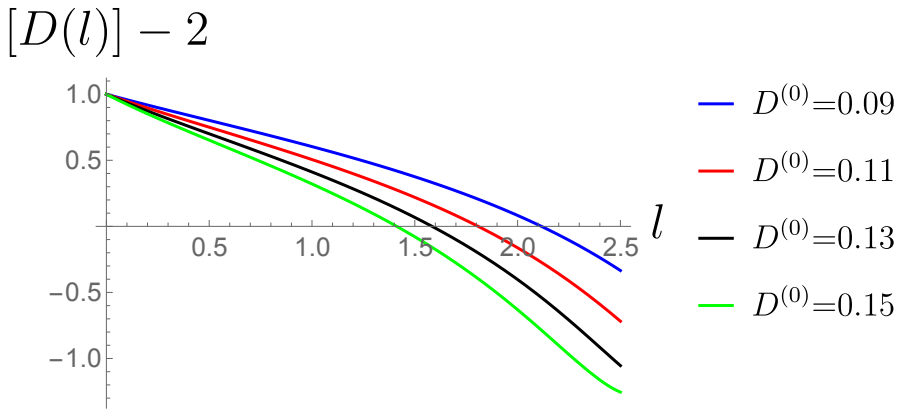

FIGURE 4.7: This graph shows the point at which the minimum in the resistivity occurs, since that corresponds to the point where $K_\rho + K_\sigma + y - 2 = 0$. This graph clearly shows all disorders have a minimum in resistivity as all trajectories cross the l axis. As the strength of disorder increases, the earlier the trajectories cross the l axis.

Scaling dimension of superconductivity - 2 for varying disorders

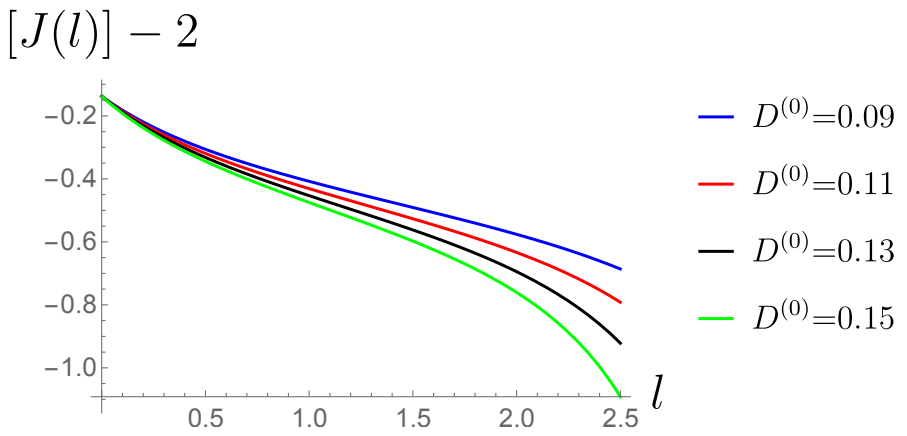

FIGURE 4.8: This graph confirms that all of the disorders give rise to superconductivity, as $J(l)$ will be increasing due to the positive exponent since all trajectories are negative. Importantly, the strongest disorder is the most negative line, and this implies that there is strong correlation with increasing disorder and inducing superconductivity.

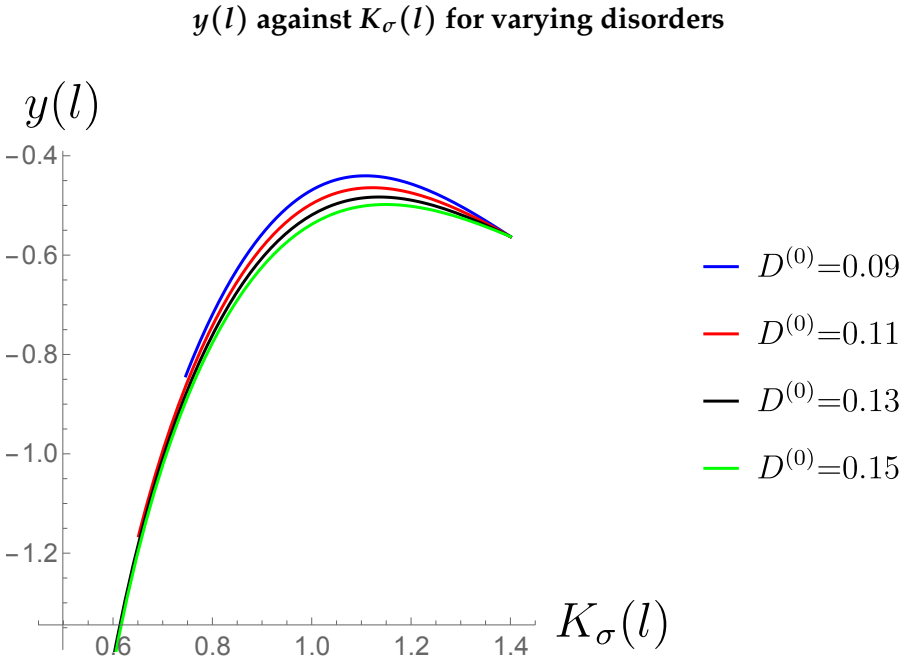

FIGURE 4.9: This is the same axis shown above for figure 4.5. Clearly when disorder is introduced, the trajectories are dramatically shifted. As the strength of disorder is increased from these initial conditions, it appears that it is tending towards diverging $y(l) \to -\infty$ as $K_\sigma(l) \to 0$. This would signify potential spin gap opening.

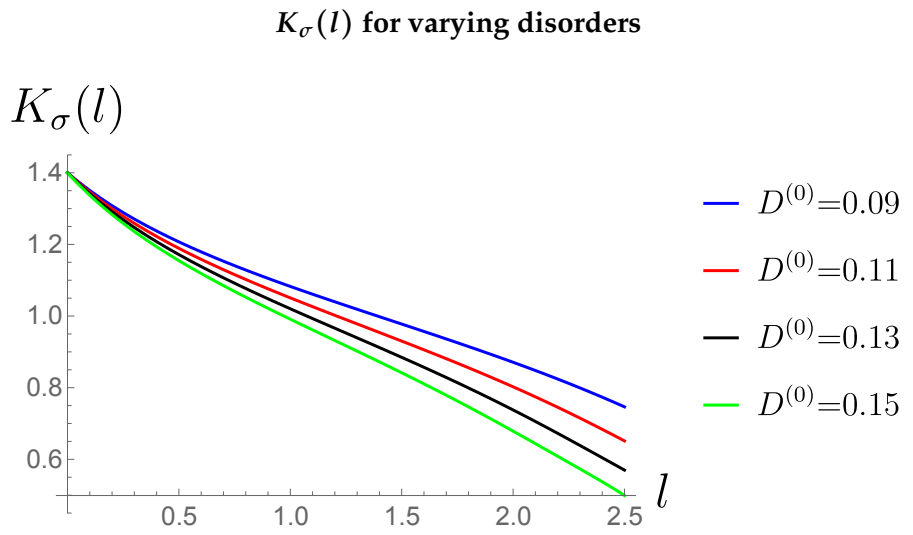

FIGURE 4.10: This graph shows that $K_\sigma(l)$ decreases as the system evolves through temperature. Additionally, the tendency is more pronounced for stronger disorder. This agrees with the $y(l)$ against $K_\sigma(l)$ graph.

$K_\rho(l)$ for varying disorders

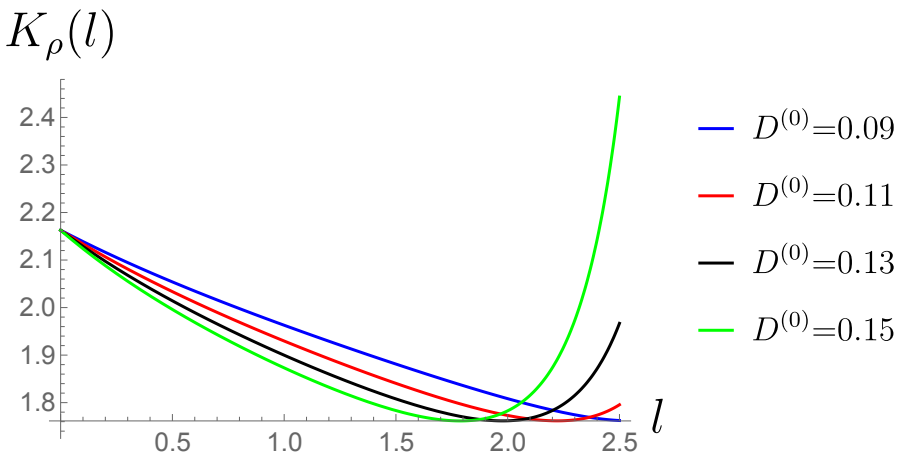

FIGURE 4.11: Similarly to the graph for $K_\sigma(l)$, there is a tendency to decrease $K_\rho(l)$ with increasing disorder. The upturn occurs as the disorder and spin mechanism are becoming dominant.

$J(l)$ for varying disorders

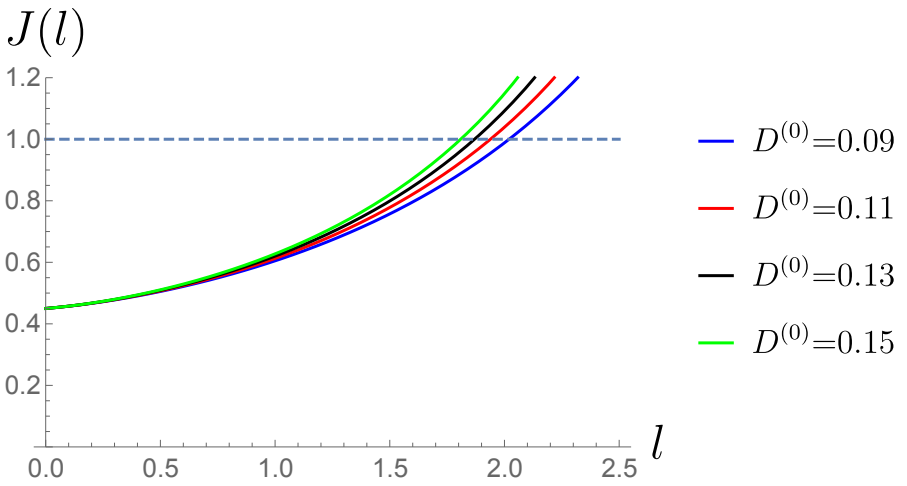

FIGURE 4.12: This graph shows the onset of superconductivity. As previously discussed, due to the RG analysis, when the interaction parameters are of order 1, the system changes into that state. Therefore the state becomes superconducting at $J(l) = 1$ within our framework. As the disorder increases, the temperature at which superconductivity occurs increases. This graph is the first numerical evidence of disorder induced superconductivity. When the trajectories cross $J(l) = 1$, this is defined as the onset of superconductivity

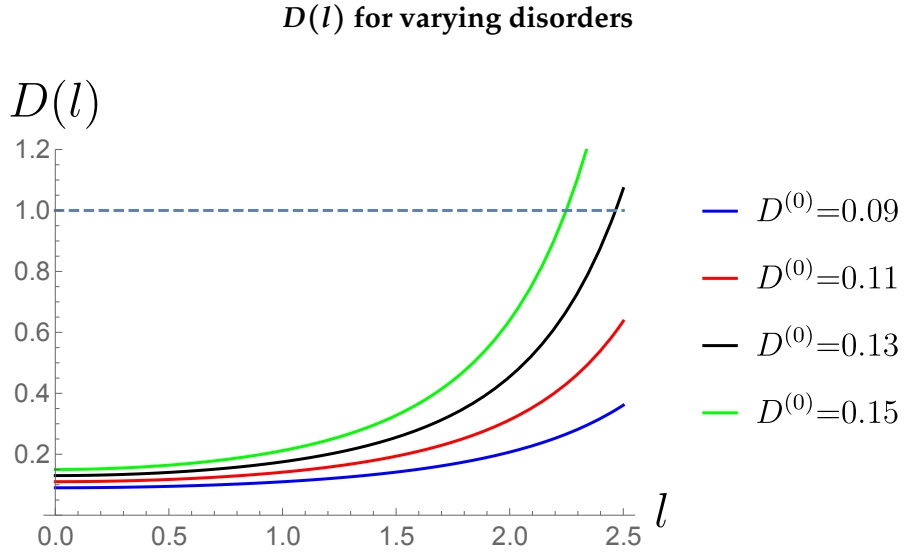

FIGURE 4.13: This graph is important as it must be checked that $D(l) < 1$ before $J(l) = 1$, otherwise the disordered state would dominate and superconductivity would not be able to occur. Fortunately, whilst the two largest disorders cross $D(l) = 1$, this happens after $J(l) = 1$, so the superconducting state is already dominating.

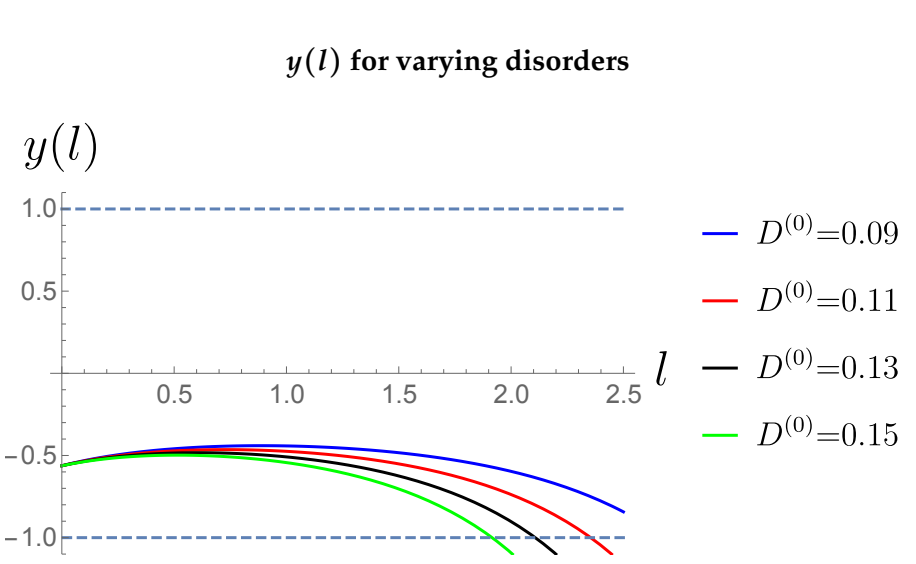

FIGURE 4.14: This graph serves a similar purpose as the disorder graph. It must be checked that $-1 < y < 1$ before $J(l) = 1$, otherwise the spin mechanism would dominate. Whilst there are disorders which cross the $y(l) = -1$ line, this occurs after $J(l) = 1$. In a similar scenario to disorder, this does not change the conclusions about disorder induced superconductivity as the restriction imposed by RG are not contradicted.

To compare our model results with the experiment [3], a scatter graph is taken of $T_{\text{min}}(K)$ and $T_{\text{peak}}(K)$ against the initial values of disorder. Using $l = -\ln T$ to rescale the variables, the graphs are shown in figures 4.15 and 4.16.

The value of l at the minimum for the resistivity against the initial disorder

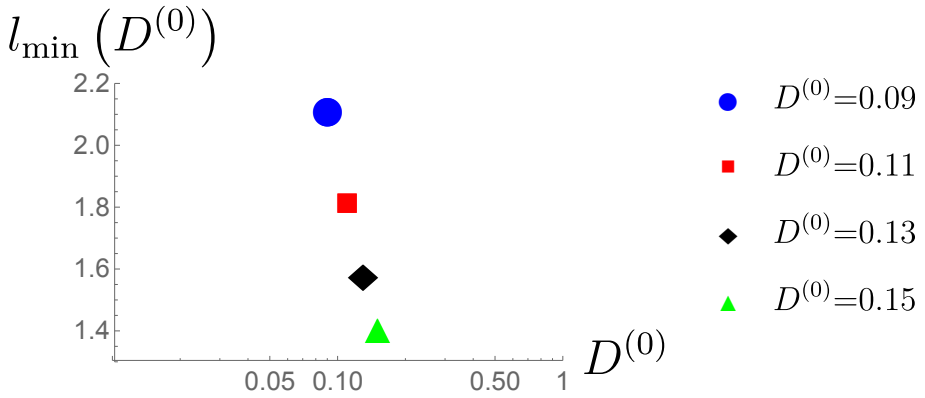

FIGURE 4.15: This graph shows some tendency towards figure 4.4, as it appears to correspond to the middle four disorders which show an increase in T (decrease in l). However, this theory currently does not explain the largest and smallest disorders in the experimental graph.

The value of T at the minimum for the resistivity against the initial disorder

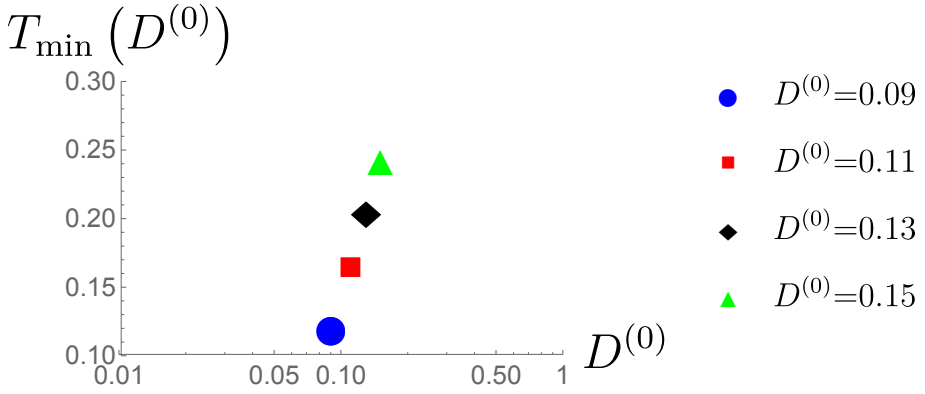

FIGURE 4.16: This graph is now in the form shown in the experiment [3], as in figure 4.4 and this appears to correspond to the middle four disorders in the experiment. As the disorder is increased comparably to the experiment, the jump in $T_{\min}(K)$ is more than doubled, in agreement with the experiment. It is clear that the smallest and largest disorders of the experiment are not explained. A similar logarithmic scale has been used for $D^{(0)}$ to match figure 4.4. If the disorders are extended it remains linear which suggests this does not fully explain the experiement, and the smallest and strongest disorders may occur via a different mechanism. To reconcile the theory with experiment, there must be a plateau for the strong and weak disorders.

To find the peak of the resistivity and thus the onset of superconductivity, the values when $J(l) = 1$ are found for each corresponding disorder, and these values can be plotted.

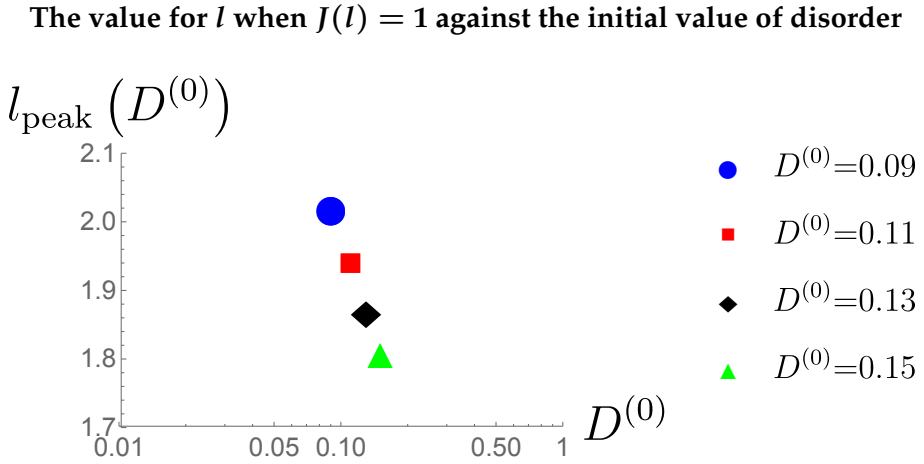

FIGURE 4.17: This graph confirms that disorder does induce superconductivity in this model. As the disorder is increased, the value of l_{peak} is decreased, which corresponds to a higher temperature.

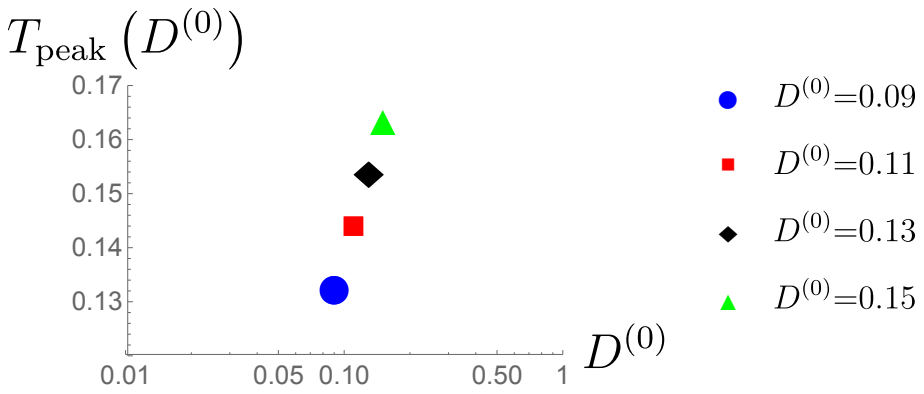

FIGURE 4.18: This graph shows that the onset of superconductivity increases with an increase in disorder. This again confirms the conclusion of disorder induced superconductivity. However, this does not fully match the experimental evidence, as T_{peak} does not increase with disorder as much as expected.

Aditionally, the full resistivity graph can be drawn, where the stop in the graph indicates the onset of superconductivity. This is shown in figure 4.19

The full plots of resistivity, $\rho(T)$ including the onset of superconductivity

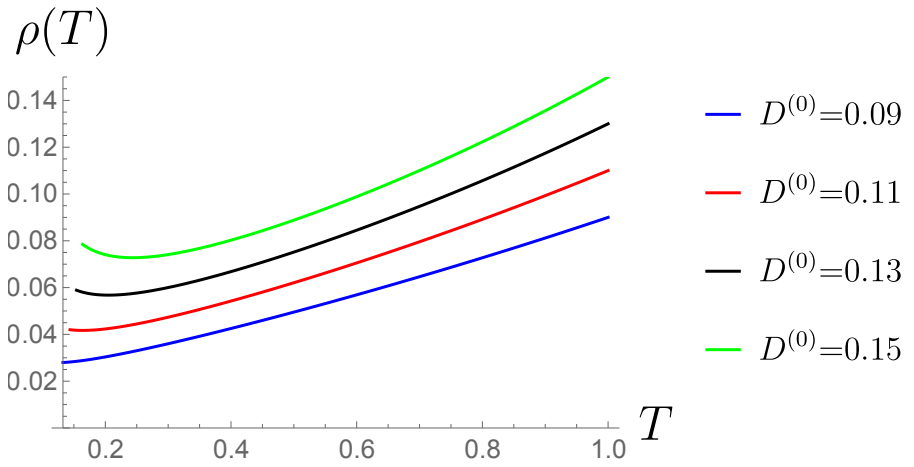

FIGURE 4.19: This graph shows how the resistivity goes through a minimum, and then starts to increase before $J(l) = 1$ occurs, and thus the onset of superconductivity occurs. When this happens, the lines are stopped to indicate the resistivity would vanish at these points.

This section has succeeded in one of the aims of this thesis; to design a theory which describes disorder induced superconductivity. As is clear in figure 4.18, the temperature at which superconductivity occurs is higher for increasing disorder. However, this theory does not currently explain the full experiment, in particular the signature for the graph of $T_{\text{min}}(K)$ against initial disorder. The lowest and strongest disorder still need to be explained. This is where the RG can be exploited, since when $y(l) = \pm 1$, this yields a new set of coupled differential equations. This is explored in the next section.

4.3 Spin Gapped Superconductivity

In an attempt to explain the weakest and strongest disorder, it may be beneficial to consider a different underlying physical mechanism which causes the minimum in the resistivity and then consequently the onset of superconductivity. This leads to the question of what happens when $y(l) = 1$. Recall that $y = g_{1\perp}/\pi$, and g_1 denotes a spin interaction. Therefore when $y(l) = 1$, this corresponds to the spin interaction being dominant as the interaction between the spins is strong, thus fixing the spins in alignment. Since there are two ways the spins can be aligned, parallel or anti-parallel, this corresponds to two different states. The parallel alignment is the ferromagnetic state, whereas the anti-parallel alignment is an antiferromagnetic state.

It has been established that superconductivity can occur in a spin gapped state [87], therefore the aim is to try and reproduce the weakest and strongest disorders that are currently unexplained using a spin gapped mechanism. For a spin gapped system, the spins align anti-parallel, so exhibit antiferromagnetism.

To derive the new coupled differential equations, the fact that the spin is now frozen is used. This results in no spin interactions occuring. Mathematically, this means y, u_σ and K_σ no longer contribute to the evolution of the system in temperature. Therefore the new set of differential equations is given by

$$\frac{dK_\rho}{dl} = -\frac{1}{2}K_\rho^2 D + \frac{1+K_\rho^2}{4}(3-K_\rho)D, \tag{4.55}$$

$$\frac{dD}{dl} = -(K_\rho - 3)D, \tag{4.56}$$

$$\frac{dJ}{dl} = \Big(2 - \frac{1}{K_\rho}\Big)J. \tag{4.57}$$

These equations can be solved in a similar way to before. However before solving them, information can be extracted from the equations analytically. Since the spin gap opening needs to represent the minimum in resistivity, the exponent for resistivity must be positive. By following the same analysis as equation (4.52), the exponent changes sign as $K_\rho = 2$. Since the exponent is negative for $K_\rho > 2$, in order for the resistivity to have a minimum, $K_\rho < 2$. If $K_\rho > 2$ then the resistivity will continue to decrease with no upturn. Therefore it is imperative to ensure that when $y(l) = \pm 1$, $K_\rho < 2$ simultaneously, otherwise the spin gap opening will not describe the experiment as there would be no minimum in resistivity.

Additionally, the superconducting exponent must still be positive to ensure superconductivity will occur as T is decreased. For this to happen $K_\rho > 1/2$, since that means the exponent for J is positive. This restricts $K_\rho \in (1/2, 2)$. All the constraints from using RG will still apply in these new set of equations, which imposes that $J(l) = 1$ has to occur before $D(l) = 1$.

4.3.1 Numerical Results

To find a set of initial conditions which takes into account the disorder induced superconductivity, but also contains a spin gapped mechanism is difficult. A set of conditions was found that may describe all the points except the strongest disorder. This set of conditions

is given by $K_\sigma^{(0)} = 0.8$, $y^{(0)} = 0.25$, $K_\rho^{(0)} = 1.95$, $u_\sigma^{(0)} = 4$, $u_\rho^{(0)} = 0.5$, $J^{(0)} = 0.115$. Then by choosing a disorder range which varies as $D^{(0)} = 0.02, 0.18, 0.19, 0.2, 0.21, 0.22$, this allows three different types of mechanism to occur. The spin gapped scenario when $y(l) = -1$, the real minimum scenario shown in section 4.2, and the spin gapped scenario for $y(l) = 1$. Similar graphs as shown previously are plotted, and comparisons are drawn about the scenario.

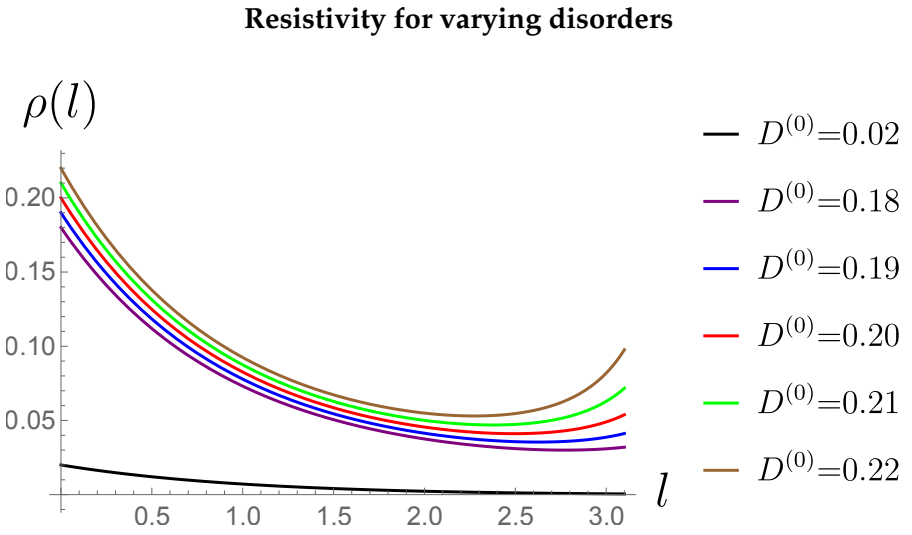

FIGURE 4.20: The smallest disorder does not have an upturn in resistivity, whereas all of the other disorders have this upturn. As expected, the higher disorders are higher in the graph.

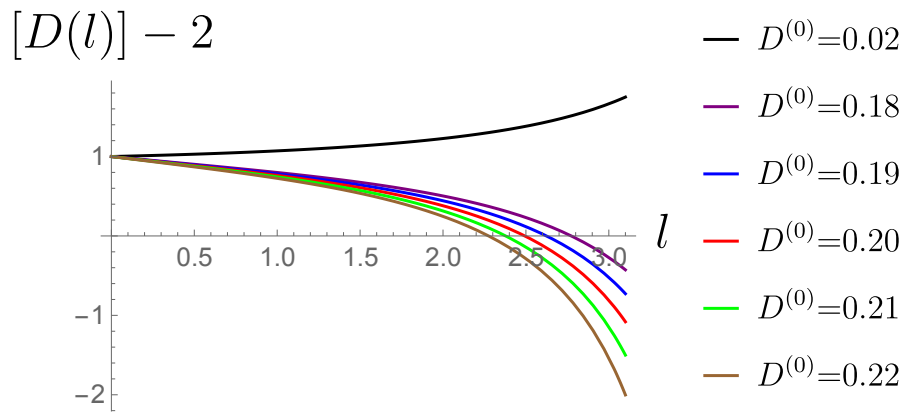

FIGURE 4.21: This graph confirms that for the five strongest disorders there is a minimum in resistivity. Moreover for the weakest disorder there is no minimum in resistivity which initially appears to contradict the experimental results.

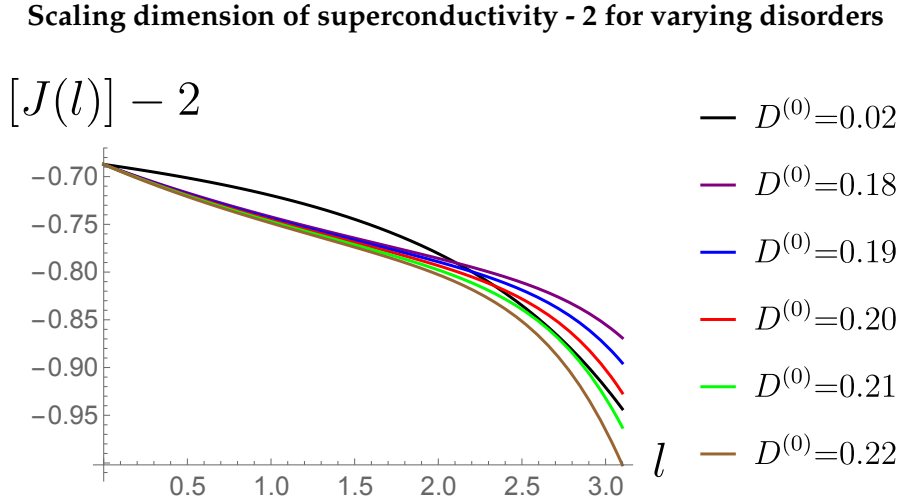

FIGURE 4.22: This graph shows that $J(l)$ is always increasing due to the negative values of $[J(l)]-2$. There is interesting behaviour as there is a crossover for some of the disorders with the weak disorder which suggests that the weak disorder may induce superconductivity faster. However, for the strongest two disorders these would induce superconductivity faster than the weakest disorder.

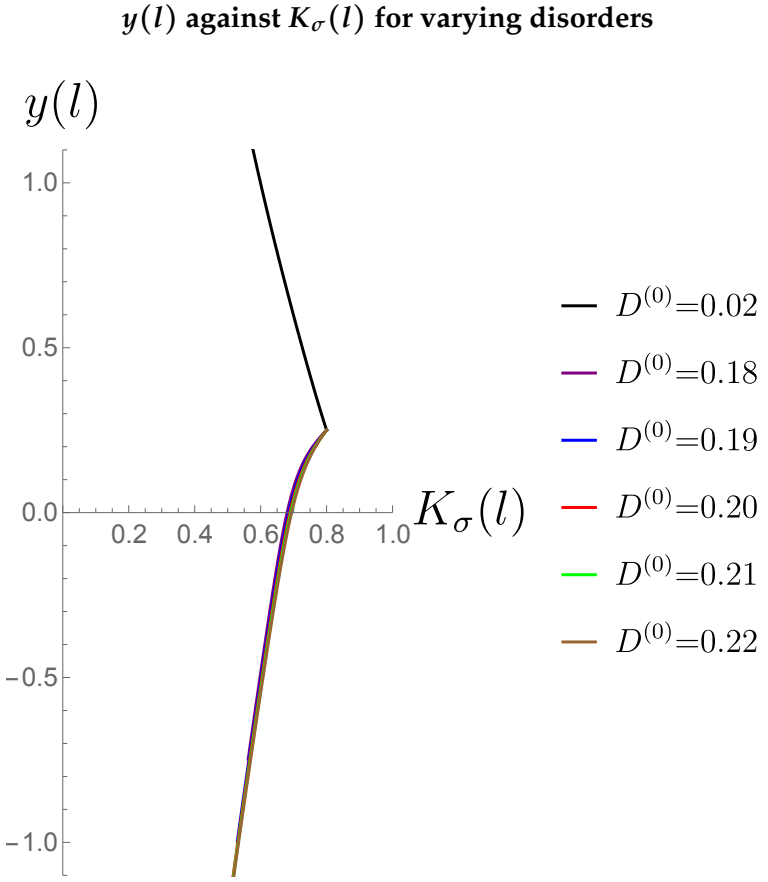

FIGURE 4.23: This graph shows how varying disorder can change the behaviour of the system dramatically. This shows at some point the weak disorder will cross $y(l) = 1$, and conversely the stronger disorder will cross $y(l) = -1$. The other graphs still need to be considered as the system may already be superconducting, or the disorder may be too large, before any of the spin gaps open.

$K_\sigma(l)$ for varying disorders

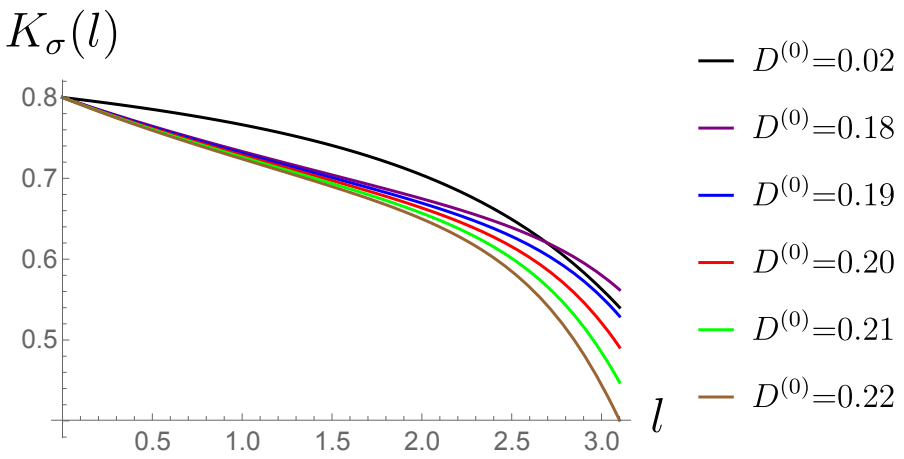

FIGURE 4.24: This graph shows that $K_\sigma(l)$ decays for all disorders. The trajectories decay strongest with the strongest disorder. This appears to agree with figure 4.23.

$K_\rho(l)$ for varying disorders

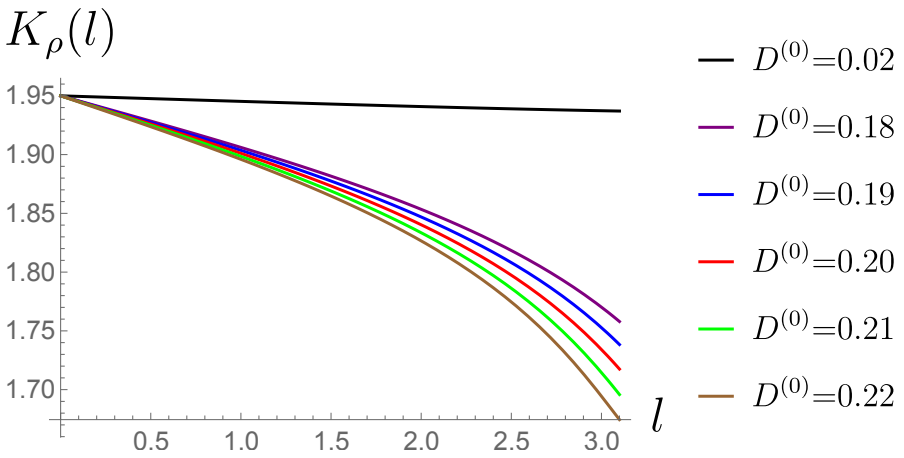

FIGURE 4.25: This graph shows that $K_\rho < 2$ for all disorders which is important. This implies that for any spin gap opening, a minimum will occur and the exponent in resistivity will be positive and therefore resistivity must be increasing. Additionally, this shows that as disorder increases, the rate of increase in resistivity increases.

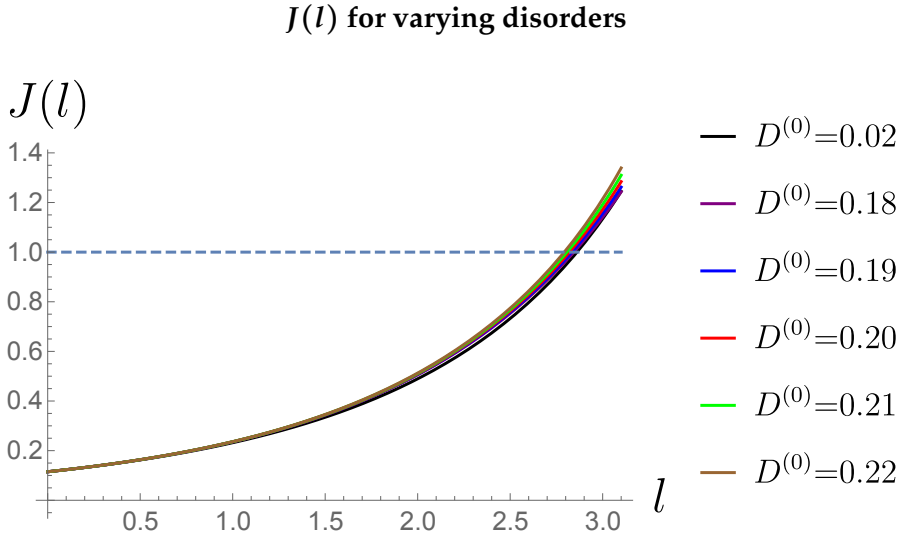

FIGURE 4.26: This graph shows that $J(l) = 1$ occurs for all disorders. This happens in close proximity for all disorders. The strongest disorder appears to occur first. This is confirmed in table 4.1.

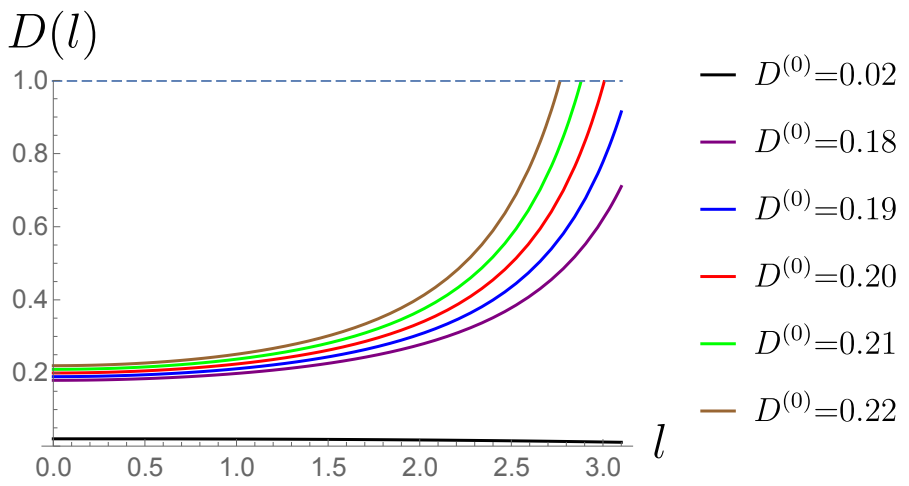

FIGURE 4.27: This graph shows that the three strongest disorders cross with $D(l) = 1$. This is important, as all the relevant physics within the system must occur before this happens for each corresponding disorder, otherwise the RG equations become invalid.

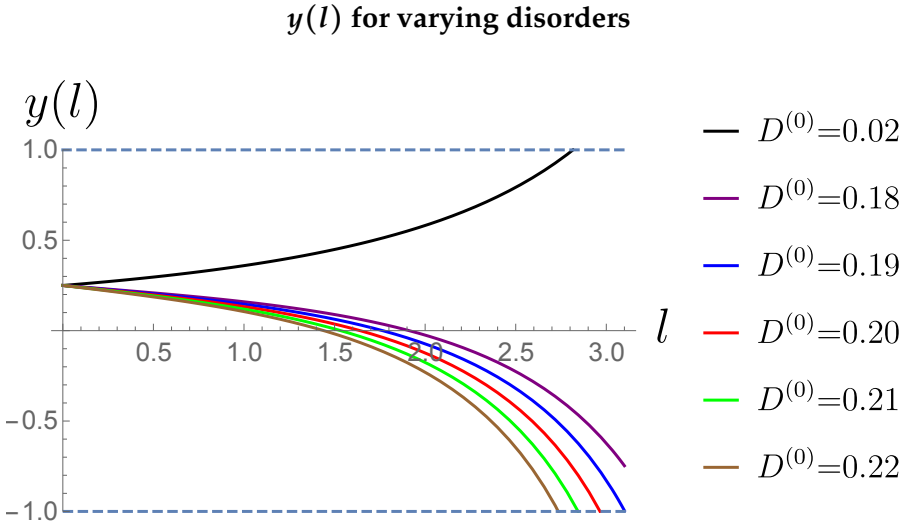

FIGURE 4.28: This graph confirms the observations from figure 4.23. The weakest disorder crosses $y(l) = 1$, and therefore would open up a spin gap when that occurs. Similarly, the strongest three disorders open up a spin gap at $y(l) = -1$. This graph is useful at showing when the spin gaps open.

To compare all of the physics regarding spin gaps, superconductivity, and disorder divergence occurring, the points at which these corresponding phenomena occur need to be found. This is found by numerically computing the values of l, when $D(l) = 1$, $J(l) = 1$, $y(l) = \pm 1$. Additionally, since the experiment shows there must be a minimum in resistivity, which could be due to a spin gap, or $[D(l)] - 2 = 0$, the minimum must also be considered. This is all shown in table 4.1.

TABLE 4.1: This table shows the values for l when all of these important features occur. This does not show what the true $J(l) = 1$ would be for the spin gap scenarios since new equations must be solved. This is since for the weakest disorder $y(l) = 1$ occurs before $J(l) = 1$ and similarly for the strongest disorder, $y(l) = -1$ occurs before $J(l) = 1$. The blank spaces represent the scenarios where the features did not occur, and there was no solution for l.

$D^{(0)}$	0.02	0.18	0.19	0.2	0.21	0.22
$D(l) = 1$		3.313	3.150	3.009	2.882	2.767
$J(l) = 1$	2.861	2.844	2.833	2.820	2.807	2.793
$y(l) = 1$	2.817					
$y(l) = -1$				2.966	2.844	2.734
$[D(l)] - 2 = 0$		2.774	2.624	2.493	2.378	2.275

By studying table 4.1, and knowing that $K_\rho < 2$ for these set of initial conditions, the

minima for resistivity can be plotted. It is seen that the weakest disorder has a minimum which is due to a spin gap opening since $y(l) = 1$. The other disorders have minima which occur due to the exponent in resistivity changing sign in the expected way, as shown in section 4.2. Importantly, these minima occur before any other physical phenomena for the corresponding disorders. In terms of temperature, this means that as the samples are cooled, the first phenomena that are seen are the minima in resistivity. The values for $l_{\min}(D^{(0)})$ and therefore $T_{\min}(D^{(0)})$ are plotted in figures 4.29 and 4.30.

The value of l at the minimum for the resistivity against the initial disorder

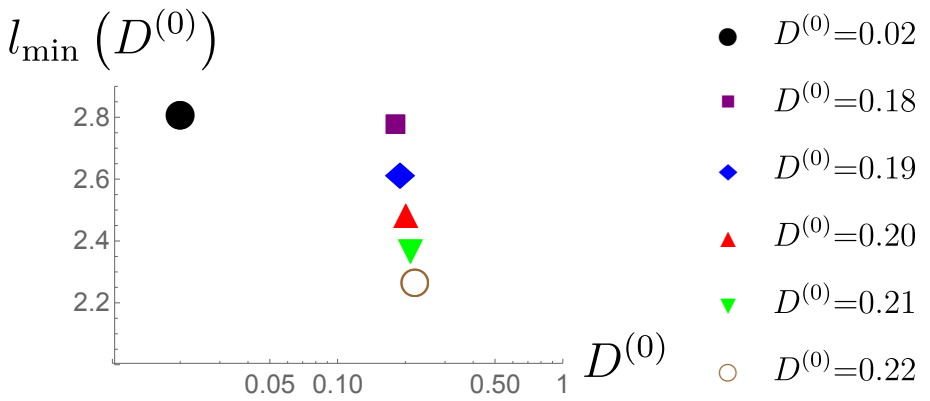

FIGURE 4.29: This graph shows that the weakest disorder appears to display similar characteristics to the experiment. This is since the minimum occurs at a similar temperature, but the value of disorder is significantly lower. This mimics the behaviour of the experiment. Unfortunately the strongest disorder does not plateau as expected. If disorder is increased further, then $l_{\min}(D^{(0)})$ occurs at a similar rate to what is seen currently.

The value of T at the minimum for the resistivity against the initial disorder

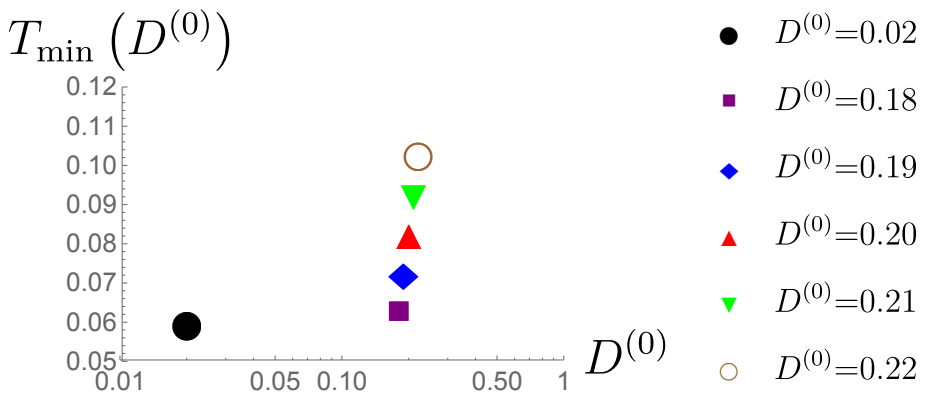

FIGURE 4.30: This graph shows close resemblance to the experimental graph. As disorder is increased there is a plateau, then at a critical disorder a jump in the minimum of resistivity. This appears to be due to the differing mechanisms. However, this still requires investigation. The strongest disorder does not plateau as expected.

Interestingly, there is evidence in the experiment which suggests that the first three disorders occur due to a spin gap mechanism which would suggest this $T_{\min}(D^{(0)})$ graph is incorrect. Therefore it could be coincidence that the form appears correct. This could be worth further investigation in the future.

Previously, the $T_{\text{peak}}(D^{(0)})$ graph was plotted by extracting the points where $J(l) = 1$ for each disorder and plotting these on a scatter graph. In this circumstance, the two spin gap disorders; the weakest and the strongest, have new equations which require solving to find the new values of $J(l) = 1$ for each disorder. This is done by extracting the new initial conditions for equations (4.56), (4.57) and (4.55) by finding the value of these parameters when $y(l) = \pm 1$ for the weak and strong disorder respectively, and substituting that l_c into $K_\rho(l_c)$, $D(l_c)$ and $J(l_c)$. This gives the new set of initial conditions. The equations are subsequently solved and must obey all the standard RG rules.

The new values of $J(l) = 1$ are found, whilst keeping $D(l) < 1$. This is plotted in figure 4.31.

The value for l when $J(l) = 1$ against the initial value of disorder

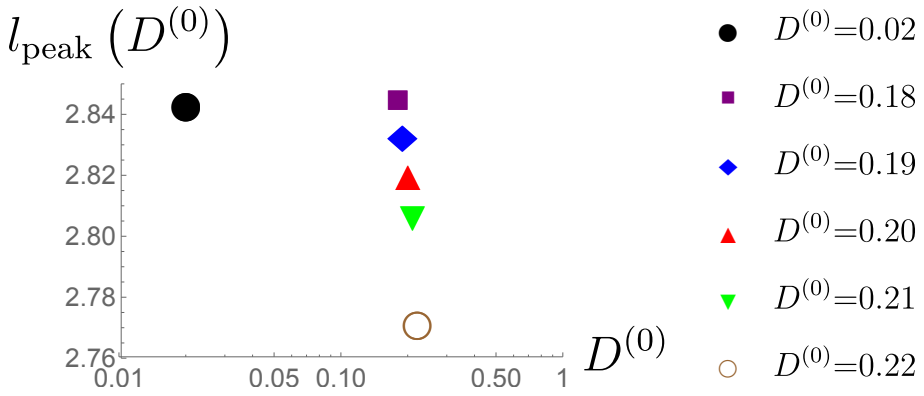

FIGURE 4.31: This graph does confirm that this scenario has disorder induced superconductivity. The value for l_{peak} at the weakest disorder is still similar to what it would have been without the spin gap due to how close $y(l) = 1$ and $J(l) = 1$ occuring was. However, for the strongest disorder the spin gap has decreased l_{peak} more than otherwise. This implies that a spin gap opening increases the rate at which superconductivity occurs.

The value for T when $J(T) = 1$ against the initial value of disorder

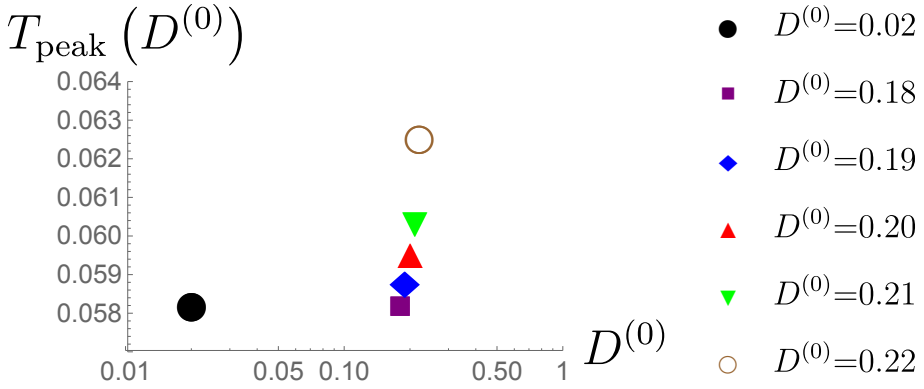

FIGURE 4.32: This graph shows disorder induced superconducting in T as expected. This does not exactly correspond to the experimental graph as there is expected to be a larger gap between the disorders. Additionally it is expected that the strongest disorder would start to plateau as in the case for T_{min}. This could be due different mechanisms being required.

Now the resistivities for all of the disorders can be plotted. Due to the differing mechanisms it is beneficial to plot each mechanism individually.

The full plots of resistivity, $\rho(T)$ including the onset of superconductivity for the real minimum

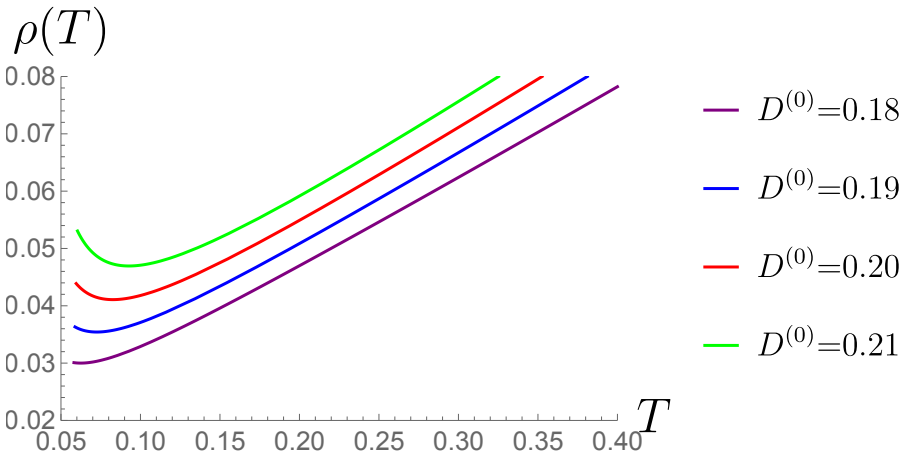

FIGURE 4.33: This graph is similar to figure 4.19 however the values for T_{peak} are much closer in this graph. The resistivities follow the expected trajectory from experiment where as T is decreasing, a minimum occurs and then $J(l) = 1$ signalling the onset of superconductivity.

The full plot of resistivity for the weak spin gapped disorder

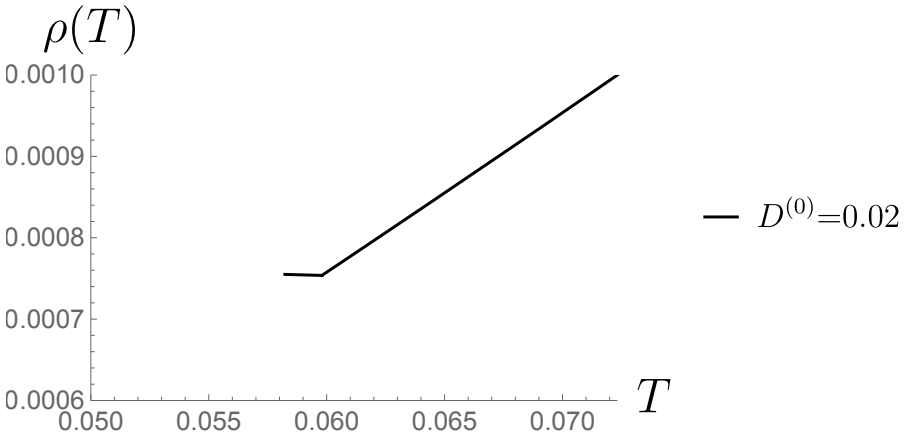

FIGURE 4.34: This graph shows similar behaviour to figure 4.33 in the sense there is a minimum in resistivity and then quickly the onset of superconductivity occurs. This corresponds with the results from table 4.1. The main striking difference is the value of $\rho(T_{\text{peak}})$ which is two orders of magnitude lower than figure 4.33.

The full plot of resistivity for the strong spin gapped disorder

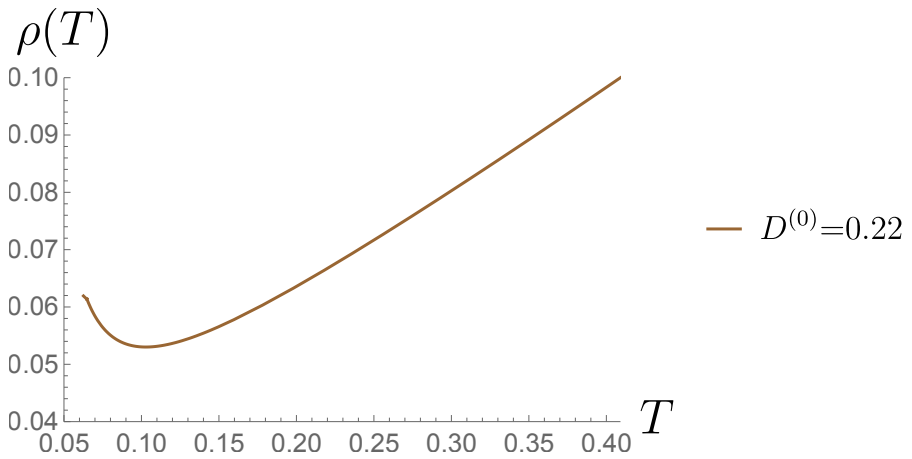

FIGURE 4.35: This graph appears to follow the same template as figure 4.33, including a similar value for $\rho(T_{\text{peak}})$. Therefore the spin gapped scenario does not always give drastically different behaviour in resistivity.

Another graph that is shown in the experiment is the values for $\rho(T_{\text{peak}})$ against $D^{(0)}$. This reveals the difference in the mechanisms in another way due to the large difference between $\rho(T_{\text{peak}})$ for the smallest disorder compared to the other disorders.

The value of $\rho(T_{\text{peak}})$ against initial values of disorder

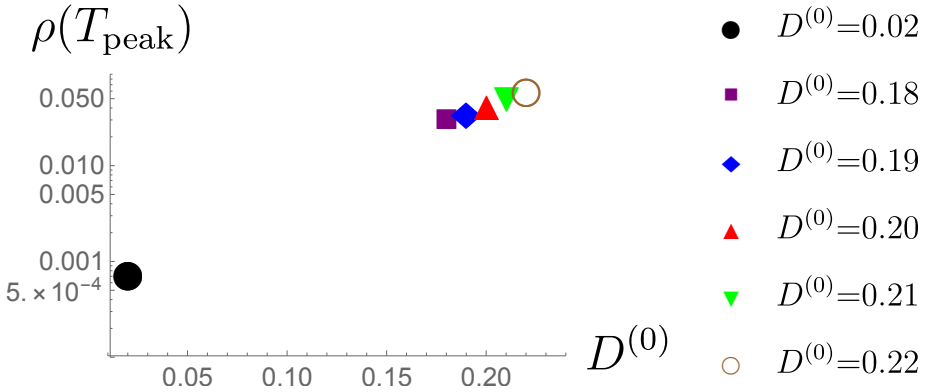

FIGURE 4.36: This graph confirms there is a large difference of about two orders of magnitude in the value of $\rho(T_{\text{peak}})$. In the experiment the three weakest disorders appear to have a $\rho(T_{\text{peak}}) \approx 10^{-5}$ which suggests the three weakest disorders should occur via the spin gap mechanism for $y(l) = 1$ which contradicts what is found here.

4.4 Discussion

The main result of this section is a possible explanation of the jump in the minimum of the resistivity, by using different mechanisms to explain different parts of the experiment. Ultimately the strongest disorder was not able to reproduce the experiment for the set of parameter initial conditions chosen. The disorder could not be raised further either since if this occured then $D(l) = 1$ would occur in the spin gapped scenario before $J(l) = 1$ so the RG equations would lose their validity. It is an interesting question to speculate what might happen when $D(l) = 1$ occurs, as that could possibly explain the physics of the strongest disorder point in figure 4.4.

Additionally $\rho(T_{\text{peak}})$ was found to vary by two orders of magnitude by changing mechanisms from spin gapped for $y(l) = 1$ to $[D] - 2 = 0$. This showed some correspondence to the experiment except for their change in magnitude was approximately four orders of magnitude. Currently there is no explanation for this. Additionally, the experiment had the three weakest disorders which had $\rho(T_{\text{peak}})$ being consistent with the $y(l) = 1$ spin gapped scenario in this model. Therefore this implies that the first three disorders may need to all occur via this mechanism. This could be looked into in the future, however there was no current evidence a $T_{\text{min}}(D^{(0)})$ could be reproduced to match the experiment via this mechanism. Due to the number of initial conditions and the sensitivity of the system on these initial conditions, the scenario may exist and is yet to be found.

In summary, disorder induced superconductivity has been found numerically within this theory, which in itself is a novel and exciting observation, other experimental signatures are also found within the theory suggesting there is promise in pursuing and developing the theory, as this could be the first theoretical description of disorder induced superconductivity which correctly describes what is seen in experiment.

Chapter 5

Conclusions and Future Work

The primary novel research of this thesis was presented in chapters 3 and 4. In chapter 3, an analytical derivation of a non trivial topological superconductor was presented where the topology was dependent on the chemical potential. When the chemical potential was found to be zero, this resulted in a trivial topological state, however the ground state for this system was unusual since it had a continuum of ground states along the diagonals of the Brillouin zone. This scenario is particularly interesting as it shows that a widely held assumption, the gap field being homogeneous for a translationally invariant system, may not hold in all cases. This is because it has been shown that the gap field may depend on momentum for certain scenarios.

Experimental work is needed to check this prediction. A potential way to find this topological phase transition would be to compute the specific heat. This should give a jump as the system goes through the transition. Once the expected behaviour jump is confirmed theoretically, it would give experimentalists a signature to study, and the dependence of the translational invariance of the gap field on chemical potential could potentially be found. This piece of research yields an exciting opportunity for collaborative work between theorists and experimentalists. The benefit of topological superconductors has been widely discussed within this thesis, culminating in potentially finding a material which could be used for quantum computing. This branch of research is worth pursuing in the future.

From a theoretical perspective, the most significant discovery was the dependence of the gap field on momentum if chemical potential is zero. This at the time of writing was not known. Therefore there may be other theories which must account for this caveat. Additionally, it demonstrates how a highly symmetrical model could potentially yield non trivial topology. This implies a link between symmetry and topological properties. This prediction

could be used as another way of designing a topological material.

The novel research explained in chapter 4 has significant implications both theoretically and experimentally. There are few theories that describe how disorder could induce superconductivity, and currently at the time of writing, there is no theory that is widely accepted which agrees with any of the experiments which suggest disorder-induced superconductivity. This could be the first theory which agrees, at least partially, with experiment. Part of this reason is by design. The action that was written is a quasi-1D model which reflects the experiment. After solving the action in terms of RG equations, this allows the study of how the parameters affect the system. This is where the bulk of the research was developed within chapter 4. One issue with this theory is the dependence on the initial conditions. Since slightly changing the initial conditions can significantly change the behaviour of the system, it is difficult to predict whether the full experiment can be explained by this theory. Nevertheless, a clear jump in T_{min} is found, which is one of the main signatures of the experiment. Most importantly, there are scenarios in which disorder is numerically found to induce superconductivity.

Another fascinating discovery is how superconductivity can occur in different states within this model, and the competition between them. The difference between spin gapped states and the normal state was studied extensively. The $y(l) = 1$ spin gapped state corresponds to a spin density wave (SDW) system, and the $y(l) = -1$ state corresponds to a charge density wave (CDW) state. It appears the order of increasing superconductivity with disorder starts with SDW, and goes through a transition to the normal state, and then finishes with a CDW. The competition between these states disregarding superconductivity is an interesting theoretical find.

Unfortunately, the theory does not align perfectly with the model. The main discrepancy is that experimentally there is a plateau in both the T_{min} and T_{peak} graphs for the strongest disorder. This is not seen in the theory for the range of initial conditions attempted. It was believed this plateau may be due to a different mechanism, namely the CDW. However this was not seen. Another difficulty with the strong disorder point, was that the RG equations did not allow the true strongest disorder to be chosen, as the experimental strong disorder is about four times larger than the middle four points. When attempting to do this in numerical simulations, the strong disorder renormalised to unity before any superconductivity or spin gap could occur. Therefore the RG approach limits the model. There are also results

which suggest this is only a two-mechanism scenario, not a three-mechanism scenario as is being proposed in this model. One of the graphs in the experiment shows how the peak of resistivity at the onset of superconductivity differs by five orders of magnitude from the three weakest disorders to the three strongest disorders. This implies there are only two mechanisms. However numerical simulations that describes the T_{min} graph could not be found for such a scenario. The only mechanism which gave a significantly different $\rho(T_{\text{peak}})$ was the SDW state. For this model it was approximately two orders of magnitude different. The largest limitation of this theory is the dependence on initial conditions. Since there is an abundance of physics contained within the theory, it is difficult to extract the complete experimental results. This does not mean a relevant set of initial conditions do not exist. Consequently, this could be an opportunity for collaboration with machine learning experts to use interpolation techniques to decisively determine whether there is a set of initial conditions within this theory which can reproduce the experiment.

The future work that can be performed from this research is extensive. From the theoretical perspective, our set of inital conditions was fixed, and the only changing parameter was the initial disorder. If it could be shown justifiably that disorder itself changes the initial conditions of the other parameters, then matching the theory to the experiment would be a much simpler task. Moreover, an ambitious task, but nonetheless important, would be to try and definitively confirm the mechanism for this type of superconductivity, and the detail of how disorder enhances this mechanism. Understanding this could lead to other theories based on this mechanism in non quasi-1D scenarios. This could ultimately lead to a higher T_c superconductor, and potentially a room temperature superconductor.

Appendix A

Calculating the Jacobian

This appendix provides the detail relevant to the derivation of the Luttinger liquid Hamiltonian in section 4.1.1. This derivation is computed at zero temperature. Starting from

$$Z_\eta = \int \mathcal{D}\bar{\psi}\mathcal{D}\psi \exp\left(iS_{0\eta}\right) = J(\alpha_\eta) \int \mathcal{D}\bar{\psi}'\mathcal{D}\psi' \exp\left(iS'_{0\eta}\right) = J(\alpha_\eta) Z'_\eta, \tag{A.1}$$

it can be seen that the Jacobian can be written as

$$J(\alpha_\eta) = \frac{Z_\eta}{Z'_\eta}. \tag{A.2}$$

Now recall equation (1.19), which states

$$Z = \int \mathcal{D}\bar{\psi}\mathcal{D}\psi \exp\left(i\bar{\psi}A\psi\right) = \det A, \tag{A.3}$$

when calculated in real time. This identity is true for fermions. For bosons the result is $1/\det(A)$. In this relation A is typically denoted by G^{-1}, which is the Green's function. This is discussed in more detail in chapter 3. Now by using the results for $S_{0\eta}$ and $S'_{0\eta}$, the result for the Jacobian becomes

$$J(\alpha_\eta) = \frac{\det\left(G_\eta^{-1}\right)}{\det\left(G_\eta^{-1} - \alpha_\eta\right)} = \frac{\det\left(G_\eta^{-1}\right)}{\det\left(G_\eta^{-1} - \alpha_\eta\right)}. \tag{A.4}$$

By then using the relation

$$\ln\det(A) = \mathrm{Tr}\ln(A), \tag{A.5}$$

equation (A.4) becomes

$$\begin{aligned} J(\alpha_\eta) = \exp\Big[\operatorname{Tr}\ln G_\eta^{-1} - \operatorname{Tr}\ln\left(G_\eta^{-1} - \alpha_\eta\right)\Big] &= \exp\Big[-\operatorname{Tr}\ln\left(1 - \alpha_\eta G_\eta\right)\Big] \\ &= \exp\Big[-\operatorname{Tr}\sum_{n=2}^{\infty}\frac{\left(\alpha_\eta G_\eta\right)^n}{n}\Big]. \end{aligned} \tag{A.6}$$

The $n = 1$ term is a global term so is cancelled without the gauge transformation, however for $n > 2$ all the terms vanish due to the Dzyaloshinskii-Larkin theorem [88]. This implies that

$$\begin{aligned} \ln J_\eta &= -\frac{1}{2}\operatorname{Tr}\left(\alpha_\eta G_\eta\right)^2 \\ &= -\frac{1}{2}\int d\xi d\xi' \alpha_\eta(\xi) G_\eta(\xi - \xi') G_\eta(\xi' - \xi)\alpha_\eta(\xi'), \end{aligned} \tag{A.7}$$

where $\xi = (x, t)$. In momentum space this is

$$\ln J_\eta = -\frac{1}{2}\int d\mathbf{k}\alpha_\eta(\mathbf{k})\alpha_\eta(-\mathbf{k})\int d\mathbf{p} G_\eta(\mathbf{p}) G_\eta(\mathbf{p}+\mathbf{k}), \tag{A.8}$$

where $\mathbf{k} = (k, \omega)$ and $\mathbf{p} = (p, \Omega)$. Compute the $\mathbf{p}$ integral such that

$$\begin{aligned} \int d\mathbf{p} G_\eta(\mathbf{p}) G_\eta(\mathbf{p}+\mathbf{k}) \\ = \int d\mathbf{p}\frac{1}{\Omega + \omega - \eta v(p+k) + i\delta sgn(\Omega+\omega)}\frac{1}{\Omega - \eta v p + i\delta sgn\Omega}, \end{aligned} \tag{A.9}$$

which becomes

$$\begin{aligned} \int d\mathbf{p} G_\eta(\mathbf{p}) G_\eta(\mathbf{p}+\mathbf{k}) &= 2\pi i \int dp \frac{\eta(H_p - H_{p+k})}{\omega - \eta v k + i\delta sgn\omega} \\ &= \frac{2\pi i k\eta}{(\omega - \eta v k + i\delta sgn\omega)} = 2\pi i k \eta G_\eta(\mathbf{k}), \end{aligned} \tag{A.10}$$

where H_p and H_{p+k} represent the heaviside step functions, and arise from the complex integration. From this, the $\mathbf{k}$ integral becomes

$$\ln J_\eta = -\pi i \eta \int d\mathbf{k}\alpha_\eta(\mathbf{k})\alpha_\eta(-\mathbf{k})\mathbf{k} G_\eta(\mathbf{k}), \tag{A.11}$$

which can be transformed back to real space to give

$$\ln J_\eta = \frac{\eta}{4\pi}\operatorname{Tr}\Big[\alpha_\eta \partial_x G_\eta \alpha_\eta\Big], \tag{A.12}$$

then remember that $\alpha_\eta \equiv \partial_\eta \theta_\eta$ and $G_\eta \equiv -i\partial_\eta^{-1}$, which implies $G_\eta \alpha_\eta = -i\theta_\eta$. Therefore

$$\ln J_\eta = -\frac{i\eta}{4\pi} \operatorname{Tr}\Big[\partial_\eta \theta_\eta \partial_x \theta_\eta\Big], \tag{A.13}$$

which means the full Jacobian is

$$J(\theta_R, \theta_L) = \exp\Big[-\sum_\eta \frac{i\eta}{4\pi} \operatorname{Tr}\Big(\partial_\eta \theta_\eta \partial_x \theta_\eta\Big)\Big]. \tag{A.14}$$

Appendix B

Derivation of a Renormalisation Group Equation

This will show the derivation of the $g_\perp$ RG equation and is based on the derivations in [81, 85, 86]. Starting with the partition function for the action in equation (4.39) in chapter 5, only including the $g_\perp$ term, the result is

$$Z = \int \mathcal{D}\phi(x,\tau) \exp\big(-S(\phi(x,\tau))\big), \tag{B.1}$$

where ϕ includes both the spin and charge components. The first step of RG is to write ϕ in Fourier modes as

$$\phi(\mathbf{x},\tau) = \frac{1}{\beta\Omega}\sum_{\mathbf{k},\epsilon} \exp\big(i(\mathbf{k}.\mathbf{x} - \epsilon t)\big)\phi(\mathbf{k},\epsilon). \tag{B.2}$$

Then these modes can be decomposed into fast and slow modes which represent different energy scales. This is done by imposing cutoffs, Λ, Λ' and writing $\phi(\mathbf{r}) = \phi^{>}(\mathbf{r}) + \phi^{<}(\mathbf{r})$, where

$$\phi^{>}(\mathbf{r}) = \frac{1}{\beta\Omega}\sum_{\Lambda' \geq |\mathbf{q}| \leq \Lambda} \exp\big(i\mathbf{q}.\mathbf{r}\big)\phi(\mathbf{q}), \tag{B.3}$$

and

$$\phi^{<}(\mathbf{r}) = \frac{1}{\beta\Omega}\sum_{\mathbf{q}<\Lambda'} \exp\big(i\mathbf{q}.\mathbf{r}\big)\phi(\mathbf{q}). \tag{B.4}$$

For the quadratic in $\phi(\mathbf{r})$ part of the action, write as $S_0(\mathbf{r}) = S_0^>(\mathbf{r}) + S_0^<(\mathbf{r})$. Divide the interacting partition function by the non-interacting partition function and expand such that

$$\begin{aligned}\frac{Z}{Z_0} = \frac{1}{Z_0}\int \mathcal{D}\phi(\mathbf{r},\mathbf{r_1},\mathbf{r_2})\exp\big(-S_0^>-S_0^<\big)\Big[1-\\ \frac{2g_{1\perp}}{(2\pi\alpha)^2u}\int d^2\mathbf{r}\cos[\sqrt{8}(\phi^>(\mathbf{r})+\phi^<(\mathbf{r}))]+\frac{2g_{1\perp}^2}{(2\pi\alpha)^4u^2}\\ \int d^2\mathbf{r_1}\int d^2\mathbf{r_2}\cos[\sqrt{8}(\phi^>(\mathbf{r_1})+\phi^<(\mathbf{r_1}))]\cos[\sqrt{8}(\phi^>(\mathbf{r_2})+\phi^<(\mathbf{r_2}))]\Big].\end{aligned} \tag{B.5}$$

The fast modes can now be integrated out, to leave the action only dependent on the slow modes. This yields

$$\begin{aligned}\frac{Z}{Z_0^<} = \frac{1}{Z_0}\int \mathcal{D}\phi(\mathbf{r},\mathbf{r_1},\mathbf{r_2})\exp\big(-S_0^<\big)\Big[1-\\ \frac{2g_{1\perp}}{(2\pi\alpha)^2u}\int d^2\mathbf{r}\cos[\sqrt{8}\phi^<(\mathbf{r})]\exp\big(-4\langle(\phi^>\mathbf{r})^2\rangle\big)\\ +\frac{g_{1\perp}^2}{(2\pi\alpha)^4u^2}\sum_{\nu=\pm1}\int d^2\mathbf{r_1}\int d^2\mathbf{r_2}\cos[\sqrt{8}(\phi^<(\mathbf{r_1})+\nu\phi^<(\mathbf{r_2}))]\\ \exp\big(-4\langle(\phi^>(\mathbf{r_1})+\nu\phi^>(\mathbf{r_2}))^2\rangle\big)]\Big].\end{aligned} \tag{B.6}$$

Now the equation must be reexponentiated to get it in the form of the effection action. This results in

$$\begin{aligned}\frac{Z}{Z_0^<} = \frac{1}{Z_0}\int \mathcal{D}\phi(\mathbf{r},\mathbf{r_1},\mathbf{r_2})\exp\Big[-S_0^<-\frac{2g_{1\perp}}{(2\pi\alpha)^2u}\\ \int d^2\mathbf{r}\cos[\sqrt{8}\phi^<(\mathbf{r})]\exp\big(-4\langle(\phi^>\mathbf{r})^2\rangle\big)\Big]\\ \exp\Big[\frac{g_{1\perp}^2}{(2\pi\alpha)^4u^2}\sum_{\nu=\pm1}\int d^2\mathbf{r_1}\int d^2\mathbf{r_2}\cos[\sqrt{8}(\phi^<(\mathbf{r_1})+\nu\phi^<(\mathbf{r_2}))]\\ \exp\big(-4\langle(\phi^>(\mathbf{r_1})+\nu\phi^>(\mathbf{r_2}))^2\rangle\big)]\Big]\\ \exp\Big[-\frac{g_{1\perp}^2}{(2\pi\alpha)^4u^2}\int d^2\mathbf{r_1}\int d^2\mathbf{r_2}\cos[\sqrt{8}(\phi^<(\mathbf{r_1})]\exp\big(-4\langle\phi^>(\mathbf{r_1})\rangle\\ \cos[\sqrt{8}(\phi^<(\mathbf{r_2})]\exp\big(-4\langle\phi^>(\mathbf{r_2})\rangle\Big].\end{aligned} \tag{B.7}$$

At this stage, the first terms can be compared. In this equation it is only in terms of the slow modes. To relate it back to the original action, the momentum, position and time must be

rescaled such that

$$\begin{aligned} d\mathbf{k} &= \frac{\Lambda'}{\Lambda} d\mathbf{k}, \\ dx &= \frac{\Lambda}{\Lambda'} dx', \\ d\tau &= \frac{\Lambda}{\Lambda'} d\tau'. \end{aligned} \tag{B.8}$$

From this, the coupling constant $g_{1\perp}$ has been rescaled such that

$$\begin{aligned} g_{1\perp}(\Lambda') =& \Big(\frac{\Lambda}{\Lambda'}\Big)^2 g_{1\perp}(\Lambda) \exp\big(-4\langle(\phi^{>}(\mathbf{r})^2\rangle\big) \\ =& \Big(\frac{\Lambda}{\Lambda'}\Big)^2 g_{1\perp}(\Lambda) \exp\Big[-\frac{4}{\beta\Omega} \sum_{\Lambda' \geq |\mathbf{q}| \leq \Lambda, \epsilon} \frac{\pi K u}{\epsilon^2 + u^2\mathbf{q}^2}\Big]. \end{aligned} \tag{B.9}$$

The correlation function has been evaluated and the derivation is found in [81]. To further evaluate this equation, $\beta = L \to \infty$, and the sum over Matsubara frequencies is computed. This gives

$$g_{1\perp}(\Lambda') = \Big(\frac{\Lambda}{\Lambda'}\Big)^2 g_{1\perp}(\Lambda) \exp\big(-2\int_{\Lambda'}^{\Lambda} d\mathbf{q} \frac{K}{\mathbf{q}}\big) = \Big(\frac{\Lambda}{\Lambda'}\Big)^2 g_{1\perp}(\Lambda) \exp\Big[-2K \ln\Big(\frac{\Lambda}{\Lambda'}\Big)\Big]. \tag{B.10}$$

Now parameterise the cutoff as $\Lambda(l) = \Lambda_0 \exp(-l)$, where Λ_0 is the bare cutoff. Then an infinitesimal change is applied such that $\Lambda(l)' = \Lambda_0 \exp(-l - dl)$, and therefore

$$g_{1\perp}(l + dl) = g_{1\perp}(l) \exp\big((2 - 2K(l))dl\big), \tag{B.11}$$

and therefore the RG equation is initially

$$g'(l) = g(l)(2 - 2K(l)). \tag{B.12}$$

This in terms of $y(l)$ is

$$y'(l) = y(l)(2 - 2K(l)). \tag{B.13}$$

This is not the full RG equation. This is because as $y(l)$ renormalises, D also renormalises with it since the action terms are both cosines. These can be combined for $g_{1\perp}$ to give

$$\begin{aligned} yD \int dx \cos\Big(\sqrt{8}\phi_\sigma(x)\Big) \int dx' \exp\Big(i\sqrt{2}\phi_\rho(x')\Big) \cos\Big(\sqrt{2}\phi_\sigma(x')\Big) \\ = yD \int dx \int dx' \exp\Big(i\sqrt{2}\phi_\rho(x')\Big) \cos\Big(\sqrt{2}\phi_\sigma(x)\Big), \end{aligned} \tag{B.14}$$

which is the definition of a disorder term from Giamarchi [81]. Therefore when solving the RG equations for $y(l)$, there must be a disorder term. Since in the action the disorder term comes with a minus sign, the full RG equation is

$$y'(l) = y(l)(2 - 2K(l)) - D(l). \tag{B.15}$$

The remaining RG equations are derived in a similar way. For full details see [81, 86, 85].

Bibliography

[1] I. Karnaukhov. “Spontaneous breaking of time-reversal symmetry in topological superconductors”. In: *Scientific Reports* 7 (2017), pp. 7008–7015.

[2] A. Lowe, M. Ortuno, I. Yurkevich. “Topological Phase Transition in Superconductors with Mirror Symmetry”. In: *Journal of Physics: Condensed Matter* 32 (2019), pp. 035603 –035609.

[3] A. Petrović, D. Ansermet, D. Chernyshov, M. Hoesch, D. Salloum, P. Gougeon, M. Potel, L. Boeri, C. Panagopoulos. “A disorder-enhanced quasi-one-dimensional superconductor”. In: *Nature Communications* 7 (2016), pp. 12262–12272.

[4] H. Onnes, G. Sizoo. “Further experiments with liquid helium. D. On the change of electric resistance of pure metals at very low temperatures, etc. V. The disappearance of the resistance of mercury.” In: *Commun. Phys. Lab. Univ. Leiden* 122b (1911), pp. 264–266.

[5] F. Arute, K. Arya, R. Babbush, D. Bacon, J. Bardin, R. Barends, R. Biswas, S. Boixo, F. Brandao, D. Buell, B. Burkett, Y. Chen, Z. Chen, B. Chiaro, R. Collins, W. Courtney, A. Dunsworth, E. Farhi, B. Foxen, A. Fowler, C. Gidney, M. Giustina, R. Graff, K. Guerin, S. Habegger, M. Harrigan, M. Hartmann, A. Ho, M. Hoffmann, T. Huang, T. Humble, S. Isakov, E. Jeffrey, Z. Jiang, D. Kafri, K. Kechedzhi, J. Kelly, P. Klimov, S. Knysh, A. Korotkov, F. Kostritsa, D. Landhuis, M. Lindmark, E. Lucero, D. Lyakh, S. Mandrà, J. McClean, M. McEwen, A. Megrant, X. Mi, K. Michielsen, M. Mohseni, J. Mutus, O. Naaman, M. Neeley, C Neill, M. Niu, E. Ostby, A. Petukhov, J. Platt, C. Quintana, E. Rieffel, P. Roushan, N. Rubin, D. Sank, K. Satzinger, V Smelyanskiy, K. Sung, M. Trevithick, A. Vainsencher, B. Villalonga, T White, J. Yao, P. Yeh, A. Zalcman, H. Neven, J. Martinis. “Quantum Supremacy using a Programmable Superconducting Processor”. In: *Nature* 574 (2019), pp. 505–510.

[6] I. Burmistrov, I. Gornyi, A. Mirlin. "Enhancement of the Critical Temperature of Superconductors by Anderson Localization". In: *Physical Review Letters* 108 (2012), pp. 017002–017007.

[7] J. Bednorz, K. Müller. "Possible high Tc superconductivity in the BaLaCuO system". In: *Zeitschrift für Physik B Condensed Matter* 64 (1986), pp. 189–193.

[8] W. Meissner, R. Ochsenfeld. "Ein neuer Effekt bei Eintritt der Supraleitfähigkeit". In: *Die Naturwissenschaften* 21 (1933), pp. 787–788.

[9] F. London, H. London. "The Electromagnetic Equations of the Supraconductor". In: *Proceedings of the Royal Society of London. Series A - Mathematical and Physical Sciences* 149 (1935), pp. 71–88.

[10] K. Binder. "Theory of First-Order Transitions". In: *Reports on Progress in Physics* 50 (1987), pp. 783–859.

[11] L. Landau. "On the Theory of Phase Transitions". In: *Nature* 138 (1936), pp. 840–841.

[12] V. Ginzburg. "On the Theory of Superconductivity". In: *Institute of Physics of the Academy of Science of the USSR* 2 (1955), pp. 1234–1250.

[13] E. Schrodinger. "An Undulatory Theory of the Mechanics of Atoms and Molecules". In: *Physical Review* 28 (1926), pp. 1049–1070.

[14] W. Harrison. *Solid State Theory*. McGraw-Hill, 1970.

[15] J. Bardeen, L. Cooper, J. Schrieffer. "Theory of Superconductivity". In: *Physical Review* 108 (1957), pp. 1175–1204.

[16] L. Cooper. "Bound Electron Pairs in a Degenerate Fermi Gas". In: *Physical Review* 104 (1956), pp. 1189–1190.

[17] J. Negele, H. Orland. *Quantum Many-particle Systems*. Addison-Wesley, 1988.

[18] R. Stratonovich. "On a Method of Calculating Quantum Distribution Functions". In: *Soviet Physics Doklady* 2 (1958), pp. 416–419.

[19] P. Debye. "Zur Theorie der Spezifischen Warmen". In: *Annalen der Physik* 344 (1912), pp. 789–839.

[20] A. Drozdov, P. Kong, V. Minkov, S. Besedin, S. Kuzovnikov, L. Mozaffari, F. Balicas, D. Balakirev, V. Graf, E. Prakapenka, D. Greenberg, M. Knyazev, M. Tkacz, M. Eremets. "Superconductivity at 250K in Lanthanum Hybride under High Pressures". In: *Nature* 569 (2019), pp. 528–531.

[21] G. Eliashberg. "Temperature Green's Function for Electrons in a Superconductor". In: *Sov. Phys. JETP* 38 (1961), pp. 696 –702.

[22] L. Oliveira, E. Gross, W. Kohn. "Density-Functional Theory for Superconductors". In: *Physical Review Letters* 60 (1988), pp. 2430–2433.

[23] T. Lemberger, S. Lee. "Disorder Induced Pair Breaking in Superconductors". In: *Novel Superconductivity*. Ed. by S. Wolf, V. Kresin. Springer, 1987.

[24] P. Anderson. "Absence of Diffusion in Certain Random Lattices". In: *Physical Review* 109 (1958), pp. 1492–1505.

[25] D. Pesin, A. Andreev. "Suppression of Superconductivity in Disordered Interacting Wires". In: *Physical Review Letters* 97 (2006), pp. 117001–117005.

[26] B. Gao, A. Komnik, R. Egger, D. Glattli, A Bachtold. "Evidence for Luttinger-Liquid Behavior in Crossed Metallic Single-Wall Nanotubes". In: *Physical Review Letters* 92 (2004), pp. 216804–216808.

[27] J. Voit. "One-dimensional Fermi Liquids". In: *Reports on Progress in Physics* 58.9 (1995), pp. 977–1116.

[28] R Peierls. *Quantum Theory of Solids*. Clarendon, Oxford, 1955.

[29] J. Luttinger. "An Exactly Soluble Model of a Many-Fermion System". In: *Journal of Mathematical Physics* 4 (1963), pp. 1154–1162.

[30] V. Vescoli, F. Zwick, W. Henderson, L. Degiorgi, M. Grioni, G. Gruner, L. Montgomery. "Optical and Photoemission Evidence for a Tomonaga-Luttinger Liquid in the Bechgaard Salts". In: *European Physical Journal B* 13 (2000), pp. 503–511.

[31] D. Jérome, A. Mazaud, M. Ribault, K. Bechgaard. "Superconductivity in a Synthetic Organic Conductor $(TMTSF)_2PF_6$". In: *J. Physique Lett.* 41 (1980), pp. 95–98.

[32] M. Rother, W. Wegscheider, R. Deutschmann, M. Bichler, G. Abstreiter. "Evidence of Luttinger Liquid Behavior in GaAs/AlGaAs Quantum Wires". In: *Physica E: Low Dimensional Systems and Nanostructures* 6 (2000), pp. 551–554.

[33] M. Atala, M. Aidelsburger, M. Lohse, J. Barreiro, B. Paredes, I. Bloch. "Observation of Chiral Currents with Ultracold Atoms in Bosonic Ladders". In: *Nature Physics* 10 (2014), pp. 588–593.

[34] M. Chang. "Chiral Luttinger Liquids at the Fractional Quantum Hall Edge". In: *Reviews of Modern Physics* 75 (2003), pp. 1449–1505.

[35] Y. Ran, Y. Zhang, A. Vishwanath. "One-Dimensional Topologically Protected Modes in Topological Insulators with Lattice Distortions". In: *Nature Physics* 5 (2009), pp. 298–303.

[36] E. Lieb, F. Wu. "Absence of Mott Transition in an Exact Solution of the Short-Range, One-Band Model in One Dimension". In: *Physical Review Letters* 20 (1968), pp. 1445–1448.

[37] N. Plakida. "Superconductivity in the t-J model". In: *Condensed Matter Physics* 5 (2002), pp. 707–727.

[38] L. Pryadko, S. Kivelson, O. Zachar. "Incipient Order in the t-J Model at High Temperatures". In: *Physical Review Letters* 92 (2004), pp. 067002–067006.

[39] H. Zhai, M. Rechtsman, Y. Lu, K. Yang. "Focus on Topological Physics: From Condensed Matter to Cold Atoms and Optics". In: *New Journal of Physics* 18 (2016), pp. 080201–080205.

[40] K. Klitzing, G. Dorda, M. Pepper. "New Method for High-Accuracy Determination of the Fine-Sructure Constant Based on Quantized Hall Resistance". In: *Physical Review Letters* 45 (1980), pp. 494–497.

[41] D. Thouless, M. Kohmoto, M. Nightingale, M. den Nijs. "Quantized Hall Conductance in a Two-Dimensional Periodic Potential". In: *Physical Review Letters* 49 (1982), pp. 405–408.

[42] J. Kosterlitz, D. Thouless. "Ordering, Metastability, and Phase Transitions in Two-Dimensional Systems". In: *Journal of Physics: Condensed Matter* 6 (1973), pp. 1181–1203.

[43] L. Sheng, D. Sheng, C. Ting, F. Haldane. "Nondissipative Spin Hall Effect via Quantised Edge Transport". In: *Physical Review Letters* 95 (2005), pp. 136602–136606.

[44] C. Kane, E. Mele. "Z_2 Topological Order and the Quantum Spin Hall Effect". In: *Physical Review Letters* 95 (2005), pp. 146802–146806.

[45] A. Kitaev. "Fault-Tolerant Quantum Computation by Anyons". In: *Annals of Physics* 303 (2003), pp. 2–30.

[46] P. Roushan, J. Seo, C. Parker, Y. Hor, D. Hsieh, D. Qian, A. Richardella, M. Hasan, R. Cava, A. Yazdani. "Topological Surface States Protected From Backscattering by Chiral Spin Texture". In: *Nature* 460 (2009), pp. 1106–1109.

[47] C. Kane, E. Mele. "Quantum Spin Hall Effect in Graphene". In: *Physical Review Letters* 95 (2005), pp. 226801–226805.

[48] A. Bernevig, T. Hughes, S. Zhang. "Quantum Spin Hall Effect and Topological Phase Transition in HgTe Quantum Wells". In: *Science* 314 (2006), pp. 1757–1761.

[49] J. Leinaas, J. Myrheim. "On the Theory of Identical Particles". In: *Il Nuovo Cimento B* 37 (1977), pp. 1–23.

[50] P Shor. "Scheme for Reducing Decoherence in Quantum Computer Memory". In: *Physical Review A* 52 (1995), pp. 2493–2496.

[51] R. Willet, C. Nayak, K. Shtengel, L. Pfeiffer, K. West. "Magnetic-Field-Tuned Aharonv-Bohm Oscillations and Evidence for Non-Abelian Anyons at $\nu = 5/2$". In: *Physical Review Letters* 111 (2013), pp. 186401–186406.

[52] N. Read, D. Green. "Paired State of Fermions in Two Dimensions with Breaking of Parity and Time-Reversal Symmetries, and the Fractional Quantum Hall Effect". In: *Physical Review. B* 61 (2000), pp. 10267–10297.

[53] A. Kitaev. "Unpaired Majorana Fermions in Quantum Wires". In: *Physics-Uspekhi* 44 (2001), pp. 131–136.

[54] E. Majorana. "Teoria Simmetrica Dell'elettrone e del Positrone". In: *Il Nuovo Cimento* 14 (1937), pp. 171–185.

[55] S. Nadj-Perge, I. Drozdov, J. Li, H. Chen, S. Jeon, J. Seo, A. MacDonald, A. Bernevig, A. Yazdani. "Observation of Majorana Fermions in Ferromagnetic Atomic Chains on a Superconductor". In: *Science* 346 (2014), pp. 602–607.

[56] D. Wang, L. Kong, P. Fan, H. Chen, S. Zhu, W. Liu, L. Cao, Y. Sun, S. Du, J. Schneeloch, R. Zhong, G. Gu, L. Fu, H. Ding, H. Gao. "Evidence for Majorana Bound States in an Iron-Based Superconductor". In: *Science* 362 (2018), pp. 333–335.

[57] A. Fornieri, A. Whiticar, F. Setiawan, E. Portolés, A. Drachmann, A. Keselman, S. Gronin, C. Thomas, T. Wang, R. Kallaher, G. Gardner, E. Berg, M. Manfra, A. Stern, C. Marcus, F. Nichele. "Evidence of Topological Superconductivity in Planar Josephson Junctions". In: *Nature* 569 (2019), pp. 89–92.

[58] E. Noether. "Invariante Variationsprobleme". In: *Math-Phys. Klasse.* 1918 (1918), pp. 235–257.

[59] A. Altland, M Zirnbauer. "Novel Symmetry Classes in Mesoscopic Normal Superconducting Hybrid Structures". In: *Physical Review. B* 55 (1997), pp. 1142–1162.

[60] C. Chiu, T. Jeffrey, A. Schnyder, S. Ryu. "Classification of Topological Quantum Matter with Symmetries". In: *Reviews of Modern Physics* 88 (2016), pp. 035005–035068.

[61] S. Chern. "Characteristic Classes of Hermitian Manifolds". In: *Annals of Mathematics* 47 (1946), pp. 85–121.

[62] M. Sigrist. "Introduction to Unconventional Superconductivity". In: *AIP Conference Proceedings*. Vol. 789. 2005, pp. 165–244.

[63] D. Osheroff, R. Richardson, D. Lee. "Evidence for a New Phase of Solid He_3". In: *Physical Review Letters* 28 (1972), pp. 885–888.

[64] D. Lawson, H. Bozler, D. Lee. "Anisotropy in Superfluid ^{3}He and the Attenuation of Zero Sound". In: *Physical Review Letters* 34 (1975), pp. 121–124.

[65] Y. Liu. "Phase-Sensitive-Measurement Determination of Odd-Parity, Spin-Triplet Superconductivity in Sr_2RuO_4". In: *New Journal of Physics* 12 (2010), pp. 075001–075021.

[66] K. Nelson, Z. Mao, Y. Maeno, Y. Liu. "Odd-Parity Superconductivity in Sr_2RuO_4". In: *Science* 306 (2004), pp. 1151–1154.

[67] P. Monthoux, A. Balatsky, D Pines. "Weak-Coupling Theory of High-Temperature Superconductivity in the Antiferromagnetically Correlated Copper Oxides". In: *Physical Review B* 46 (1992), pp. 14803–14817.

[68] C. Tsuei, J. Kirtley, Z. Ren, J. Wang, H. Raffy, Z. Li. "Pure $d_{x^2-y^2}$ Order Parameter Symmetry in the Tetragonal Superconductor $Tl_2Ba_2CuO_{6+\delta}$". In: *Nature* 387 (1997), pp. 481–483.

[69] B. Grenier, R. Ballou. "Crystallography: Symmetry Groups and Group Representation". In: *EPJ Web of Conferences*. Vol. 22. 2012, pp. 00006–00053.

[70] T. McQueen, A. Williams, P. Stephens, J. Tao, Y. Zhu, V. Ksenofontov, F. Casper, C. Felser, R. Cava. "Tetragonal-to-Orthorhombic Structural Phase Transition at 90K in the Superconductor $Fe_{1.01}Se$". In: *Physical Review Letters* 103 (2009), pp. 057002–057006.

[71] T. Moriya. "Developments of the Theory of Spin Fluctuations and Spin Fluctuation-Induced Superconductivity". In: *Proceedings of the Japan Academy. Series B, Physical and Biological Sciences* 82 (2006), pp. 1–16.

[72] T. Moriya, K. Ueda. "Spin Fluctuations and High Temperature Superconductivity". In: *Advances in Physics* 49 (2000), pp. 555–606.

[73] G. Esirgen, N. Bickers. "Fluctuation Exchange Analysis of Superconductivity in the Standard Three-Band CuO_2 Model". In: *Physical Review B* 57 (1998), pp. 5376–5393.

[74] D. Manske. *Theory of Unconventional Superconductors - Cooper-Pairing Mediated by Spin Excitations*. Springer Berlin Heidelberg, 2004.

[75] Y. Yanase, T. Jujo, T. Nomura, H. Ikeda, T. Hotta, K. Yamada. "Theory of Superconductivity in Strongly Correlated Electron Systems". In: *Physics Reports* 387 (2003), pp. 1–149.

[76] J. Wheatley, T. Hsu, P. Anderson. "Interlayer Pair Hopping: Superconductivity from the Resonating-Valence-Bond State". In: *Physical Review B* 37 (1987), pp. 5897–5900.

[77] P. Anderson. "The Resonating Valence Bond State in La_2CuO_4 and Superconductivity". In: *Science* 235 (1987), pp. 1196–1198.

[78] N. Mott. "The Basis of the Electron Theory of Metals, with Special Reference to the Transition Metals". In: *Proceedings of the Royal Society* 62 (1949), pp. 416–422.

[79] K. Chao, J. Spałek, A. Oles. "Canonical Perturbation Expansion of the Hubbard Model". In: *Physical Review B* 18 (1978), pp. 3453–3464.

[80] A. Mobius. "Über die Bestimmung des Inhaltes eines Polyëders". In: *Mathematisch-Physische Klasse.* 17 (1865), pp. 31–68.

[81] T. Giamarchi. *Quantum Physics in One Dimension*. Clarendon, Oxford, 2004.

[82] A. Luther, I. Peschel. "Calculation of critical exponents in two dimensions from quantum field theory in one dimension". In: *Physical Review B* 12 (1975), pp. 3908–3917.

[83] A. Pelissetto, E. Vicari. "Critical Phenomena and Renormalization-Group Theory". In: *Physics Reports* 368 (2002), pp. 549–727.

[84] K. Wilson. "Renormalization Group and Critical Phenomena. I. Renormalization Group and the Kadanoff Scaling Picture". In: *Physical Review. B* 4 (1971), pp. 3174–3183.

[85] T. Giamarchi, H. Schulz. "Anderson Localization and Interactions in One-Dimensional Metals". In: *Physical Review B* 37 (1988), pp. 325–340.

[86] I. Gornyi, A. Mirlin, D. Polyakov. "Electron Transport in a Disordered Luttinger Liquid". In: *Physical Review B* 75 (2007), pp. 085421–085457.

[87] D. Shelton, A. Tsvelik. "Superconductivity in a Spin Liquid - A One Dimensional Example". In: *Physical Review B* 53 (1996), pp. 14036–14039.

[88] I. Dzyaloshinskii, A. Larkin. "Correlation Function for a One-Dimensional Fermi System with Long-Range Interaction". In: *Sov. Phys. JETP* 38 (1974), pp. 411–426.